Elucidation of Ionomer/Electrode Interfacial Phenomena in Polymer Electrolyte Fuel Cells

Xiao Gao

Contents

Chapter 1 General Introduction

1.1 Background

A lot of researchers believe that we are encountering problem with energy sources, (oil, coal, *et.al.*) becoming scarcer.[1,2] Energy is closely related to the development of our society. It is said that people are impossible to reach the present level of wellbeing and quality of life without energy source. Fossil fuels, which are the most utilized, useful source of energy are facing a downside. However, our energy system is still not prepared for it since highly concentrated forms of energy are both in short supply and act important roles in our industrial system. Because energy is the foundation of all activity, this dysfunction propagates throughout all of our daily life and interactions with environment, manifesting as problems: deforestation, ocean acidification, biodiversity loss, mass poverty, pollution of water and air, diseases, water table depletion and so on

If there is no enough energy resources, the modern economic development will be significantly restricted. Additionally, the more critical problem is that fossil fuels are a source of pollution of the environment in many cases and have great impact on air. As a consequent, the energy problem has several impact bellows:

(1) Major oil producers tend to conceal their ability of supply, in order to reveal the importance of oil prices

(2) Global warming has become unmistakably important, especially climate changes, and rising sea levels.

Thus, it is urgent to develop a kind of alternative sustainable, renewable energy source to support modern society. In order to fulfill these demands, recent researchers are focusing new energy (e.g. lithium ion battery (LIB), fuel cell, photovoltaic generation system) development. In these, although LIB is most widely used secondary battery for further energy source, while the further utilization is limited by immature technology such as ageing, safety problem.[3] One more attractive alternating solution is the polymer electrolyte fuel cells. Although there are many types of fuel cells, such as

phosphoric acid fuel cells, alkaline fuel cells, solid oxide fuel cells, polymer electrolyte fuel cells are receiving the most attention for automotive and small stationary applications.[4-7] Compared with other energy sources, PEFCs has following advantages:[8,9]

(1) Non-pollutant, the only by-product at point of use is water

(2) Low operation temperature (80°C), compactable

(3) Operating times are much longer than with batteries

Since PEFCs have various advantage compared to conventional energy sources. PEFCs are expected to become the alternating energy sources in the 21st century.

In this manuscript, we focus the ionomer/electrode interface to investigate the properties and morphology of polymer electrolyte in form of thin film.

1.2 Current Development of Polymer Electrolyte Fuel Cells (PEFCs)

The PEFCs has received extraordinary attention as a new generation power converter, which are expected to be applied to automotive power and stationary power of microelectronics. As the high energy density and low operation temperature, PEFC is expected to be one of the most promising energy sources.[8,10-12] A fuel cell vehicle (FCV) manufactured by Toyota was released at the November 2014. Up to now, global sales totaled more 5000 Mirais.

Figure 1 shows an example schematic image of PEFCs. PEFC use a solid state polymer membrane (electrolyte) as a separator. This proton conducting membrane is sandwiched between the anode and cathode. A very thin catalyst layer mixed with carbon support are cast to either side of the membrane and to the electrodes. The membrane electrode assembly is set between the middle separators to fabricate a unit cell. Two bipolar plates are positioned to the adjacent electrode, one on each side of the MEA. If H_2 gas is used as the fuel, it oxidized at the anode and release electrons and proton as following equation

$$H_2 \rightarrow 2H^+ + 2e^- \qquad [1]$$

The hydrogen reaction is an oxidation reaction because electrons are being liberated by the reaction. The generated protons are transported across the electrolyte membrane and react with oxygen to generate water

$$4H^+ + 4e^- + O_2 \rightarrow 2H_2O \quad [2]$$

The oxygen reaction that occurred in cathode is a reduction reaction because electrons are being consumed by this reaction. In particular, multiple elementary reaction pathways are possible at each electrode. hydrogen electrode and oxygen electrode can be either positive or negative. For a galvanic cell, the anode is the negative electrode and the cathode is the positive electrode.[1,6,13]

To commercialize successfully PEFCs, the cost must be economically reduced.[14-17] The approach to solve this problem is considered as simplification of reaction system, increasing durability and lifetime, improving cell performance, and decreasing the cost of the raw material. In all these issues, the most crucial point is to reduce the cost of the extremely expensive platinum catalysts. To solve this problem, several strategies have been efforted to enhance the activity of Pt-based catalysts through increasing effective surface area and/or intrinsic activity site.[10,17-20]

Another crucial point is the proton conducting polymer. Since the hydrogen gas has to transport through electrolyte membrane, the gas permeation, proton transport property

1.3 Nafion State

1.3.1 Perfluoirnated Sulfonic-acid (PFSA) ionomers

Perfluorinated sulfonic-acid ionomers are members of proton conducting materials famous for its significant high proton conductivity, thermal stability and mechanical stability. Nafion®, a registered trademark of proton conducting material, is the most widely used for various electrochemical devices. Dupont de Nemous was the first one in 1962 to develop this proton conducting material. Beside Nafion, PFSAs with short side-chain chemistries shown in Figure 2, have received conservable attention to

optimize chemical and phsical properties, such as Aquivion, Flemion and other improved PFSAs, such as Gore-SELECT, GORE-SELECT and GORE.[21-24]

As a kind of diblock copolymer, Nafion consist of semicrystalline polytetrafluoro-ethylene (-CF_2) backbone and a side-chain with a pendant sulfonic acid group, SO_3H shown in Figure 2.[25,26] The molecular weight of the Nafion is not easy to determine which is only can be considered it changing all the time. Normally, the equivalent weight (EW), defined as the grams of dry polymer per mole of sulfonate acid groups, was used to evaluate the relative number of sulfonate groups in Nafion molecule.[27]

In fact, proton conductivity, water content, hydrogen stability at high temperatures, mechanical/thermal and oxidative stability are important properties that must be controlled in the practical design of these membranes.[11,28-30] Since the Nafion /catalyst interface act as a chemical reaction field, it is crucial to further understanding the interface morphology and various phenomena occurred in this regime.[31]

1.3.2 Phase Separation

Different with monomer, one of the most unique feature of a diblock copolymer is the repulsion of sequences.[21] Normally, sequence tend to accumulate, but as they are chemically bonded, for which the segregation result in a phase separation only exhibit as crosslink of polymer chain. However, in the case of a completely incompatibility diblock copolymer system, phase separation occurs: nanodomains rich in A or in B are formed and vice versa.[21,32,33]

In case of the perfluorinated ion-exchange membrane, hydrophilic domains are described as cluster formed by hydrophilic function groups-sulfonate groups where the hydrophobic domains consist of the perfluorinated and polyaromatic backbone. It is well known that the hydrophilic/hydrophobic phase-separated morphology that support PFSAs considerably high ion transport capabilities. As Figure 3 shown, the difference in chemical structure of the covalently bonded pendant sulfonate group and CF_2 chains induce nature hydrophilic/hydrophobic phase separation and it will be enhanced by hydration. Under hydrated condition, PFSA membrane separates at nanoscales then

form a proton-conducting hydrophilic phase and a nonconductive hydrophobic phase with complex morphologies having mesoscale connectivity.

This phase separation phenomena of PFSAs have been studied extensively by using small angle X-ray scattering (SAXS), wide angle X-ray scattering (WAXS) and small angle neutrons scattering (SANS).[32,34-54] In the case of high humidity level, the generally accepted theoretical model is that a continuous water-rich cluster surrounded by partially crystallized perfluorinated matrix which acts as physical crosslinks preventing a complete dissolution. On the other hand, under comparatively dry condition, Nafion tends to form inverted-micelle with the polymer backbones on the outside and the sulfonate group lining water channel.

1.3.3 Nafion Model

Over the past two decades, on the basis of information gathered from SAXS and WAXS, various models of free-standing Nafion membrane have been proposed. Based on the changes in the Nafion ionomer peak position and intensity as a function of hydration has been studies by various groups.[45,47,55,56]

(a) Cluster-network model: such structural changes was firstly proposed by Hsu, who suggest that the coalescence of water-swollen clusters that would result in the increased spacing of periodic clusters as shown in Figure 4(a).[55,57]

(b) Parallel water channel model: The author Rohr assumed in their simulations that the ionomer peak increase due to thickness change was slightly larger than that of both lateral dimensions. Based on the simulation, the characteristic ionomer peak around 1-2 nm^{-1} result from long periodic hydrophilic cluster but otherwise randomly packed water channels surrounded by partially hydrophobic matrix, forming inverted-micelle cylinders shown in Figure 4(b). It is noticeable that Nafion with crystallites of 10 vol%, which form physical crosslinks that are significantly important for the mechanical properties of Nafion films, are elongated and parallel to the water channels.[2,58]

(c) Locally flat ribbon-like (ribbon) model: This model was created ideally to

demonstrate the ionomer peaked, around 1-2 nm^{-1}, in SAXS data and measured its domain spacing. Based on these results, parameters, such as the *d*-spacing, cluster size *et. al.* depend on humidity level can be estiamted.[27,47,59,60]

(d) Other models: For instance, the structure, at low hydration, correspond exhibit connected water-rich spherical hydrophilic domains embedded in hydrophobic polymer matrix. As the humidity increased, it tend to form a connected network, rod-like polymer shown in Figure 4(d).[41]

In early stages, a hydrophilic domain has been considered as a spherical cluster-network geometry, which was widely accepted in this area. However, recent studies and the current state of understanding requires a more general description on phase segregation but not a prescribed geometric shape as before. While, if we recognize the specific perspective by which a particular model was proposed, a number of valuable disparities between the different models may be reconciled. For instance, a rodlike model, which was widely accepted, has been refined to the structure that may have e possibility of cylinder aggregates. Furthermore, it may assemble locally at low humidity.[47]

The morphological information and demonstration for Nafion revealed the fact that a connected ionic cluster network through which polar solvents and ionic species permeate. It is still controversial to preset a certain morphology and geometry of PFSA ionomers. It can be said that the morphology of Nafion is complicated. The current model summarized in Figure 4 are the model of current research. The data analysis techniques utilized in these studies are providing a wealth of new morphological information which is can be related to other morphological and/or physical property research to give a total elucidation of the PFSA ionomer structure.

1.3.4 Thin Film and Interface

In practical PEFC catalyst layers, proton conducting ionomers are fabricated as layer with nanometers thick on the surface of catalyst particles, which is responsible for proton transport and gas and/or water transport to and from catalytic active sites.[11,18,61-

[67] As the thickness confined to nano levels, its properties significantly depend on ionomer thickness and ionomer/substrate interactions.[61,68-71] Now days, several effort has been conducted toward elucidation of PFSA thin film, which present distinctive property compared to free standing Nafion membrane due to confinement effects as the film thickness decreased to the domain size of the Nafion ionomer.[61,68,69,72-82] In this regime, several factor such as thickness, processing, substrate type and humidity are considered to have a great impact on film morphology.[68,69,77,82-84]

In thin film, ionomer/catalyst interactions and confinement are known to have a great impact on the phase separation of diblock-copolymers, Nafion.[82,85-87] Thus, self-assembly Nafion thin film exhibit anisotropy in domain orientation. As a result, confinement effects in Nafion films have attracted much attention mainly for two reasons:

(1) To understanding the surface morphology, properties of free-standing membranes, where the ionomer is considered to form a distinctive layer

(2) To further understand the morphology changes and behavior of ionomer films in practical PEFCs electrode[11,18,61,62,88,89]

Generally, Nafion thin film are fabricated by casting method a diluted Nafion dispersion onto a certain substrate, such as SiO_2, Au. In other words, the relationship between structure and property of PFSA thin-film is strongly influence by fabrication processing as well as ionomer/substrate interactions. To probe the thin film cast on substrate, techniques such as quartz-crystal microbalance (QCM) and ellipsometry are used for weight and thickness measurement, respectively. Recently, grazing-incidence small (GISAXS) / grazing-incidence wide angle X-ray scattering (GIWAXS) experiments and neutron reflectivity (NR) were developed for thin film morphological characterization. Since the investigation of transport property is difficult to conducted in thin film, most studies relay on swelling measurements, such as *in-situ* ellipsometry. These results are further supported by nanostructural characterization for anticipating ionomer thin-film proton transport behavior.

Recent research have revealed that when the film thickness topologically confined nanometers, significant deviations in its physical properties as well as morphological

changes occur compared to free standing Naifon membrane. Compared to free-standing membrane, Nafion films thin with thickness under 50 nm exhibit significantly decreased thickness swelling, water uptake,[31,68,69,73,74,76,78,81-84,90] decreased proton conductivity and increased activation energy,[67,75-77,84,91,92] lower water diffusion rate,[74,78,82,90,93,94] lower intrinsic permeation,[95]higher modulus,[96,97] and lower permeability.[62,89] These trends are pronounced to stronger as the film thickness decreased to under 30 nm.[31,69,73-75,80] Additionally, confinement effect and the interactions between substrate and ionomer affect the molecular ordering of the CF_2 chains, which as confirmed by Fourier-transform infrared spectroscopy,[98] neutron reflectometry,[74,98] and grazing incidence small angle X-ray scattering[31,69] results, where alignment of CF_2 chains and water domain brought in comparatively lower water uptake[72,76,82,83] and transport processes.[72,76,82,83] The above phenomenon observed in thin film can be explained by (1) the decreased swelling; (2) anisotropic orientation (3) a less phase separated structure.

It is considered that the thin film is available to use as model system to investigate and mimic catalyst/Nafion interface.[11,18,61] A good performance ionomer must have two points (1) high oxygen permeability (2) high proton conductivity. While in case of thin film, the decreased property of oxygen permeability and conductivity is mainly determined by the confinement effect, is also strongly influenced by the ionomer/catalyst interaction, with chemical affinity (specific adsorption) between sulfonate group and Pt substrate. Therefore, elucidating the influence of ionomer on transport mechanism under confinement effect and ionomer/substrate interactions is still a challenging theme. Additionally, the impact of morphological changes on proton transport is strongly dependent on the transport direction in which the conductivity is probed along in-plane and out-of-plane direction. For instance, a DPD model of Nafion thin film with thickness of 5-10 nm on carbon substrate elucidated anisotropic diffusion; higher along the in-plane direction, while lower in out-of-plane direction.[99] Considering the electrostatic interactions arising from ionic groups, which is responsive to humidity level, wetting interactions, a high level of complexity in structure is observed in Nafion thin film. As an energy conversion system, additional studies such like operando

measurements need to be conducted to reveal the potential impact on morphology and properties of intrest.

1.4 Nanomorphology Features

1.4.1 Small/Wide Angle X-ray Scattering (SAXS/WAXS)

Small/Wide angle X-ray scattering (SAXS/WAXS) is a technique by which nanoscale density differences in a sample can be quantified. Figure 5(a) shows the simplified schematic of a SAXS/WAXS measurement. The scattered radiation is measured in transmission mode within an angular angle. The intensity is recorded as a function of the q, scattering wave vector, which characterize the distance in Fourier space.

Over the past decades, several morphological results obtained by a varieties of scattering and/or diffraction analysis method of PFSA ionomer has been released t to give a reasonable elucidation of PFSA ionomers in term of the nanostructure organization under a variety of environmental condition or physical states.

In Figure 5(b), we summarized the useful information can be extracted from scattering profile are list below:

(1) A widen peak, around 0.2 nm^{-1}<q<1 nm^{-1}, corresponding to the intercrystalline spacing between the crystalline domains of the polymer matrix, generally called matrix knee.

(2) The single peak, around q=1-2 nm^{-1}, corresponding to a structural correlation length for hydrophilic domains formed by aggregation of sulfonate groups and interpreted as the spacing between hydrophilic domains on the order of nanometers.

(3) The amorphous and crystalline WAXS peaks appear at q=12.4, can be interpreted to the inter spacing of the fluorocarbon (-CF_2-) chains and the peak around 26 nm^{-1} are illustrated as the intracrystalline spacing of the fluorocarbon (-CF_2-) chains in the crystalline structure,

SAXS/WAXS analysis is difficult due to the backgournd that scattering method only

provide data in inverted space. The conversion of raw data to real space in three-dimensional space is necessary. Additionally, due to the fact that the relative random hydrophilic/hydrophobic phase separation, peaks (ionomer peak, amorphous/crystalline peak) has amorphous-like widen peak. As a result, the quantitative interpretation of the scattering results is controversial. Therefore, the researchers are required to compare the experimentally obtained scattered profiles with that predicted by conceptive models assumed for the structure. While, the SAXS/XRD patterns of these polymers generally obtained extremely limited information. Mot research groups have focus on elucidating the influence of swelling, post-treatment on the scattering profiles for comparison and validation of conceptive model as mentioned above. Moreover, recent studies of the morphological continuum from the dry condition through the hydrated condition, have accumulated valuable questions about the organization of hydrophilic and hydrophobic domains and so on of the morphology of PFSA.

Recalling the previous search used SAXS,[32,34,35,44,45,47,48,56] these distinctive models have each certain hypothesis result in significantly difference in quantitative and/or qualitative detail. Finally, some of these results have weathered the test time but still remain the focus of debate. The perspective continuesly focus continues on fundamental elucidation of the structure nature of the hydrophilic (ionic) domains, especially the cluster size, shape, and spatial distributions. Although the ionic hydrophilic cluster are known as a result from the hydrophilic/hydrophobic phase separation between polar and nonpolar constituents of the diblock copolymer, Nafion, the concept or the illustration of dispersed ionic clusters or contiguous hydrophilic ionic domains rely on the perspective of the method used to probe.

1.4.2 Grazing Incidence Small/Wide Angle X-ray Scattering (GISAXS/GIWAXS)

The GISAXS technique was originally introduced by Jonna and his coworkers, but it has come to be a widely accepted method for the study of nanostructured thin film only in the past 10years.[100,101] It is a technique that combines features from SAXS and

diffuse X-ray reflectivity.[102] One of the key point that distinguishes the GISAXS from the transmission method is the reflection scattering wave, which its intensity has almost the same amplitude as that of the incident beam. Scattering from the reflected beam is called multiple scattering since it is scattered at least two times.[103] In case of the GISAXS, there are multiple scattering wave in addition to the interferences between the scattered radiation the reflected beam and the incident beams. As a result, kinematic scattering theory makes an assumption that no multiple scattering is no longer be taken into consideration unless the reflectivity is negligible.[104] Although the full dynamic scattering theory should be taken into account for the grazing-incidence measurement, a relatively simpler principle distorted-wave Born approximation (DWBA), has been gradually accepted, for the reason that the former does not limit how many times the incident photon is scattered, while the latter assumes that it undergoes a maximum of a reflection events and a scattering events by a nanostructure object. In briefly, GISAXS is a powerful tool for charactering nanoscale structure, orientation, the morphological information like the shape and/or size of nanoscopic object at surface or bulky part for thin films.

In order to extract useful information from incidence x-ray scattering pattern, a specific grazing incidence angle (α_i), must be strictly selected between the critical angle of the substrate ($\alpha_{c,s}$) and the critical angles of the film material ($\alpha_{c,f}$). In briefly, it could be expressed as the following relationship: $\alpha_{c,f} < \alpha_{c,f} < \alpha_{c,s}$. In practice, the actual choice of α_i depends on the object to be studied. To obtain high quality data, largest scattering cross sections are need to be achieved, which require the incident angle must set to the value as close to the critical angle of objective film. However, in case of this, multiple scattering effects needs to be considered to properly model the results. If the incident angle is more or less above the critical angle of the substrate, dynamic scattering effect will be much reduced.

Different with SAXS, the samples used for GISAXS measurement can be cast on various substrate to mimic the reaction field of practical PEFCs. By now, GISAXS is still a new tool to investigate the morphology of the Nafion thin film. Up to now, only less than 10 papers about Nafion thin film have been published, including wetting

interaction[83], substrate influence[69], confinement effect[77], EW of PFSA ionomer[31], atmosphere impact[105]. All these investigations give a fundamental insight of morphology of Nafion thin film with thickness under 300 nm. In briefly, the phenomenon discussed above are related to hydrophilic/hydrophobic phase separation, substrate/ionomer interaction *et.al* and consequently affect the proton transport property.

1.4.3 Direct imaging of AFM and SEM

Accurate visualization technique is need to clarify morphology, although it is still a challenge due to sample processing method, radiation damage *et al*.[106,107] By using TEM, a phase-separated nanostructure consist of circular domains with thickness under 10 nm has been visualized in lower humidity level.[108-110] Recently, Allen *et al*. revealed that the hree dimensional nanoscale image of PFSA thin film as shown in Figure 7(a) by suing cryo-TEM tomography.[106] The direct evidence of the three dimensional structure and demonstrate some of the previously conceptive model proposed by using SAXS/SANS, in practical, the l elongated cylinders are interconnected via sub-domains with various size. It should be noticed that this directly obtained structure was measured under 100%RH humidity level. For the cases under low humidity level, like the spherical domains with weaker connections, it is also expected to be validate. Additionally, after the calculation of Fourier transform of images, one can yielded a scattering peak result from ionic domain, around $q \approx 1\ nm^{-1}$, which is comparable to the experimental observation.

1.5 Proton Transport Properties and Mechanism

1.5.1 Transport Phenomena

The transport of proton in PFSA is dependent on humidity level as well as the circumstance of water, where the sulfonate site and water interact. In addition to that, the segmental motions of the polymer chains also have impact on proton transport,

which is temperature sensitive. Therefore, the proton transport consist of multiple sub-process, (1) firstly, the dissociation of the proton from sulfonate groups (2) secondly, the formation of an ion-pair with water and sulfonate group at the molecular scale, (3) thirdly, water-mediated transport through the hydrophilic ionic domains at the nanoscale (4) long-range mobility within the connected cluster network at the mesoscale. In general, proton conduction in PFSA is directly correlated to water behavior, humidity level at multiple length from molecular to meso scale and time scales, wherein the relationship between conductivity and water diffusivity is possible to be developed.

Over the last decades, although the proton conductivity of PFSA ionomers was extensively investigated over 200 papers, the impact of possible interfacial resistance on impedance results is still under debate due to fact that the measurement techniques and decoupling with contact resistance.[111-114]

1.5.2 Proton Conductivity of Nafion membrane and thin film

The conventional method to obtain proton conductivity are electrochemical impedance, dielectric spectroscopy and for some cases it can be determined from self-diffusion. If structural diffusion/hopping mechanism exist, the obtained value is vehicular conductivity and fails to represent conductivity.[25] Previous studies on conductivity of Nafion membrane are normally considering these parameters hydration,[115] thickness,[116,117] interfacial resistance,[111,113,114] pretreatment,[118-122] annealing.[118,119,123-127]

As the proton conductivity in Nafion membrane does not exhibit a totally random, it is considered that the proton conductivity is not entirely isotropic. Therefore, the anisotropic behavior of proton conductivity of PFSA membranes has been widely studied by measuring conductivity along in-plane and out-of-plane direction. The gap between in conductivity along in-plane and out-of-plane were discussed by Cooper and his cowokers,[112,113] who released that the conductivity ratio of is 1.00±0.07 if the out-of-plane conductivity is corrected. The similar observation was confirmed by Jiang *et*

al.[111] and Thompson *et al*.,[128]

Regarding the conductivity values, the most of the previous research about conductivity is focus on Nafion 1100 EW. One thing has to noticed that pre-treatment induced the changes in conductivity as well as the water-uptake capacity, in which annealing treatment tends to reduce a membrane's water uptake, proton conductivity, and whereas these can be increased by preboiling.[120,129] [115,122,125] Additionally, a common tendency in PFSA membrane studies is that the proton conductivity is increased with decreasing EW, which is considered that decreased EW induce an increase in ion-exchange capacity and charge carriers per sulfonate site.[130] On the other hand, the *d*-spacing of ionomer peak is smaller for lower EW ionomers under a certain humidity level, which indicate a more well-defined distribution of sulfonate-acid groups and shorten proton conducting pathway tortuosity, consequently enhanced proton conductivity.[131,132] Thus, the increased EW is considered to reduce the fractional proton concentration thus further influence on the proton conductivity. While this suggest that EW influence proton conductivity through water-uptake, this should not get rid of additional role of chemical.

In case of the Nafion thin film, as the other transport properties, the conductivity of Nafion membrane/thin film increase with hydration and temperature shown in Figure 8. Compared to the freestanding Nafion membrane, the conductivity of recast Nafion thin film showed comparatively lower value, which is considered to the confinement effect and/or substrate/ionomer interaction.[69] As for the recast thin film, thickness can be exactly controlled. All previous research proposed that the proton conductivity showed not only humidity dependence, but also thickness dependence.[66,75,92,133,134]

1.5.3 Conduction Mechanism

Although there are variety of proton conductive materials can be used as separator, the inherent proton are only solvated by only limited types of solvent. These are essentially water, oxyacid anions or oxyacid, heterocycles, or oxide ions. Some of these species take part in the formation of proto and the its transport process. The conduction

mechanism will be demonstrated in following two parts.

(1) In homogeneous media, the usually high mobility of protons in aqueous solutions has been investigated since last decades. The essential features of the present can be refer to the previous work conducted by Eigen *et.al.*[135,136] They firstly illustrate that "structure diffusion", where the excess proton is "tunneling" back and forth, is the rate-determining step. There is controversial point that whether the region containing the excess proton, which can be considered as a hydrated ion. [137]

(2) Most of the fuel cells, operated at comparatively low temperature, depend on the properties of heterogeneous separator materials.

1.6 Thermal History

1.6.1 Thermal Induced Mechanical Transitions

Dynamic mechanical analysis is a technique sensitive to the stress, which is response under an applied sinusoidal strain wave across a wide range of temperature and frequency. This technique provides the information of molecular origins of the transition temperatures, in other words, such as the glass transition temperature is also been revealed by this method.

Nafion membrane present three thermal transitions temperature: α, β, γ, which is corresponded to distinct 3 relaxation mechanism as shown in Figure 10.

(1) α transition: T_α, around -90 to 120°C, can be assigned to the onset of long-range mobility of the chains surrounding the ionic cluster.

(2) β transition: T_β is also called the glass transition (-40 to 20°C) of the PFSA matrix, which is assigned to the onset of segmental main-chain motion.

(3) γ transition: T_γ, around -120 to -90°C, is assigned to the local motions of the polytetrafluoroethylene backbone.[127,131,138-142]

Here, compared to T_γ, T_α and T_β are more depend on humidity level, EW, side-chain chemistry and cation-form of the Nafion ionomer.[139,143,144] The T_β is known as the segmental main-chain motion, while the T_α is mainly controlled by the times that an ion pair before hopping to neighbouring site.

Regarding T_α, increasing humidity level, is linked to decreased T_α because the water molecule can act as plasticizer, which is responsible for enhance the mobility of hydrophilic cluster thus reduce the onset of ion-hopping.[142,145-147] Change in with other alkaline cation will induce T_α to higher temperature side. Because their comparatively strong electronic interactions, which is considered to stabilizes the electrostatic network, will stiffening the ionomer thus restrict its chain mobility.[145,148,149] One thing has to be noticed that the ion-hopping transition, illustrated as the ionic cluster transition, also named as α transition, is different with the conventional T_g.[139,144,150]

As well as shift in Tα, T_β also shifts to lower temperatures by introducing larger counterions, which demonstrate that main-chain motions and electrostatic crosslink are coupled through the side-chains.[139,143,144,150]

1.6.2 Temperature Effects and Activation Energy

It is well known that the temperature has a positive impact on proton transport., including water diffusion/self-diffusion and proton conductivity. The temperature dependence for a PFSA membrane property of proton conductivity, diffusion *et.al*., can be represented by Arrhenius equation:

$$\Psi\left(=D, D_\mu, \kappa\right) \propto \exp\left(-\frac{E_{a,\Psi}}{RT}\right) \qquad [3]$$

Up to now, several processes related to activation energy of Nafion ionomers are extensively investigated. The difficult point is that the assignment of single value of the energy of a given process. Previous investigation of E_a for a certain process are list in Table 1.

For instance, the slopes represent the activation energy of Arrhenius plot in term of temperature and proton conductivity are Figure 11. Generally, the E_a shows decreasing tendency with humidity level because the motion of water, proton, and polymer chains are restricted. On the other hand, the effect of hydration on thermal activation is the stronger for proton conductivity than the activation energy for self-diffusion of water. In practical, the proton transport phenomenon a is complex process, mainly including

3 process: (1) water-mediated transport (2) proton hopping and (3) segmental motions of chains, these three processes strongly influence on the thermally activated kinetics that dependent on humidity.

The temperature dependence of proton conductivity for Nafion thin film/membrane was systematically investigated and reported by Giffin *et al*, who proposed that the conductivity-temperature follows Arrhenius relationship and the determining mechanism can be considered as hopping. However, in the case of high temperature (>120ºC), conductivity of hydrated Nafion exhibit Vogel-Tamman-Fulcher (VTF) relationship, which indicate that segmental motion of the polymer chains with long range as well as their viscosity were also considered to have a impact on transport process, and consequently influence mediating proton exchange.[131] The VTF relationship can be expressed as following

$$\Psi\left(=D_{\mu},\kappa\right)\propto\exp\left(-\frac{E_a'}{R}\frac{1}{T-T_0}\right) \qquad [4]$$

Here, E_a' represent the activation energy, T_0 exhibit the thermodynamic ideal glass temperature (free volume almost equal to zero).[131] Additionally, E_a' can be used to describe the probability of a large increase in free volume formation.

1.7 Outline of the Present Thesis

In this manuscript, the present thesis consists five chapters, demonstrating the nanostructure-property relationship of high performance proton transport Nafion thin film to further understanding catalyst/ionomer interface phenomena and give a design policy for high oxygen reduction reaction electrode.

In chapter 1, polymer electrolyte fuel cells and the fundamental insight of perfluorinated sulfonic-acid ionomers, especially the interfacial phenomenon occurred in Nafion thin film was introduced in detail.

In chapter 2, The morphology changes of Nafion thin films with thicknesses from 10–200 nm on Pt substrate with various annealing histories (unannealed to 240ºC) were systematically investigated using grazing incidence small angle X-ray scattering

(GISAXS) and grazing incidence wide angle X-ray scattering (GIWAXS). The results revealed that the hydrophilic ionic domain and hydrophobic backbone in Nafion thin films changed significantly when the annealing treatment exceeded the cluster transition temperature, which decreased proton conductivity, due to the constrained hydrophilic/hydrophobic phase separation, and increased crystalline-rich domain. This research contributed to the understanding of ionomer thermal stability in the catalysts layer, which is subjected to thermal annealing during the hot-pressing process significantly changed under dry condition while shown no significant difference in wet.

In chapter 3, The electrochemical reactions occur on the carbon-supported platinum covered by a proton conducting polymer electrolyte. Thus, it is important to clarify the correlation between proton conductivity and morphology of the polymer electrolyte on Pt or carbon. In this study, the properties of thin films (50–200 nm) of Nafion, which is the typical polymer electrolyte, were investigated on platinum and carbon substrates. Grazing-incidence small/wide angle X-ray scattering and electrochemical impedance spectroscopy were used to extract morphological and proton transport information. Self-designed interdigitated array electrodes were utilized to test and compare the proton conductivity on the Pt and carbon substrates. Based on the results, the difference in anisotropic behavior of Nafion thin films on each substrate were explored, which exhibit that the proton conductivity of Pt-supported Nafion thin films has more well defined hydrophilic domain structure than that of carbon supported thin films along in-plane direction and while it showed the opposite trend in the out-of-plane direction. These datasets and analyses represented a thorough study of the behavior of Nafion thin films on model substrates of interest, i.e., Pt catalyst/carbon electrodes. These results are expected to further understanding the difference in term of proton transport pathway.

In chapter 4, The dispersion of perfluorinated sulfonic acid ionomers in catalyst inks is an important factor controlling the performance of catalyst layers in membrane electrode assemblies of polymer electrolyte fuel cells. The effect of water/alcohol compositions on morphological properties and proton transport were investigated by grazing incidence small angle X-ray scattering, grazing incidence wide angle X-ray scattering, and electrochemical impedance spectroscopy. The thin films cast by high

water/alcohol ratio Nafion dispersion has high proton conductivity and well-defined hydrophilic/hydrophobic phase separation, which indicates that proton conductivity and morphology of Nafion thin films are strongly influenced by the state of dispersion. This finding will help to further understanding of the morphologic and proton transport property of Nafion thin films with different water/alcohol ratio, which has implications for the performance on Pt/Nafion interface.

In chapter 5, Thin perfluorosulfonated ion-conducting polymer, Nafoin®, in energy-conversion devices have limitations in functionality attributed to confinement-driven and substrate/polymer interactions. In this study, we performed grazing incidence small X-ray scattering (GISAXS), grazing incidence wide angle X-ray scattering (GIWAXS) and electrochemical impedance spectroscopy (EIS) to investigate the function of water, the plasticization effect, in 50 and 200 nm-thick Nafion thin film with under a wide temperature range from 25oC to 120oC. The changes in order-disorder transition is an indicator for sulfonate groups relaxation with implication on proton transporting property, which is confirmed by EIS as well. Compared to the thin films under dry condition, water molecule act as plasticizer which improve the mobility of ionic domains and hydrophobic domains as temperature increased. Such observation is less pronounced in thinner Nafion thin films due to the relative strong ionomer/substrate interaction.

In chapter 6, based on our results shown in chapter 2-5, we summarized conclusion and prospect for the future polymer electrolyte fuel cells.

Table 1 Previous research method of Nafion thin film

Method	Thickness	Compared with membrane
NR voltammetry	60 nm	Substrate impact
QCM	20-80 nm	Lower diffusion coefficient
EIS	14-1121 nm	Decreased conductivity
AFM	230 nm	Higher modulus
GISAXS	4-160 nm	Lower phase separation
Ellipsometry	17-1000 nm	Lower water content

Table 2 The activation energy for various process measured for PFSA listed based on the measurement type

property/process	term	Range [kJ/mol]	Form
proton conductivity	κ	9-22	Membrane
proton conductivity	κ	20-115	Thin film
self-diffusion (PSGE-NMR)	D'	11-23	Membrane
self-diffusion (MD simulation)	D'	11-20	Membrane
permeation and diffusion	k	15-30	Membrane
sorption and diffusion	D_d	20-31	Membrane
gas permeation	P	15-49	Membrane
DMA, mechanical properties	E	10-12	Membrane
relation time	τ	40-60	Membrane

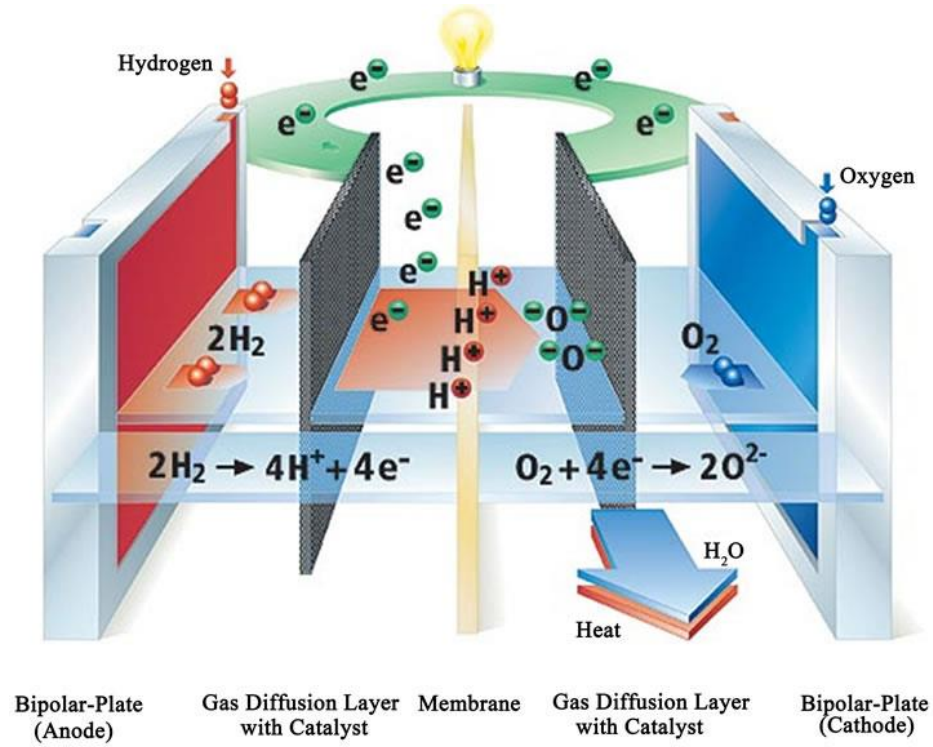

Figure 1 The schematic image of basic parts of PEFC in automotive application.

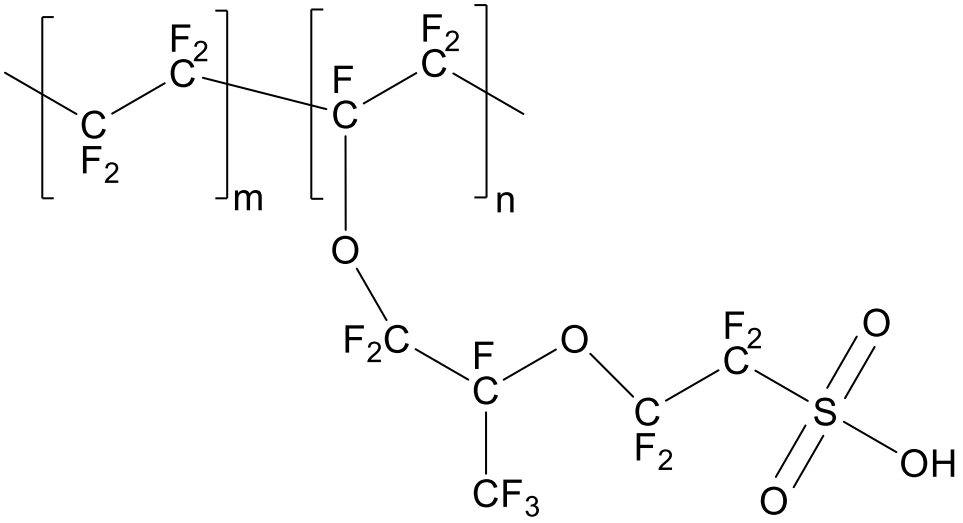

Figure 2 The chemical structure of typical PFSA ionomers used in PEFCs.

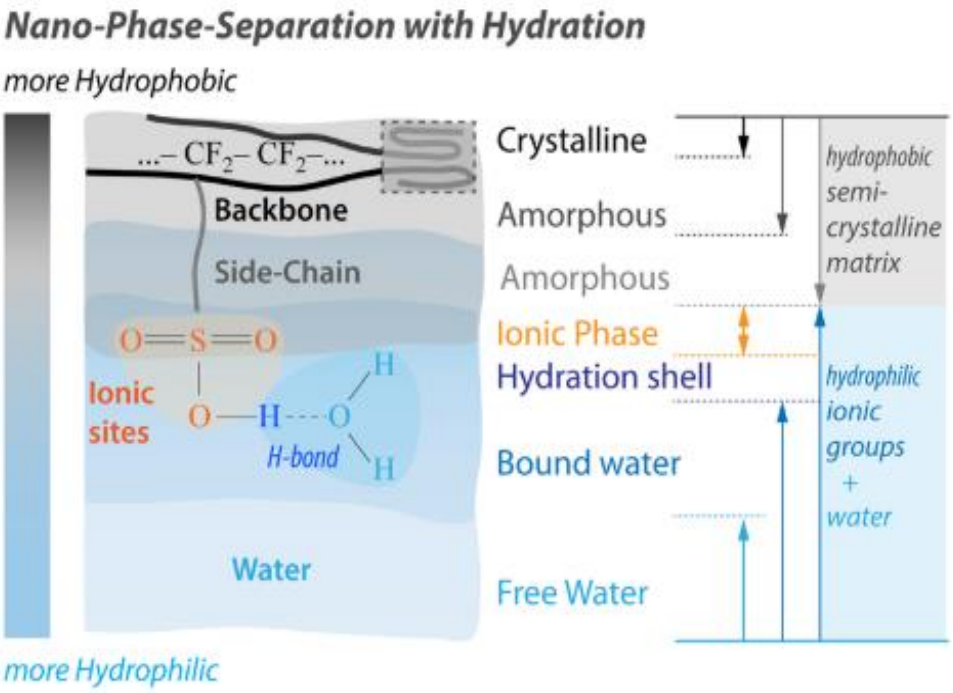

Figure 3 The nanoscale of Nafion structure under hydrated condition and the key parameters governing their phase-separated morphology and properties.

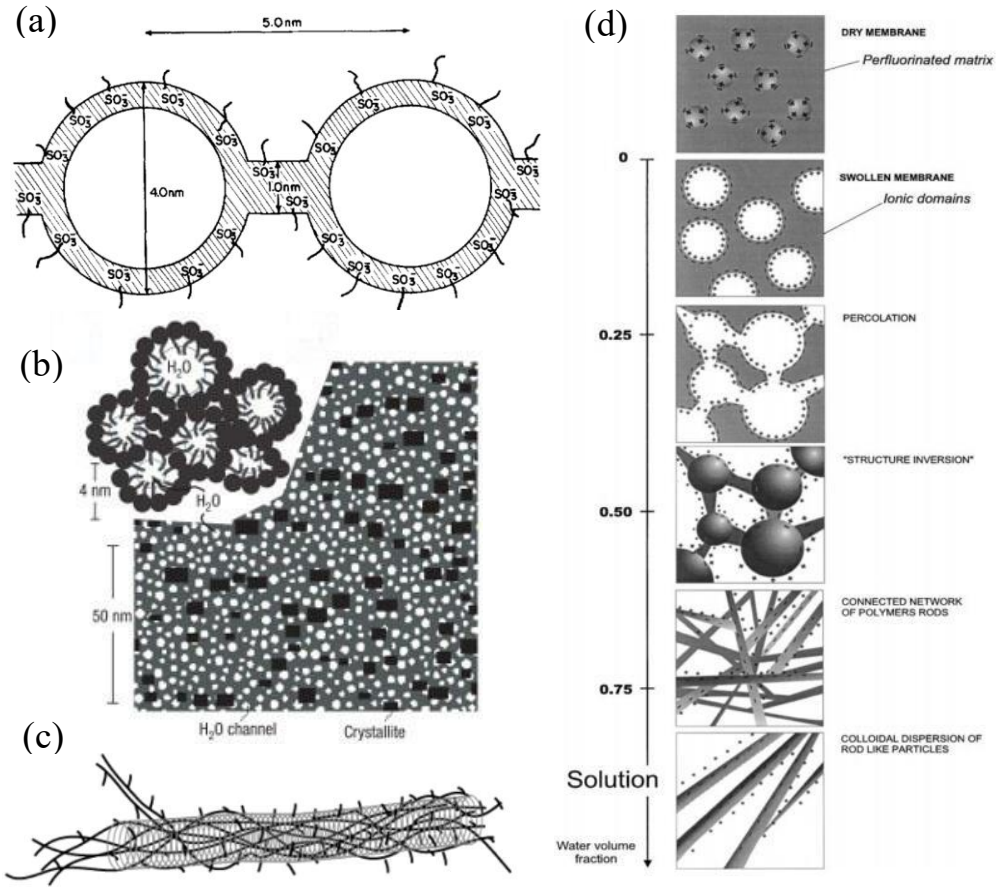

Figure 4 Proposed conceptive modeling of Nafion : (a) cluster-network model (b) parallel water channel model in hydrated membrane by simulation (c) locally flat ribbon-like model discussed by Kreuer (d) evolution morphology from spherical domains to rod-like aggregate in dispersion.

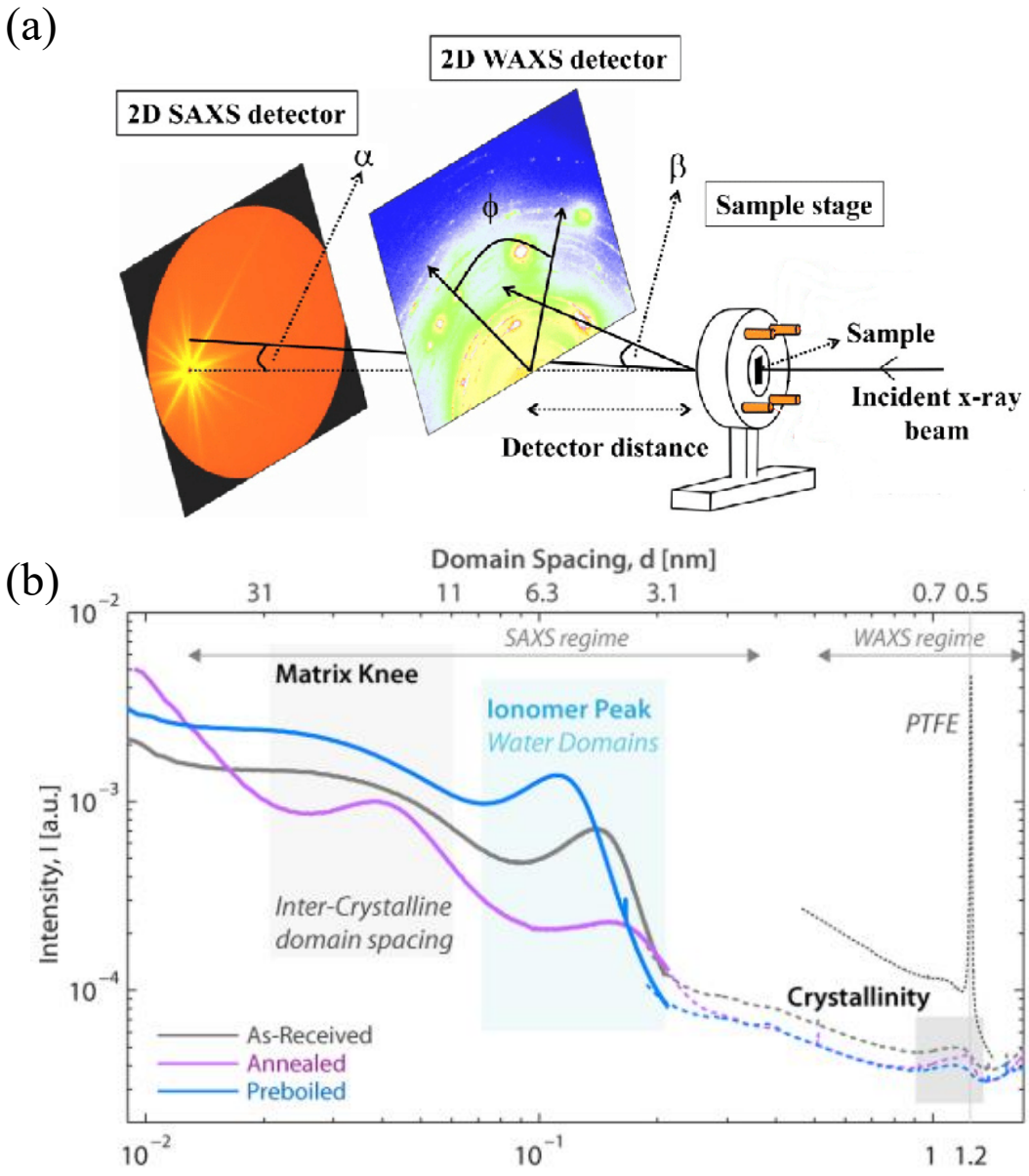

Figure 5. (a) Simplified schematic of a SAXS/WAXS measuremen. (b) Characteristic peaks and their values are shown in the plot along with SAXS/WAXS peaks.

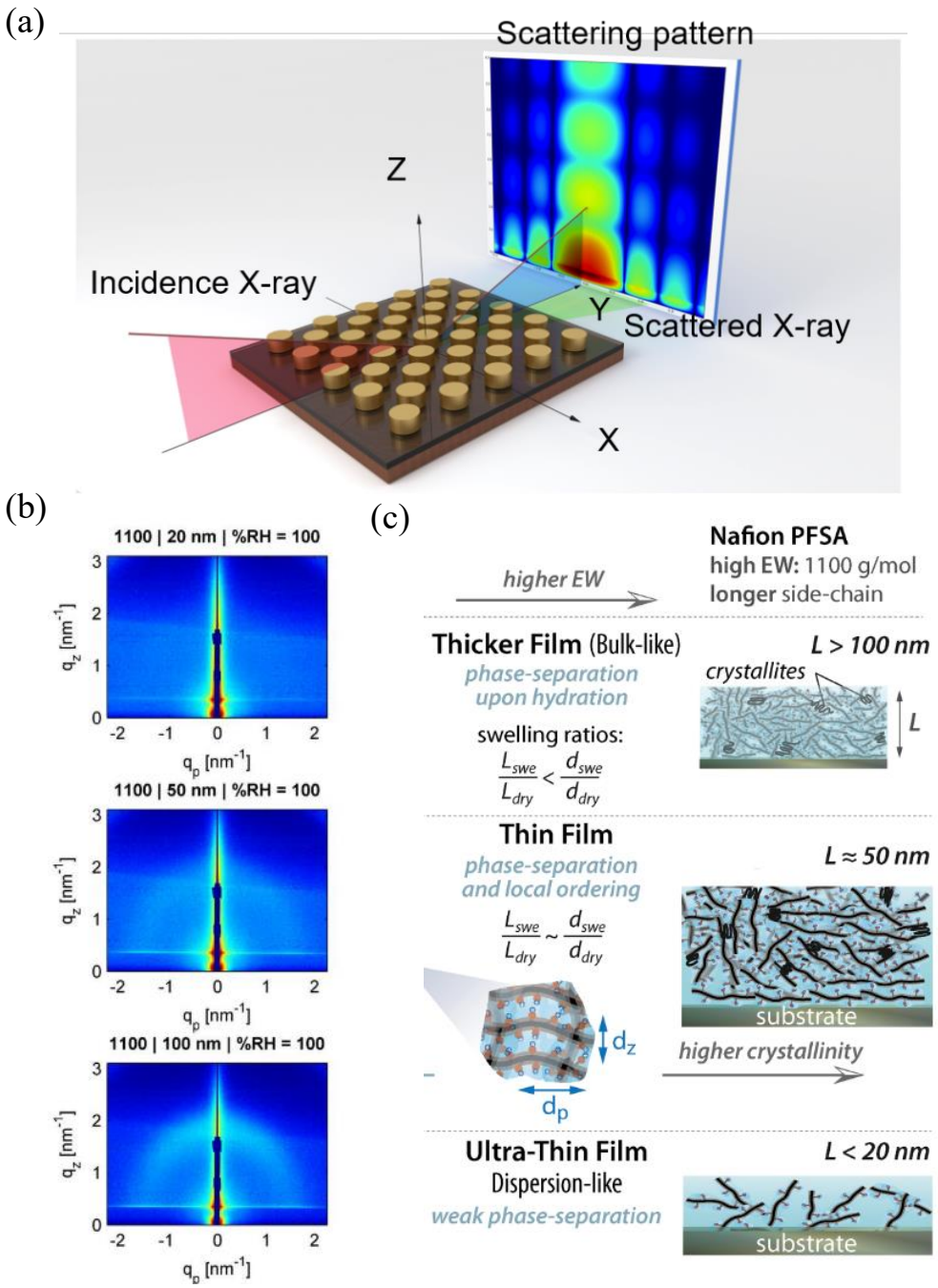

Figure 6 (a) Schematic image of GISAXS measurement (b) GISAXS pattern of Nafion thin film with various thickness under 100%RH 298K. (c) The structure--swelling relationship change in case of Nafion thin film.

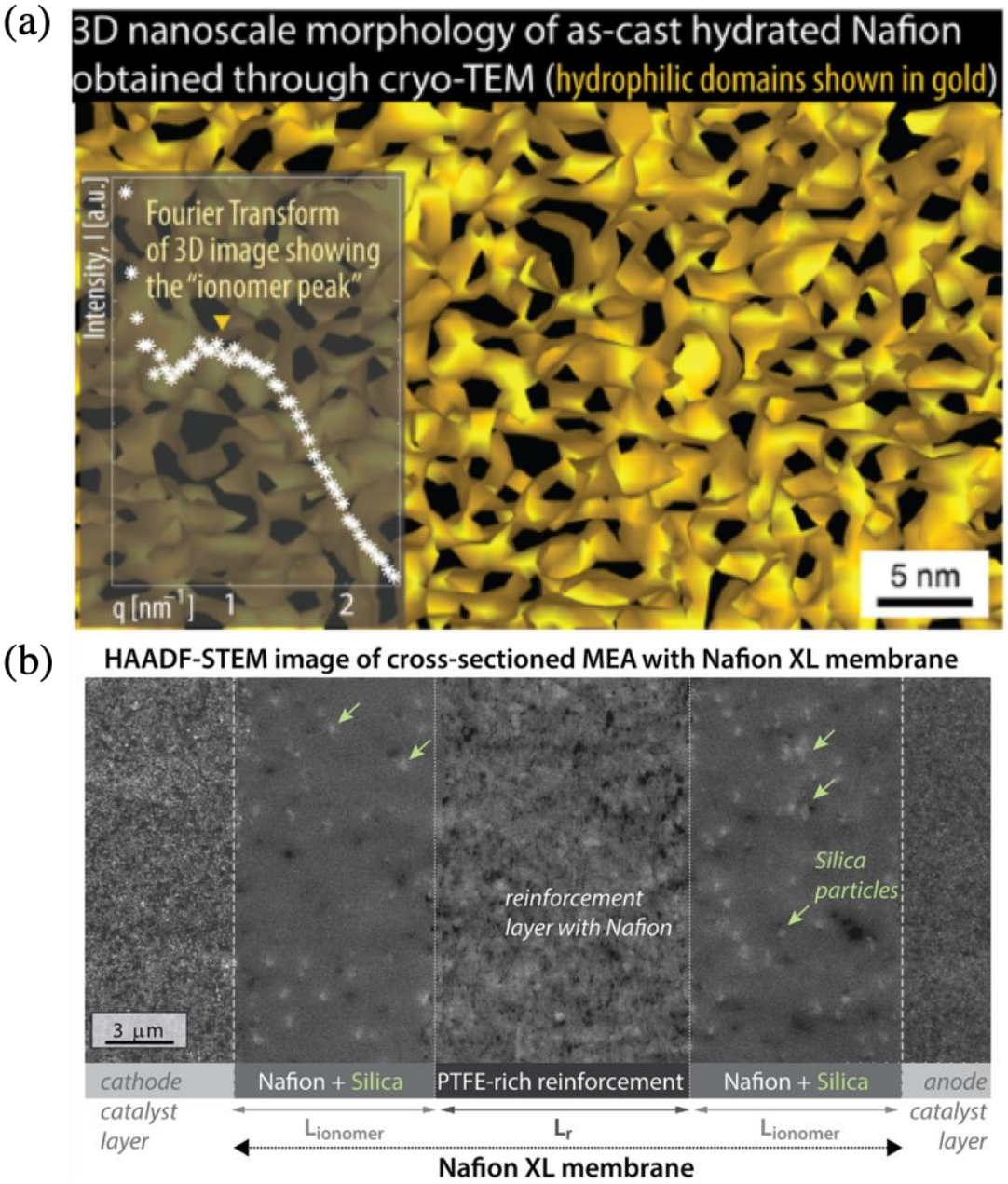

Figure 7 (a) 3D Nanostructure of hydrated Nafion film obtained through cryo-TEM tomography (b) STEM image of baseline Nafion XL membrane showing the reinforcement layer and additives.

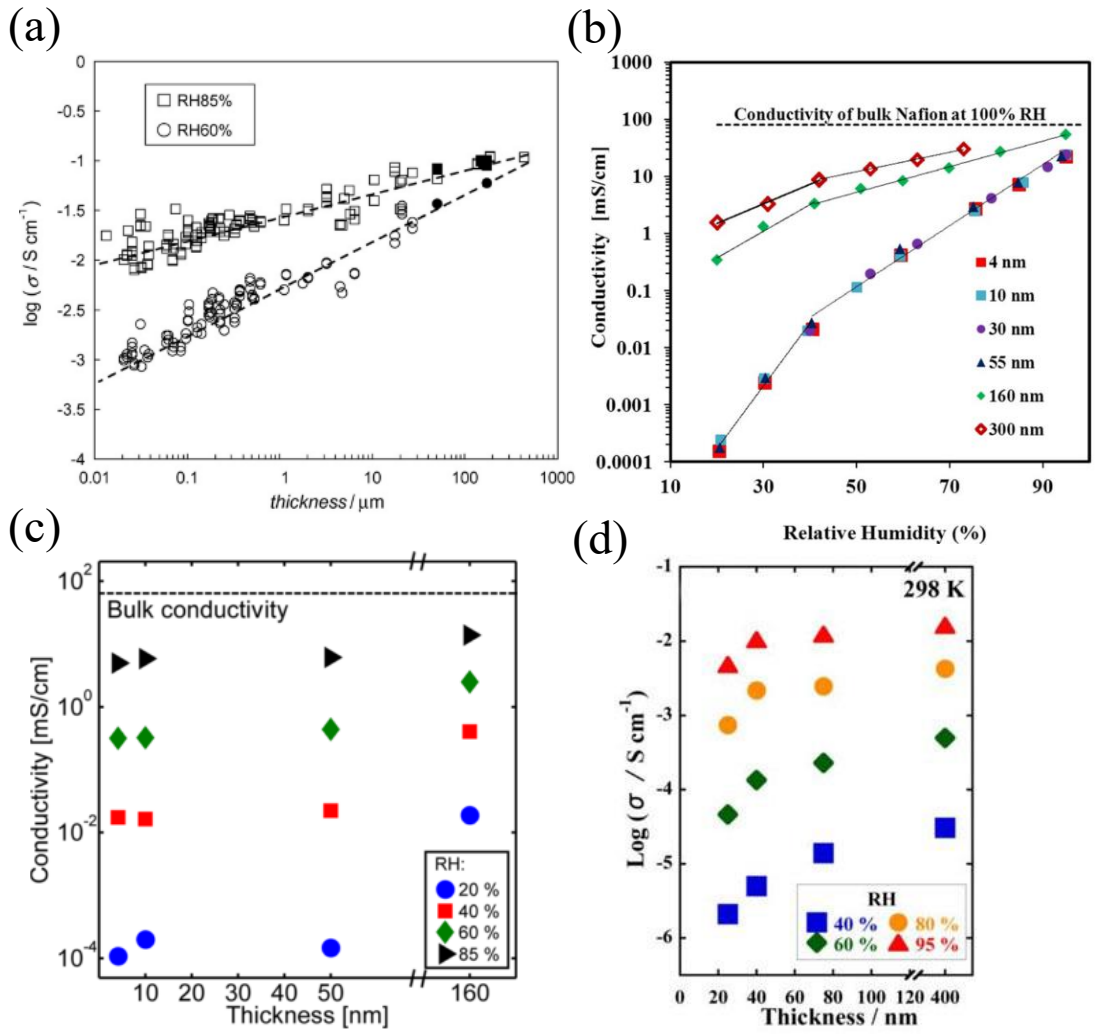

Figure 8 Previous investigation of proton conductivity of Nafion thin film (a) dependence of the conductivity of recast Nafion thin film on the thickness under 80ºC and 60ºC. Solid marks show bulk Nafion 117 membrane. The proton conductivity of Nafio thin film with various thickness ranging from (b) 4-300 nm, (c) 4-160 nm, (d) 20-400 nm, at 25ºC as a function of relative humidity. The dot line shown in (b) and (c) exhibit the bulk Nafion 117 membrane under 100%RH.

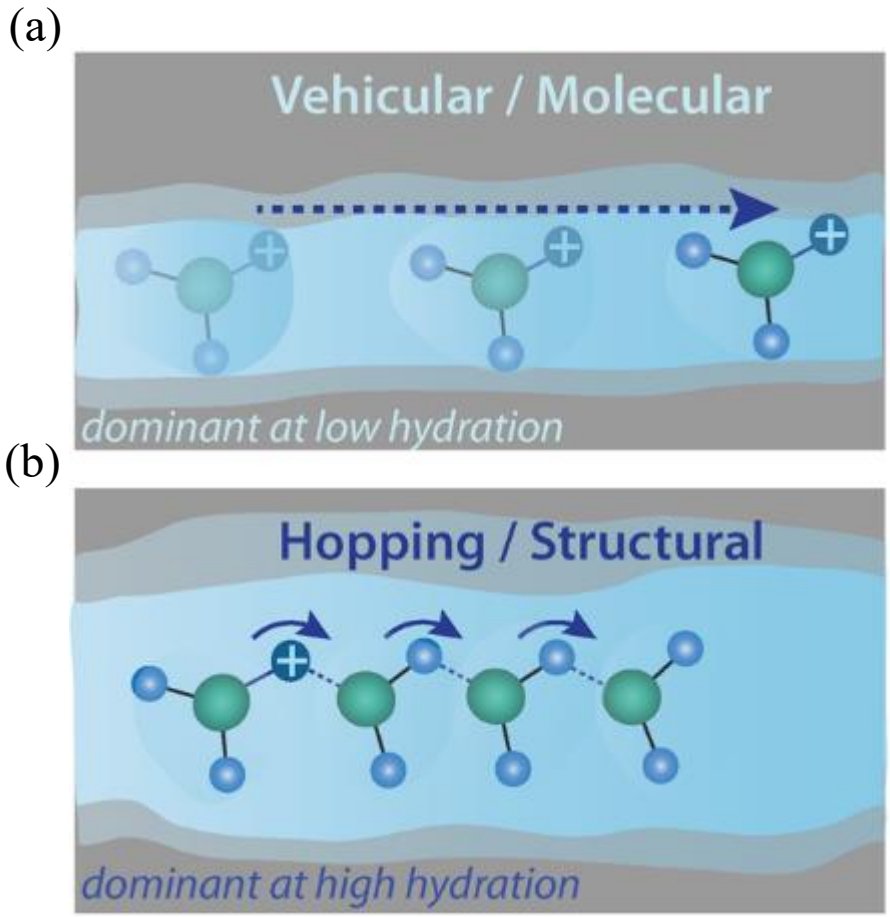

Figure 9 The proton conduction mechanism under (a) lower hydrated and (b) high hydrated condition.

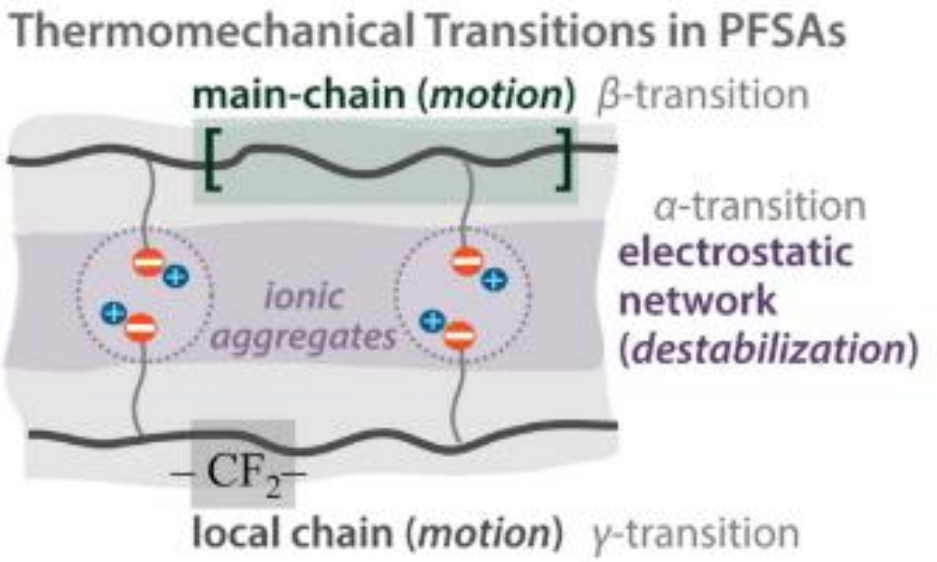

Figure 10 Typical temperature scan profiles from DMA showing the storage modulus and tan(δ)for Nafion and an illustration of thermomechanical transitions associated with PFSA morphology.

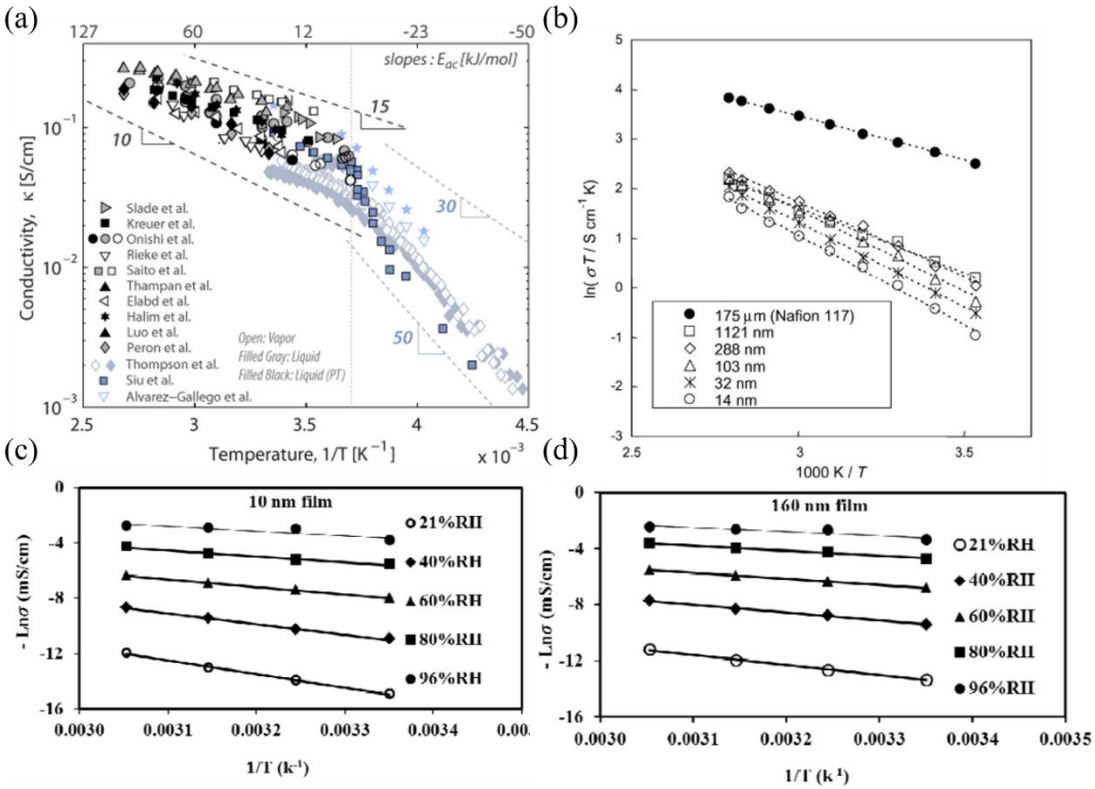

Figure 11 The Arrhenius plot of (a) Nafion membrane and (b) Nafion thin film with various thicknesses and humidity level.

Reference

(1) Goodstein, D.; Intriligator, M. *Climate Change and the Energy Problem: Physical Science and Economics Perspective Second Edition*, 2017.

(2) Stein, R. S.; Powers, J. *The Energy Problem*; World Scientific, 2011.

(3) Lin, D.; Liu, Y.; Cui, Y. Reviving the lithium metal anode for high-energy batteries. *Nat. Nanotechnol* **2017,** *12*, 194.

(4) Hacker, V.; Mitsushima, S. *Fuel Cells and Hydrogen: From Fundamentals to Applied Research*; Elsevier Science, 2018.

(5) Sammes, N. *Fuel Cell Technology: Reaching Towards Commercialization*; Springer London, 2006.

(6) Srinivasan, S. *Fuel Cells: From Fundamentals to Applications*; Springer US, 2006.

(7) Zhang, J. *PEM Fuel Cell Electrocatalysts and Catalyst Layers: Fundamentals and Applications*; Springer London, 2008.

(8) Santos, E.; Schmickler, W. *Catalysis in Electrochemistry: From Fundamental Aspects to Strategies for Fuel Cell Development*; Wiley, 2011.

(9) Zhang, J.; Wu, J.; Zhang, H. *PEM Fuel Cell Testing and Diagnosis*; Elsevier Science, 2013.

(10) Stamenkovic, V. R.; Mun, B. S.; Arenz, M.; Mayrhofer, K. J.; Lucas, C. A.; Wang, G.; Ross, P. N.; Markovic, N. M. Trends in electrocatalysis on extended and nanoscale Pt-bimetallic alloy surfaces. *Nat. Mater* **2007,** *6* (3), 241.

(11) Holdcroft, S. Fuel Cell Catalyst Layers: A Polymer Science Perspective. *Chem. Mater* **2014,** *26* (1), 381.

(12) Schmuki, P.; Virtanen, S. *Electrochemistry at the Nanoscale*; Springer New York, 2014.

(13) O'Hayre, R.; Cha, S. W.; Prinz, F. B.; Colella, W. *Fuel Cell Fundamentals*; Wiley, 2016.

(14) Greszler, T. A.; Caulk, D.; Sinha, P. The Impact of Platinum Loading on Oxygen

Transport Resistance. *J. Electrochem. Soc.* **2012,** *159* (12), F831.

(15) Hammer, B.; Nørskov, J. K. Electronic factors determining the reactivity of metal surfaces. *Surf. Sci.* **1995,** *343* (3), 211.

(16) Katsounaros, I.; Cherevko, S.; Zeradjanin, A. R.; Mayrhofer, K. J. Oxygen electrochemistry as a cornerstone for sustainable energy conversion. *Angew. Chem. Int. Ed. Engl* **2014,** *53* (1), 102.

(17) Kinoshita, K. Particle Size Effects for Oxygen Reduction on Highly Dispersed Platinum in Acid Electrolytes. *J. Electrochem. Soc.* **1990,** *137* (3), 845.

(18) Kongkanand, A.; Mathias, M. F. The Priority and Challenge of High-Power Performance of Low-Platinum Proton-Exchange Membrane Fuel Cells. *J. Phys. Chem. Lett* **2016,** *7* (7), 1127.

(19) Ohma, A.; Fushinobu, K.; Okazaki, K. Influence of Nafion® film on oxygen reduction reaction and hydrogen peroxide formation on Pt electrode for proton exchange membrane fuel cell. *Electrochim. Acta* **2010,** *55* (28), 8829.

(20) Sheng, W.; Chen, S.; Vescovo, E.; Shao-Horn, Y. Size Influence on the Oxygen Reduction Reaction Activity and Instability of Supported Pt Nanoparticles. *J. Electrochem. Soc.* **2012,** *159* (2).

(21) Leibler, L. Theory of Microphase Separation in Block Copolymers. *Macromolecules* **1980,** *13* (6), 1602.

(22) Boakye, E. E.; Yeager, H. L. Water sorption and ionic diffusion in short side chain perfluorosulfonate ionomer membranes. *J. Memb. Sci* **1992,** *69* (1), 155.

(23) Cable, K. M.; Mauritz, K. A.; Moore, R. B. Effects of hydrophilic and hydrophobic counterions on the Coulombic interactions in perfluorosulfonate ionomers. *J. Polym. Sci. B* **1995,** *33* (7), 1065.

(24) Moore, R. B.; Martin, C. R. Morphology and chemical properties of the Dow perfluorosulfonate ionomers. *Macromolecules* **1989,** *22* (9), 3594.

(25) Kusoglu, A.; Weber, A. Z. New Insights into Perfluorinated Sulfonic-Acid Ionomers. *Chem. Rev.* **2017,** *117* (3), 987.

(26) Mauritz, K. A.; Moore, R. B. State of Understanding of Nafion. *Chem. Rev.* **2004,** *104* (10), 4535.

(27) Rollet, A.-L.; Diat, O.; Gebel, G. A New Insight into Nafion Structure. *J. Phys. Chem. B* **2002,** *106* (12), 3033.

(28) Heitner-Wirguin, C. Recent advances in perfluorinated ionomer membranes: structure, properties and applications. *J. Memb. Sci* **1996,** *120* (1), 1.

(29) Inzelt, G.; Pineri, M.; Schultze, J. W.; Vorotyntsev, M. A. Electron and proton conducting polymers: recent developments and prospects. *Electrochim. Acta* **2000,** *45* (15), 2403.

(30) Kim, Y. S.; Pivovar, B. S. Moving Beyond Mass-Based Parameters for Conductivity Analysis of Sulfonated Polymers. **2010,** *1* (1), 123.

(31) Kusoglu, A.; Dursch, T. J.; Weber, A. Z. Nanostructure/Swelling Relationships of Bulk and Thin-Film PFSA Ionomers. *Adv. Funct. Mater* **2016,** *26* (27), 4961.

(32) Haubold, H. G.; Vad, T.; Jungbluth, H.; Hiller, P. Nano structure of NAFION: a SAXS study. *Electrochim. Acta* **2001,** *46* (10), 1559.

(33) Ling, X.; Bonn, M.; Parekh, S. H.; Domke, K. F. Nanoscale Distribution of Sulfonic Acid Groups Determines Structure and Binding of Water in Nafion Membranes. *Angew. Chem. Int. Ed. Engl* **2016,** *55* (12), 4011.

(34) Fujimura, M.; Hashimoto, T.; Kawai, H. Small-angle x-ray scattering study of perfluorinated ionomer membranes. 1. Origin of two scattering maxima. *Macromolecules* **1981,** *14* (5), 1309.

(35) Elliott, J. A.; Hanna, S.; Newton, J. N.; Elliott, A. M. S.; Cooley, G. E. Elimination of orientation in perfluorinated ionomer membranes. *Polym. Eng. Sci.* **2006,** *46* (2), 228.

(36) Gebel, G.; Aldebert, P.; Pineri, M. Structure and related properties of solution-cast perfluorosulfonated ionomer films. *Macromolecules* **1987,** *20* (6), 1425.

(37) ACS Appl Mater InterfacesFumagalli, M.; Lyonnard, S.; Prajapati, G.; Berrod, Q.; Porcar, L.; Guillermo, A.; Gebel, G. Fast Water Diffusion and Long-Term Polymer Reorganization during Nafion Membrane Hydration Evidenced by Time-Resolved Small-Angle Neutron Scattering. *J. Phys. Chem. B* **2015,** *119* (23), 7068.

(38) Heijden, P. C. v. d.; Rosa, A. d. l.; Gebel, G.; Diat, O. Relaxation of drawn

Nafion films studied with birefringence experiments. *Polym. Adv. Technol.* **2005,** *16* (2-3), 102.

(39) Aldebert, P.; Dreyfus, B.; Pineri, M. Small-angle neutron scattering of perfluorosulfonated ionomers in solution. *Macromolecules* **1986,** *19* (10), 2651.

(40) Loppinet, B.; Gebel, G. Rodlike Colloidal Structure of Short Pendant Chain Perfluorinated Ionomer Solutions. *Langmuir* **1998,** *14* (8), 1977.

(41) Gebel, G. Structural evolution of water swollen perfluorosulfonated ionomers from dry membrane to solution. *Polymer* **2000,** *41* (15), 5829.

(42) MacKnight, W. J.; Earnest, T. R. The structure and properties of ionomers. **1981,** *16* (1), 41.

(43) Kim, M.-H.; Glinka, C. J.; Grot, S. A.; Grot, W. G. SANS Study of the Effects of Water Vapor Sorption on the Nanoscale Structure of Perfluorinated Sulfonic Acid (NAFION) Membranes. *Macromolecules* **2006,** *39* (14), 4775.

(44) Gebel, G.; Lambard, J. Small-Angle Scattering Study of Water-Swollen Perfluorinated Ionomer Membranes. *Macromolecules* **1997,** *30* (25), 7914.

(45) Roche, E. J.; Pineri, M.; Duplessix, R. Phase separation in perfluorosulfonate ionomer membranes. **1982,** *20* (1), 107.

(46) Cable, K. M.; Mauritz, K. A.; Moore, R. B. Anisotropic ionic conductivity in uniaxially oriented perfluorosulfonate ionomers. *Chem. Mater* **1995,** *7* (9), 1601.

(47) Rubatat, L.; Rollet, A. L.; Gebel, G.; Diat, O. Evidence of Elongated Polymeric Aggregates in Nafion. *Macromolecules* **2002,** *35* (10), 4050.

(48) Barbi, V.; Funari, S. S.; Gehrke, R.; Scharnagl, N.; Stribeck, N. Nanostructure of Nafion membrane material as a function of mechanical load studied by SAXS. *Polymer* **2003,** *44* (17), 4853.

(49) Rubatat, L.; Gebel, G.; Diat, O. Fibrillar Structure of Nafion: Matching Fourier and Real Space Studies of Corresponding Films and Solutions. *Macromolecules* **2004,** *37* (20), 7772.

(50) van der Heijden, P. C.; Rubatat, L.; Diat, O. Orientation of Drawn Nafion at Molecular and Mesoscopic Scales. *Macromolecules* **2004,** *37* (14), 5327.

(51) Elliott, J. A.; Wu, D.; Paddison, S. J.; Moore, R. B. A unified morphological description of Nafion membranes from SAXS and mesoscale simulations. *Soft Matter* **2011,** *7* (15), 6820.

(52) Li, J.; Park, J. K.; Moore, R. B.; Madsen, L. A. Linear coupling of alignment with transport in a polymer electrolyte membrane. *Nat. Mater* **2011,** *10*, 507.

(53) Roche, E. J.; Stein, R. S.; Russell, T. P.; Macknight, W. J. Small-angle x-ray scattering study of ionomer deformation. **1980,** *18* (7), 1497.

(54) Loppinet, B.; Gebel, G.; Williams, C. E. Small-Angle Scattering Study of Perfluorosulfonated Ionomer Solutions. *J. Phys. Chem. B* **1997,** *101* (10), 1884.

(55) Gierke, T. D.; Munn, G. E.; Wilson, F. C. The morphology in nafion perfluorinated membrane products, as determined by wide- and small-angle x-ray studies. *J. Polym. Sci. B* **1981,** *19* (11), 1687.

(56) Roche, E. J.; Pineri, M.; Duplessix, R.; Levelut, A. M. Small-angle scattering studies of nafion membranes. **1981,** *19* (1), 1.

(57) Hsu, W. Y.; Gierke, T. D. Ion transport and clustering in nafion perfluorinated membranes. *J. Memb. Sci* **1983,** *13* (3), 307.

(58) Schmidt-Rohr, K.; Chen, Q. Parallel cylindrical water nanochannels in Nafion fuel-cell membranes. *Nat. Mater* **2008,** *7* (1), 75.

(59) Kreuer, K.-D.; Portale, G. A Critical Revision of the Nano-Morphology of Proton Conducting Ionomers and Polyelectrolytes for Fuel Cell Applications. *Adv. Funct. Mater* **2013,** *23* (43), 5390.

(60) Berrod, Q.; Lyonnard, S.; Guillermo, A.; Ollivier, J.; Frick, B.; Manseri, A.; Améduri, B.; Gébel, G. Nanostructure and Transport Properties of Proton Conducting Self-Assembled Perfluorinated Surfactants: A Bottom-Up Approach toward PFSA Fuel Cell Membranes. *Macromolecules* **2015,** *48* (17), 6166.

(61) Weber, A. Z.; Kusoglu, A. Unexplained transport resistances for low-loaded fuel-cell catalyst layers. *J. Mater. Chem. A* **2014,** *2* (41), 17207.

(62) Kudo, K.; Jinnouchi, R.; Morimoto, Y. Humidity and Temperature Dependences of Oxygen Transport Resistance of Nafion Thin Film on Platinum Electrode.

Electrochim. Acta **2016,** *209*, 682.

(63) Soboleva, T.; Malek, K.; Xie, Z.; Navessin, T.; Holdcroft, S. PEMFC Catalyst Layers: The Role of Micropores and Mesopores on Water Sorption and Fuel Cell Activity. *ACS Appl. Mater. Interfaces* **2011,** *3* (6), 1827.

(64) Iden, H.; Ohma, A.; Shinohara, K. Analysis of Proton Transport in Pseudo Catalyst Layers. *J. Electrochem. Soc.* **2009,** *156* (9), B1078.

(65) Lopez-Haro, M.; Guétaz, L.; Printemps, T.; Morin, A.; Escribano, S.; Jouneau, P. H.; Bayle-Guillemaud, P.; Chandezon, F.; Gebel, G. Three-dimensional analysis of Nafion layers in fuel cell electrodes. *Nat. Commun* **2014,** *5*, 5229.

(66) Siroma, Z.; Ioroi, T.; Fujiwara, N.; Yasuda, K. Proton conductivity along interface in thin cast film of Nafion®. *Electrochem. Commun.* **2002,** *4* (2), 143.

(67) Iden, H.; Sato, K.; Ohma, A.; Shinohara, K. Relationship among Microstructure, Ionomer Property and Proton Transport in Pseudo Catalyst Layers. *J. Electrochem. Soc.* **2011,** *158* (8), B987.

(68) Ohira, A.; Kuroda, S.; Mohamed, H. F. M.; Tavernier, B. Effect of interface on surface morphology and proton conduction of polymer electrolyte thin films. *Phys. Chem. Chem. Phys* **2013,** *15* (27), 11494.

(69) Kusoglu, A.; Kushner, D.; Paul, D. K.; Karan, K.; Hickner, M. A.; Weber, A. Z. Impact of Substrate and Processing on Confinement of Nafion Thin Films. *Adv. Funct. Mater* **2014,** *24* (30), 4763.

(70) Mohamed, H. F. M.; Kuroda, S.; Kobayashi, Y.; Oshima, N.; Suzuki, R.; Ohira, A. Possible presence of hydrophilic SO3H nanoclusters on the surface of dry ultrathin Nafion® films: a positron annihilation study. *Phys. Chem. Chem. Phys* **2013,** *15* (5), 1518.

(71) Wood, D. L.; Chlistunoff, J.; Majewski, J.; Borup, R. L. Nafion Structural Phenomena at Platinum and Carbon Interfaces. *J. Am. Chem. Soc.* **2009,** *131* (50), 18096.

(72) Bass, M.; Berman, A.; Singh, A.; Konovalov, O.; Freger, V. Surface-Induced Micelle Orientation in Nafion Films. *Macromolecules* **2011,** *44* (8), 2893.

(73) Kongkanand, A. Interfacial Water Transport Measurements in Nafion Thin

Films Using a Quartz-Crystal Microbalance. *J. Phys. Chem. C* **2011,** *115* (22), 11318.

(74) Ogata, Y.; Kawaguchi, D.; Yamada, N. L.; Tanaka, K. Multistep Thickening of Nafion Thin Films in Water. *ACS Macro Lett.* **2013,** *2* (10), 856.

(75) Siroma, Z.; Kakitsubo, R.; Fujiwara, N.; Ioroi, T.; Yamazaki, S.-i.; Yasuda, K. Depression of proton conductivity in recast Nafion® film measured on flat substrate. *J. Power Sources* **2009,** *189* (2), 994.

(76) Dishari, S. K.; Hickner, M. A. Antiplasticization and Water Uptake of Nafion Thin Films. *ACS Macro Lett.* **2012,** *1* (2), 291.

(77) Modestino, M. A.; Paul, D. K.; Dishari, S.; Petrina, S. A.; Allen, F. I.; Hickner, M. A.; Karan, K.; Segalman, R. A.; Weber, A. Z. Self-Assembly and Transport Limitations in Confined Nafion Films. *Macromolecules* **2013,** *46* (3), 867.

(78) Bertoncello, P.; Ciani, I.; Li, F.; Unwin, P. R. Measurement of Apparent Diffusion Coefficients within Ultrathin Nafion Langmuir−Schaefer Films: Comparison of a Novel Scanning Electrochemical Microscopy Approach with Cyclic Voltammetry. *Langmuir* **2006,** *22* (25), 10380.

(79) Dishari, S. K.; Hickner, M. A. Confinement and Proton Transfer in NAFION Thin Films. *Macromolecules* **2013,** *46* (2), 413.

(80) Koestner, R.; Roiter, Y.; Kozhinova, I.; Minko, S. AFM Imaging of Adsorbed Nafion Polymer on Mica and Graphite at Molecular Level. *Langmuir* **2011,** *27* (16), 10157.

(81) Paul, D. K.; Karan, K. Conductivity and Wettability Changes of Ultrathin Nafion Films Subjected to Thermal Annealing and Liquid Water Exposure. *J. Phys. Chem. C* **2014,** *118* (4), 1828.

(82) Eastman, S. A.; Kim, S.; Page, K. A.; Rowe, B. W.; Kang, S.; Soles, C. L.; Yager, K. G. Effect of Confinement on Structure, Water Solubility, and Water Transport in Nafion Thin Films. *Macromolecules* **2012,** *45* (19), 7920.

(83) Modestino, M. A.; Kusoglu, A.; Hexemer, A.; Weber, A. Z.; Segalman, R. A. Controlling Nafion Structure and Properties via Wetting Interactions. *Macromolecules* **2012,** *45* (11), 4681.

(84) Paul, D. K.; Fraser, A.; Karan, K. Towards the understanding of proton conduction mechanism in PEMFC catalyst layer: Conductivity of adsorbed Nafion films. *Electrochem. Commun.* **2011,** *13* (8), 774.

(85) Albert, J. N. L.; Epps, T. H. Self-assembly of block copolymer thin films. *Mater. Today* **2010,** *13* (6), 24.

(86) Segalman, R. A. Patterning with block copolymer thin films. *Materials Science and Engineering: R: Reports* **2005,** *48* (6), 191.

(87) Fasolka, M. J.; Mayes, A. M. Block Copolymer Thin Films: Physics and Applications. *Annu. Rev. Mater. Res.* **2001,** *31* (1), 323.

(88) Jomori, S.; Komatsubara, K.; Nonoyama, N.; Kato, M.; Yoshida, T. An Experimental Study of the Effects of Operational History on Activity Changes in a PEMFC. *J. Electrochem. Soc.* **2013,** *160* (9), F1067.

(89) Suzuki, T.; Kudo, K.; Morimoto, Y. Model for investigation of oxygen transport limitation in a polymer electrolyte fuel cell. *J. Power Sources* **2013,** *222*, 379.

(90) Davis, E. M.; Stafford, C. M.; Page, K. A. Elucidating Water Transport Mechanisms in Nafion Thin Films. *ACS Macro Lett.* **2014,** *3* (10), 1029.

(91) Shim, H. K.; Paul, D. K.; Karan, K. Resolving the Contradiction between Anomalously High Water Uptake and Low Conductivity of Nanothin Nafion films on SiO2 Substrate. *Macromolecules* **2015,** *48* (22), 8394.

(92) Paul, D. K.; Shim, H. K. K.; Giorgi, J. B.; Karan, K. Thickness dependence of thermally induced changes in surface and bulk properties of Nafion®nanofilms. *J. Polym. Sci. B* **2016,** *54* (13), 1267.

(93) Krtil, P.; Trojánek, A.; Samec, Z. Kinetics of Water Sorption in NafionThin Films − Quartz Crystal Microbalance Study. *J. Phys. Chem. B* **2001,** *105* (33), 7979.

(94) Bertoncello, P.; Wilson, N. R.; Unwin, P. R. One-step formation of ultra-thin chemically functionalized redox-active Langmuir–Schaefer Nafion films. *Soft Matter* **2007,** *3* (10), 1300.

(95) Nadermann, N. K.; Davis, E. M.; Page, K. A.; Stafford, C. M.; Chan, E. P. Using Indentation to Quantify Transport Properties of Nanophase-Segregated Polymer

Thin Films. *Adv. Mater* **2015,** *27* (33), 4924.

(96) Page, K. A.; Kusoglu, A.; Stafford, C. M.; Kim, S.; Kline, R. J.; Weber, A. Z. Confinement-driven increase in ionomer thin-film modulus. *Nano Lett.* **2014,** *14* (5), 2299.

(97) Page, K. A.; Shin, J. W.; Eastman, S. A.; Rowe, B. W.; Kim, S.; Kusoglu, A.; Yager, K. G.; Stafford, G. R. In Situ Method for Measuring the Mechanical Properties of Nafion Thin Films during Hydration Cycles. *ACS Appl. Mater. Interfaces* **2015,** *7* (32), 17874.

(98) Zimudzi, T. J.; Hickner, M. A. Signal Enhanced FTIR Analysis of Alignment in NAFION Thin Films at SiO2 and Au Interfaces. *ACS Macro Lett.* **2016,** *5* (1), 83.

(99) Dorenbos, G.; Pomogaev, V. A.; Takigawa, M.; Morohoshi, K. Prediction of anisotropic transport in Nafion containing catalyst layers. *Electrochem. Commun.* **2010,** *12* (1), 125.

(100) Levine, J. R.; Cohen, J. B.; Chung, Y. W.; Georgopoulos, P. Grazing-incidence small-angle X-ray scattering: new tool for studying thin film growth. *J. Appl. Crystallogr* **1989,** *22* (6), 528.

(101) Levine Parrill, J.; Georgopoulos, P.; Chung, Y.-W.; Cohen, J. GISAXS - Glancing incidence small angle X-ray scattering. **1993,** *03* (C8), C8.

(102) Müller-Buschbaum, P. In *Applications of Synchrotron Light to Scattering and Diffraction in Materials and Life Sciences*; Gomez, M.;Nogales, A.;Garcia-Gutierrez, M. C.;Ezquerra, T. A., Eds.; Springer Berlin Heidelberg: Berlin, Heidelberg, 2009, DOI:10.1007/978-3-540-95968-7_3 10.1007/978-3-540-95968-7_3.

(103) Chang, S. L. *X-Ray Multiple-Wave Diffraction: Theory and Application*; Springer, 2004.

(104) Lee, B.; Lo, C.-T.; Thiyagarajan, P.; Lee, D. R.; Niu, Z.; Wang, Q. Structural characterization using the multiple scattering effects in grazing-incidence small-angle X-ray scattering. *J. Appl. Crystallogr* **2008,** *41* (1), 134.

(105) Tesfaye, M.; MacDonald, A. N.; Dudenas, P. J.; Kusoglu, A.; Weber, A. Z.

Exploring substrate/ionomer interaction under oxidizing and reducing environments. *Electrochem. Commun.* **2018,** *87*, 86.

(106) Allen, F. I.; Comolli, L. R.; Kusoglu, A.; Modestino, M. A.; Minor, A. M.; Weber, A. Z. Morphology of Hydrated As-Cast Nafion Revealed through Cryo Electron Tomography. *ACS Macro Lett.* **2014,** *4* (1), 1.

(107) Yakovlev, S.; Balsara, N.; Downing, K. Insights on the Study of Nafion Nanoscale Morphology by Transmission Electron Microscopy. *membranes* **2013,** *3* (4), 424.

(108) Peron, J.; Mani, A.; Zhao, X.; Edwards, D.; Adachi, M.; Soboleva, T.; Shi, Z.; Xie, Z.; Navessin, T.; Holdcroft, S. Properties of Nafion® NR-211 membranes for PEMFCs. *J. Memb. Sci* **2010,** *356* (1), 44.

(109) Lin, J.; Wu, P.-H.; Wycisk, R.; Pintauro, P. N.; Shi, Z. Properties of Water in Prestretched Recast Nafion. *Macromolecules* **2008,** *41* (12), 4284.

(110) Wang, C.; Krishnan, V.; Wu, D.; Bledsoe, R.; Paddison, S. J.; Duscher, G. Evaluation of the microstructure of dry and hydrated perfluorosulfonic acid ionomers: microscopy and simulations. *J. Mater. Chem. A* **2013,** *1* (3), 938.

(111) Jiang, R.; Mittelsteadt, C. K.; Gittleman, C. S. Through-Plane Proton Transport Resistance of Membrane and Ohmic Resistance Distribution in Fuel Cells. *J. Electrochem. Soc.* **2009,** *156* (12), B1440.

(112) Cooper, K. Progress Toward Accurate Through-Plane Membrane Resistance and Conductivity Measurement. *ECS Trans.* **2009,** *25* (1), 995.

(113) Cooper, K. Characterizing Through-Plane and In-Plane Ionic Conductivity of Polymer Electrolyte Membranes. *ECS Trans.* **2011,** *41* (1), 1371.

(114) Cooper, K. R. Progress Toward Accurate Through-Plane Ion Transport Resistance Measurement of Thin Solid Electrolytes. *J. Electrochem. Soc.* **2010,** *157* (11), B1731.

(115) Cappadonia, M.; Erning, J. W.; Stimming, U. Proton conduction of Nafion® 117 membrane between 140 K and room temperature. *J. Electroanal. Chem* **1994,** *376* (1), 189.

(116) Villaluenga, J. P. G.; Seoane, B.; Barragán, V. M.; Ruiz-Bauzá, C. Thermo-

osmosis of mixtures of water and methanol through a Nafion membrane. *J. Memb. Sci* **2006,** *274* (1), 116.

(117) Tsampas, M. N.; Pikos, A.; Brosda, S.; Katsaounis, A.; Vayenas, C. G. The effect of membrane thickness on the conductivity of Nafion. *Electrochim. Acta* **2006,** *51* (13), 2743.

(118) Hensley, J. E.; Way, J. D.; Dec, S. F.; Abney, K. D. The effects of thermal annealing on commercial Nafion® membranes. *J. Memb. Sci* **2007,** *298* (1-2), 190.

(119) Wang, J.; Yang, M.; Dou, P.; Wang, X.; Zhang, H. Influences of Annealing on the Perfluorosulfonate Ion-Exchanged Membranes Prepared by Melt Extrusion. *Ind. Eng. Chem. Res* **2014,** *53* (36), 14175.

(120) Maldonado, L.; Perrin, J.-C.; Dillet, J.; Lottin, O. Characterization of polymer electrolyte Nafion membranes: Influence of temperature, heat treatment and drying protocol on sorption and transport properties. *J. Memb. Sci* **2012,** *389*, 43.

(121) Shi, S.; Weber, A. Z.; Kusoglu, A. Structure/property relationship of Nafion XL composite membranes. *J. Memb. Sci* **2016,** *516*, 123.

(122) Sone, Y.; Ekdunge, P.; Simonsson, D. Proton Conductivity of Nafion 117 as Measured by a Four-Electrode AC Impedance Method. *J. Electrochem. Soc.* **1996,** *143* (4), 1254.

(123) Hickner, M. A. Water-mediated transport in ion-containing polymers. *J. Polym. Sci. B* **2012,** *50* (1), 9.

(124) Singhal, N.; Datta, A. Reversible tuning of chemical structure of Nafion cast film by heat and acid treatment. *J. Phys. Chem. B* **2015,** *119* (6), 2395.

(125) Lee, K.; Ishihara, A.; Mitsushima, S.; Kamiya, N.; Ota, K.-i. Effect of Recast Temperature on Diffusion and Dissolution of Oxygen and Morphological Properties in Recast Nafion. *J. Electrochem. Soc.* **2004,** *151* (4), A639.

(126) Li, J.; Yang, X.; Tang, H.; Pan, M. Durable and high performance Nafion membrane prepared through high-temperature annealing methodology. *J. Memb.*

Sci **2010,** *361* (1), 38.

(127) Hassan, M. K.; Abukmail, A.; Mauritz, K. A. Broadband dielectric spectroscopic studies of molecular motions in a Nafion® membrane vs. annealing time and temperature. *Eur. Polym. J.* **2012,** *48* (4), 789.

(128) Thompson, E. L.; Jorne, J.; Gu, W.; Gasteiger, H. A. PEM Fuel Cell Operation at $-20\,^{\circ}C$.: I. Electrode and Membrane Water (Charge) Storage. *J. Electrochem. Soc.* **2008,** *155* (6), B625.

(129) Onishi, L. M.; Prausnitz, J. M.; Newman, J. Water−Nafion Equilibria. Absence of Schroeder's Paradox. *J. Phys. Chem. B* **2007,** *111* (34), 10166.

(130) Mathias, M. F. Two Fuel Cell Cars in Every Garage? *Interfaces* **2005,** *14*, 24.

(131) Giffin, G. A.; Haugen, G. M.; Hamrock, S. J.; Di Noto, V. Interplay between Structure and Relaxations in Perfluorosulfonic Acid Proton Conducting Membranes. *J. Am. Chem. Soc.* **2013,** *135* (2), 822.

(132) Schaberg, M. S.; Abulu, J. E.; Haugen, G. M.; Emery, M. A.; O'Conner, S. J.; Xiong, P. N.; Hamrock, S. New Multi Acid Side-Chain Ionomers for Proton Exchange Membrane Fuel Cells. *J. Electrochem. Soc.* **2010,** *33* (1), 627.

(133) Paul, D. K.; McCreery, R.; Karan, K. Proton Transport Property in Supported Nafion Nanothin Films by Electrochemical Impedance Spectroscopy. *J. Electrochem. Soc.* **2014,** *161* (14), F1395.

(134) Ono, Y.; Nagao, Y. Interfacial Structure and Proton Conductivity of Nafion at the Pt-Deposited Surface. *Langmuir* **2016,** *32* (1), 352.

(135) Eigen, M.; Maeyer, L. D. Self-dissociation and protonic charge transport in water and. *Proc. Royal Soc. Lond.* **1958,** *247* (1251), 505.

(136) Eigen, M. Proton Transfer, Acid-Base Catalysis, and Enzymatic Hydrolysis. Part I: ELEMENTARY PROCESSES. *Angew. Chem. Int. Ed. Engl* **1964,** *3* (1), 1.

(137) Kreuer, K. D. On the complexity of proton conduction phenomena. *Solid State Ion.* **2000,** *136-137*, 149.

(138) Moukheiber, E.; De Moor, G.; Flandin, L.; Bas, C. Investigation of ionomer structure through its dependence on ion exchange capacity (IEC). *J. Memb. Sci*

2012, *389*, 294.

(139) Page, K. A.; Cable, K. M.; Moore, R. B. Molecular Origins of the Thermal Transitions and Dynamic Mechanical Relaxations in Perfluorosulfonate Ionomers. *Macromolecules* **2005,** *38* (15), 6472.

(140) Page, K. A.; Landis, F. A.; Phillips, A. K.; Moore, R. B. SAXS Analysis of the Thermal Relaxation of Anisotropic Morphologies in Oriented Nafion Membranes. *Macromolecules* **2006,** *39* (11), 3939.

(141) Moore, R. B.; Martin, C. R. Chemical and morphological properties of solution-cast perfluorosulfonate ionomers. *Macromolecules* **1988,** *21* (5), 1334.

(142) Swee Chye Yeo; Eisenberg, A. Physical properties and supermolecular structure of perfluorinated ion-containing (nafion) polymers. *J. Appl. Polym. Sci* **1977,** *21* (4), 875.

(143) Page, K. A.; Jarrett, W.; Moore, R. B. Variable temperature 19F solid-state NMR study of the effect of electrostatic interactions on thermally-stimulated molecular motions in perfluorosulfonate ionomers. *J. Polym. Sci. B* **2007,** *45* (16), 2177.

(144) Page, K. A.; Park, J. K.; Moore, R. B.; Garcia Sakai, V. Direct Analysis of the Ion-Hopping Process Associated with the α-Relaxation in Perfluorosulfonate Ionomers Using Quasielastic Neutron Scattering. *Macromolecules* **2009,** *42* (7), 2729.

(145) de Almeida, S. H.; Kawano, Y. Thermal Behavior of Nafion Membranes. *J. Therm. Anal. Calorim* **1999,** *58* (3), 569.

(146) Bauer, F.; Denneler, S.; Willert-Porada, M. Influence of temperature and humidity on the mechanical properties of Nafion® 117 polymer electrolyte membrane. **2005,** *43* (7), 786.

(147) Di Noto, V.; Lavina, S.; Negro, E.; Vittadello, M.; Conti, F.; Piga, M.; Pace, G. Hybrid inorganic–organic proton conducting membranes based on Nafion and 5wt% of MxOy (M=Ti, Zr, Hf, Ta and W). Part II: Relaxation phenomena and conductivity mechanism. *J. Power Sources* **2009,** *187* (1), 57.

(148) Park, M. J.; Downing, K. H.; Jackson, A.; Gomez, E. D.; Minor, A. M.; Cookson, D.; Weber, A. Z.; Balsara, N. P. Increased Water Retention in Polymer Electrolyte Membranes at Elevated Temperatures Assisted by Capillary Condensation. *Nano Lett.* **2007,** *7* (11), 3547.

(149) Fan, Y.; Tongren, D.; Cornelius, C. J. The role of a metal ion within Nafion upon its physical and gas transport properties. *Eur. Polym. J.* **2014,** *50*, 271.

(150) Page, K. A.; Rowe, B. W.; Masser, K. A.; Faraone, A. The effect of water content on chain dynamics in nafion membranes measured by neutron spin echo and dielectric spectroscopy. *J. Polym. Sci. B* **2014,** *52* (9), 624.

Chapter 2 Morphology Change of Perfluorosulfonated Ionomer on Thickness and Thermal Treatment condition

2.1 Introduction

Proton electrolyte fuel cells (PEFCs), a promising energy source, has attracted attention due to its high energy density, compactness, and low operating temperature.[1-3] In PEFCs, an oxygen reduction reaction (ORR) occurs on the carbon-supported platinum (Pt/C) covered by proton-conducting perfluorosulfonated ionomers. Among these electrolyte materials, Nafion is the most widely used proton conducting material in electrochemical systems due to its high proton conductivity and mechanical stability.[4-5] Since the ionomer/electrode interface plays a role in the electrochemical reaction field, controlling the morphology of the ionomer thin film on the Pt/C catalyst is directly related to ORR activity.[6]

Nafion consists of a hydrophobic polytetrafluoroethylene backbone (-CF_2-) with perfluorinated chains on either side that are terminated by hydrophilic sulfonic acid groups (-SO3H). [7-8] In the presence of water, the hydrophilic phase forms an ionic domain responsible for proton transport, while the hydrophobic phase aggregates and provide a high-stability polymer.[9-11] For the past two decades, several researchers have investigated Nafion properties like thermal stability[12-13] and proton conductivity.[14-15] For the H^+ form perfluorosulfonic acid ionomer, this nanophase-separated structure leads to two relaxation behaviors: the ionic clustered transitions temperature (T_α) (100–120^{o}C) and the polymer matrix transition temperature, T_β (around -60–23^{o}C).[16-17]

Considering electrode fabrication, the catalyst layer undergoes hot-pressing to increase the contact of membrane components, and the setting temperature usually exceeds the Tα.[18-22] Nafion forms a semi-continuous ionomer of nano-order thickness that covers the Pt/C aggregates.[6] As the ionomer thickness approaches the domain size of the copolymers, surface interactions and the confinement effect can significantly influence the domain orientations and cause ionomer anisotropy behavior.[7, 23-27] Consequently, the properties of Nafion thin films can differ from those of free-standing

Nafion membranes. Confined Nafoin thin film has a lower proton conductivity and higher oxygen permeation resistance, which is correlated to overall PEFC performance.[16, 28-33] Thus, it is crucial to reveal the phenomena occurring within the interfacial regime during thermal treatment.

Crystalline structures can be caused by thermal annealing, which involves heating a membrane above its T_α, thereby giving the polymer chains enough mobility to reorient and pack themselves into a semi-crystalline structure.[34] Increased the crystallinity of Nafion membranes has been studied in relation to its impact on smaller *d*-spacing,[35-39] water uptake reduction,[35, 37-42] lower gas permeability,39 and proton conductivity.[12, 43-44] The morphology of annealed Nafion thin films with the thickness of 55 nm on Au substrate was investigated via GISAXS by Kusoglu *et al.*[23] The hydrophilic ionic domain was constrained compared to the pristine Nafion after an 146^{o}C annealing treatment above T_α. Several studies have been conducted to understand the relationship between the morphological information and physical properties of a free-standing membrane. However, the quantitative relationship between morphology and proton transporting properties of Nafion thin films, especially on Pt substrate, have not been systematically investigated.

In this work, Nafion thin films with thicknesses of 10 nm to 200 nm on platinum (Pt) substrate that underwent various annealing treatments from unannealed to 240^{o}C were fabricated to model the catalyst/ionomer interface regime. The correlation between morphology and proton transporting properties were systematically investigated by grazing incidence small angle X-ray scattering (GISAXS)/grazing incidence wide angle X-ray scattering (GIWAXS) and electrochemical impedance spectroscopy, respectively. These results provide fundamental insight into using thin film on Pt substrate to optimize the post-treatment temperature in PEFC design.

2.2 Experimental

Sample preparations

The Nafion dispersion solution was prepared by diluting 5 wt% Nafion (Aldrich, equivalent weight (EW)=1,100 stock dispersion) to 0.1 wt%, 0.27 wt%, 0.45 wt%, and 1.6 wt% with 99.5% 1,1,1,3,3,3-hexafluoro-2-propanol (Wako Pure Chemical Industries, Ltd). Then, Nafion thin films of varying thickness were fabricated using the spin-cast method on cleaned interdigitated array electrodes and the as-prepared Pt substrate. The prepared Nafion-thin films were annealed at 120oC, 160oC, 200oC, and 240oC under dry N_2 for 1 h.

Proton conductivity

Self-designed interdigitated array electrodes were fabricated by the Osaka Vacuum Industrial Co., Ltd., and their geometry detail is shown in Figure S1. As shown in Figure S1, a 100 nm Pt layer was precisely deposited between Au electrodes with 0.008 mm spacing to avoid direct contact. By using self-designed interdigitated array electrodes, ionomer proton conductivity on Pt can be measured. Before using the electrodes, they were soaked in an acetone solution for at least 1 h and then sonicated for 5 min each in isopropanol (Wako Pure Chemical Industries, Ltd.), acetone (Wako Pure Chemical Industries, Ltd.), and Millipore water. Finally, the interdigitated array electrodes were washed with isopropanol, acetone, and Millipore water three times and then dried at 60°C. The thin films were fabricated by dropping 150 µl prepared Nafion dispersion onto the interdigitated array electrodes, and then the sample was immediately spun at 800–1600 rpm for 2 min.

The electrochemical impedance spectroscopy was performed on the Nafion thin films on the interdigitated array electrodes under 80% relative humidity at 25oC in an N2 atmosphere with a VSP-300 Multi Potentiostat/Galvanostat (Bio-Logic). An alternating amplitude potential and frequency range was set at 100 mV and 7 MHz to 0.01 Hz, respectively. To capture the Nafion thin films resistances, the collected

impedance data were fitted using analysis software EC-lab (V.11.21) and an equivalent circuit as shown in Figure S3. The proton conductivity of the Nafion thin films (σ) was calculated using the following equation

$$\sigma = \frac{1}{R_f} \cdot \frac{d}{l(N-1)t} \quad [1]$$

where R_f is the film resistance estimated by the fitting of the impedance spectra, d is the distance between two adjacent Au electrodes, l is the electrode length, N is the electrode number, and t is the film thickness.

GISAXS/GIWAXS

First, a 20 nm Cr buffer layer was deposited on P-doped Si substrate (1 cm × 1 cm) using a magnetron sputter (MSP-30T, Vacuum Devices Inc., Japan) in an Ar atmosphere and with 150 mA for 1 min 47 s. Then, to mimic the Pt catalyst surface, a 30 nm Pt layer was fabricated in the same manner on the prepared Cr/Si substrate in an Ar atmosphere. The thin films were fabricated using the same electrochemical impedance spectroscopy procedure as mentioned previously.

The prepared Nafion thin films were placed into a cell connected to a humidity controller system for the GISAXS/GIWAXS. The relative humidity was controlled by transporting hydrated N_2 gas to maintain a constant humidity level of 80% RH at 25oC. GISAXS and GIWAXS were performed in beamline BL40B2 at SPring-8, Hyogo, Japan. The X-ray energy was 12.4 keV, and the incident X-ray angle was at 0.14o. The GISAXS 2D image was collected with a Dectris Pilatus imaging plate (0.172 mm x 0.172 mm, C9729DK-10) and a flat panel sensor (0.05 mm, Hamamatsu Photonics K. K. Japan). The X-ray exposure time for the Nafion thin films in the GISAXS and GIWAXS was 100 s and 10 s, respectively. The distance between the samples and the detector was set at 2200 mm and 60 mm for GISAXS and GIWAXS, respectively.

Silver behenate and CeO_2 were used to calibrate the beam center and the distance between the samples and detector for the GISAXS and GIWAXS, respectively. In the GISAXS/GIWAXS, the scattering vector *q*, was defined as the following equation:

$$\mathbf{q} = \begin{pmatrix} q_x \\ q_y \\ q_z \end{pmatrix} = \frac{2\pi}{\lambda} \begin{pmatrix} \cos 2\Theta \cos \alpha_f - \cos \alpha_i \\ \sin 2\Theta \cos \alpha_f \\ \sin \alpha_i + \cos \alpha_f \end{pmatrix} \quad [2]$$

where the λ is the wavelength of the incidence X-ray. The detailed GISAXS/GIWAXS setup is shown in Figure S2.

Thickness Characterization

The thickness of the Nafion thin films was examined by ellipsometry (FE-5000, Ostuka, Electronics Co., Ltd). The Cauchy model was used to estimate the thickness of the prepared Nafion thin films.[24]

$$n(\lambda) = A + \frac{B}{\lambda^2} + \frac{C}{\lambda^4} \quad [3]$$

Here, λ is the wavelength and A, B, and C are the material coefficients that can be determined by fitting the equation to the refractive incidence. The thickness of the prepared Nafion thin films were 10 nm, 30 nm, 50 nm, and 200 nm.

2.3 Results and Discussion

The thickness of the prepared Nafion thin films were 10 nm, 30 nm, 50 nm, and 200 nm, which were characterized by ellipsometry combined with Cauchy model fitting. Figure 1 shows the proton conductivity of the Nafion thin films before and after the annealing treatment at various temperatures under 80% RH at 25°C. The electrochemical impedance spectra are shown in Figure S3. For the Nafion thin films with 200 nm thickness, the proton conductivity decreased from 23 mS/cm^{-1} (unannealed) to 5.92 mS/cm^{-1} as the annealing temperature increased to 240°C. For thin films with a

thickness of 50 nm, the conductivity declined smoothly; unannealed thin films with a thickness of 50 nm had a conductivity of 7.9 mS/cm^{-1}, and after annealing at 240°C, the conductivity decreased to 2.7 mS/cm. However, for the 10 nm thick Nafion thin film, proton conductivity of the unannealed film decreased from 2.3 mS/cm^{-1} to 1.1 mS/cm^{-1} after an annealing treatment at 240°C. The conductivity of the samples annealed at 240°C was approximately one order of magnitude lower than that of the unannealed ones. The arrow presented in Figure 1 shows the region in which proton conductivity significantly decreased: at 120–160°C for 200 nm-thick films, 160–200°C for 50 nm-thick films, and 200–240°C for 30 nm and 10 nm-thick films. Similar results were observed by Karan, who revealed that the proton conductivity of Nafion thin film with a thickness of 160 nm and 60°C annealing treatment decreased drastically compared to that of a thinner Nafion film with a thickness of 10 nm.[20]

To examine the morphological changes of Nafion thin films with varying thicknesses and annealing temperatures, GISAXS and GIWAXS were performed on the Nafion thin films. Figure 2 exhibits the GISAXS 2D profiles of the Nafion thin films with different thicknesses and annealing treatment temperatures under 80% RH 25°C. The scattering

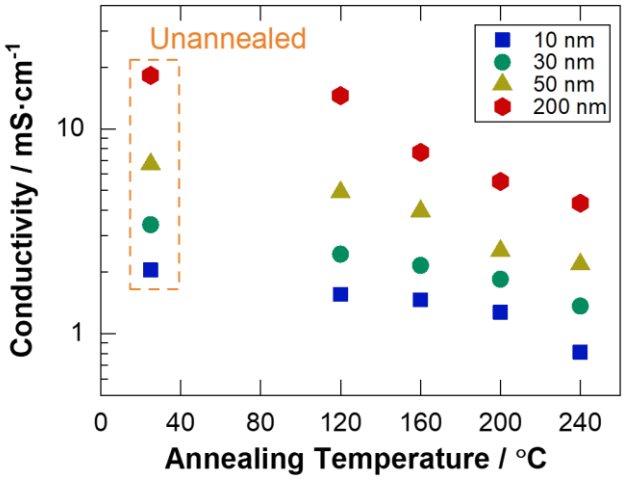

Figure 1. Proton conductivity of Nafion thin films with various thicknesses ranging from 10–200 nm before and after an annealing treatment at 120–240 °C. The conductivity was examined under 80% RH at 25°C. The arrow shows the region where proton conductivity significantly decreased.

patterns were plotted as scattering vector q in 2D. The unannealed Nafion thin film 200 nm in thickness exhibited a scattering ring around q=1.5-2 nm^{-1}. The scattering peak is attributed to the ordered structure of hydrophilic domains in Nafion thin films, which is named the "ionomer peak".[45] The ionomer peak observed in the Nafion thin film 200 nm in thickness was weaker in the Nafion thin film 50 nm in thickness, and it was even less pronounced in the Nafion thin films with thicknesses below 30 nm. For the Nafion thin films with 200 nm and 50 nm thicknesses, the ionomer peak generally weakened when the annealing temperature increased to 160°C and 200°C, respectively. In contrast, the scattering pattern of the Nafion thin films with 30 nm and 10 nm thicknesses did not exhibit obvious changes after the annealing treatments.

To further understand how the ionic domain orientation change was influenced by thickness and annealing treatment, 1D line-integrated analyses along the equatorial (in-plane) and meridional directions (out-of-plane) were extracted from the GISAXS 2D profiles. The typical 1D line profile along the in-plane direction is shown in Figure S4. The scattering vector q expressed in reciprocal space can be converted to d spacing, which is the distance of the periodic structure in real space, using equation [4].

$$d = \frac{2\pi}{q} \qquad [4]$$

To further understand the shift in the ionomer peak observed in Figure S4, the ionomer peaks were fitted using the Gaussian function along the in-plane and out-of-plane directions to extract their precise positions. In Figure 3(a), the *d*-spacing along the in-plane direction for film with a thickness of 200 nm decreased from 4.1 nm to 3.5 nm with an increase in annealing temperature, which indicates that the hydrophilic domain shrank significantly. The unannealed 50 nm-thick Nafion thin film had smaller *d*-spacing (3.6 nm) than that of the thin film with a thickness of 200 nm, and the *d*-spacing decreased to 3.3 nm as the annealing temperature increased to 240°C. However, there is no ionomer peak observed in the case of 10 nm-thick film. Similar annealing effects

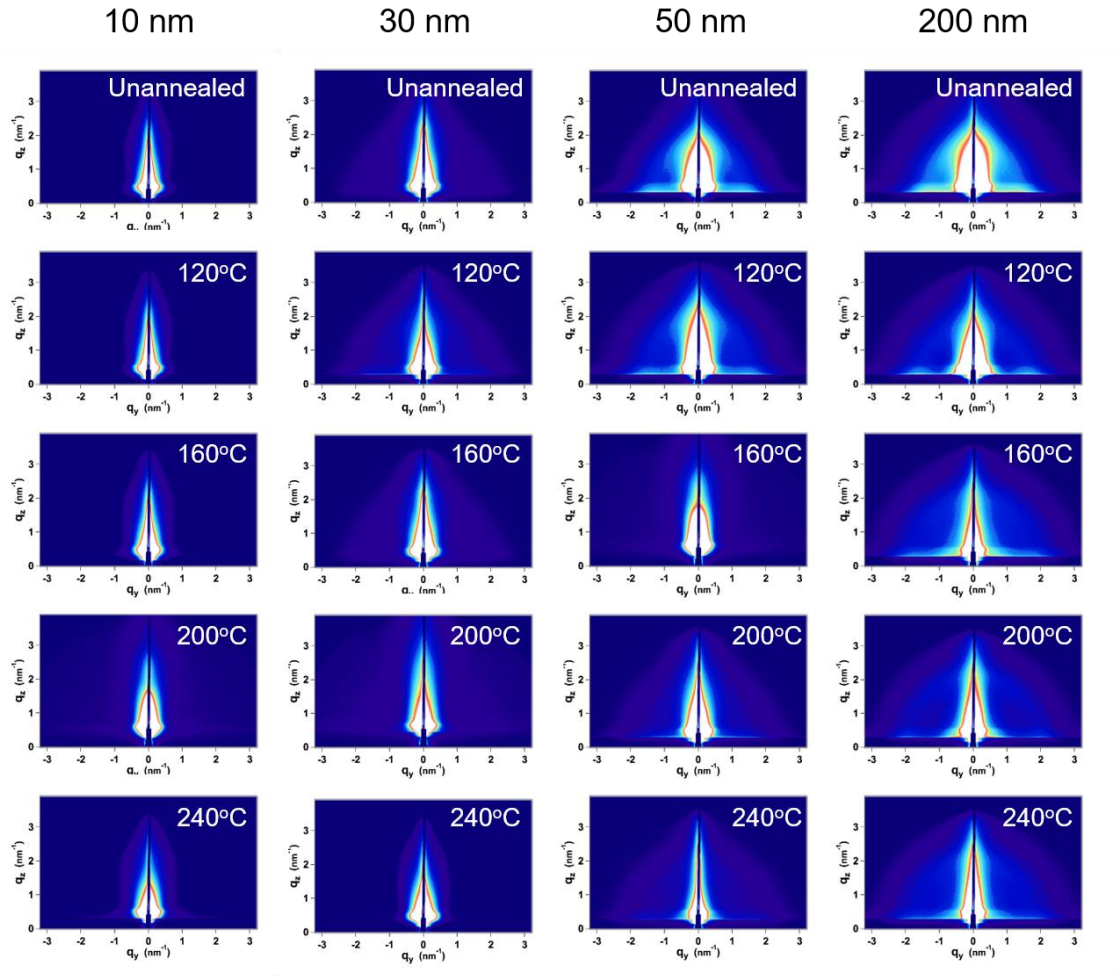

Figure 2 GISAXS 2D patterns of Nafion thin films of various thicknesses and annealing conditions measured under 80% RH at 25°C.

on thin films have also been observed in previous research, as reported by Kusoglu and Karan.[20, 23]

Suppressed proton conductivity can be directly explained by the results of the GISAXS. The ionomer peak in the GISAXS reflects the growth of the hydrophilic domain which is responsible for proton and water transport and is gradually suppressed as annealing temperature increases and abrupt suppressed when annealing temperature exceeds the Tα. Ionomer/substrate interactions were significantly higher when film thickness was below 30 nm because the polymer chain mobility was severely limited in both the in-plane and out-of-plane directions, thus enhancing the polymer chain orientation and consequently increasing the Tα. Therefore, the conductivity and

GISAXS results support the conclusion that thinner films under 30 nm in thickness are comparatively stable and less sensitive to annealing treatments because the chains become topologically confined as the film thickness approaches the crystalline size.

To quantitatively compare the intensity of the ionomer peak along the meridional and equatorial axes, I_1 and I_2 are utilized, respectively. We normalized the curves by setting the integrated intensity around the ionomer peak to q=1-2 nm^{-1}. It is assumed that I_1 (out-of-plane) and I_2 (in-plane) are both Gaussian distribution functions of the azimuthal angle, φ, shown in Figure S4, with peaks along the meridional (φ=0°) and equatorial (φ=90°) directions. The $I_1(\varphi)$ and $I_2(\varphi)$ were then used to determine the normalized integral intensity, I(q), which is defined by following equation.[46]

$$I_i(q) \approx \int_0^{\frac{\pi}{2}} I_i(\varphi) 2\pi q \left|\sin\varphi\right| d\varphi \qquad [5]$$

The normalized integral intensity of the ionomer peak along the meridian (i=1) and the equator (i=2) was evaluated using Equation [5]. In this study, the meridian and equator scattering patterns represent the in-plane and out-of-plane directions. The estimated normalized integrated intensity of 30–200 nm-thick Nafion thin films with various annealing treatments was shown in Figure 3(c). For the 10 nm and 30 nm-thick films, it is extremely difficult to extract the contribution from the ionomer peak due to the lack of ionomer peak discernibility. Overall, the results in Figure 3(c) clearly show that the ionic domain along the out-of-plane direction makes less of a contribution ($I_1(q_{ionic})/\{I_1(q_{ionic}) + I_2(q_{ionic}) < 50\%$) compared to that of the in-plane direction, which indicates that the hydrophilic ionic domain is more inclined to be aligned parallel to the Pt substrate. Additionally, for a given thickness, the $I_1(q_{ionic})$ (%) value slightly increased with an increase in annealing temperature and then decreased after a certain a temperature (50 nm: 200°C, 200 nm: 160°C), reflecting that the hydrophilic ionic domain tends to be random after the Tα has been exceeded.

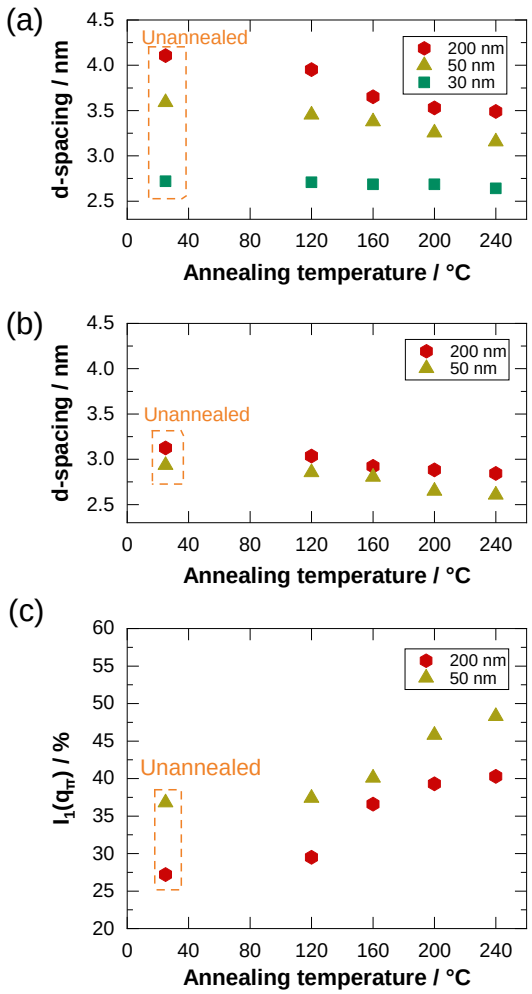

Figure 3. The plot of ionomer peak *d*-spacing extracted from Figure S4 along the (a) in-plane and (b) out-of-plane directions. (c) $I_1(q_\pi)$ were calculated on the basis of $I_1(q_{ionic})/\{I_1(q_{ionic}) + I_2(q_{ionic}) \times 100$, which indicates the ionic domain contribution along the out-of-plane direction.

Annealing treatment affects the hydrophilic ionic domain in the Nafion thin films and the crystallinity of the hydrophobic CF_2 backbone. To examine the molecular aggregation in the hydrophobic domain of the Nafion thin films, GIWAXS was performed under 80% RH at 25°C. The GIWAXS 1D line profiles along the in-plane direction extracted from 2D GIWAXS patterns are shown in Figure S6. In temperature-dependent wide angle X-ray scattering (WAXS) studies, the disappearance of the

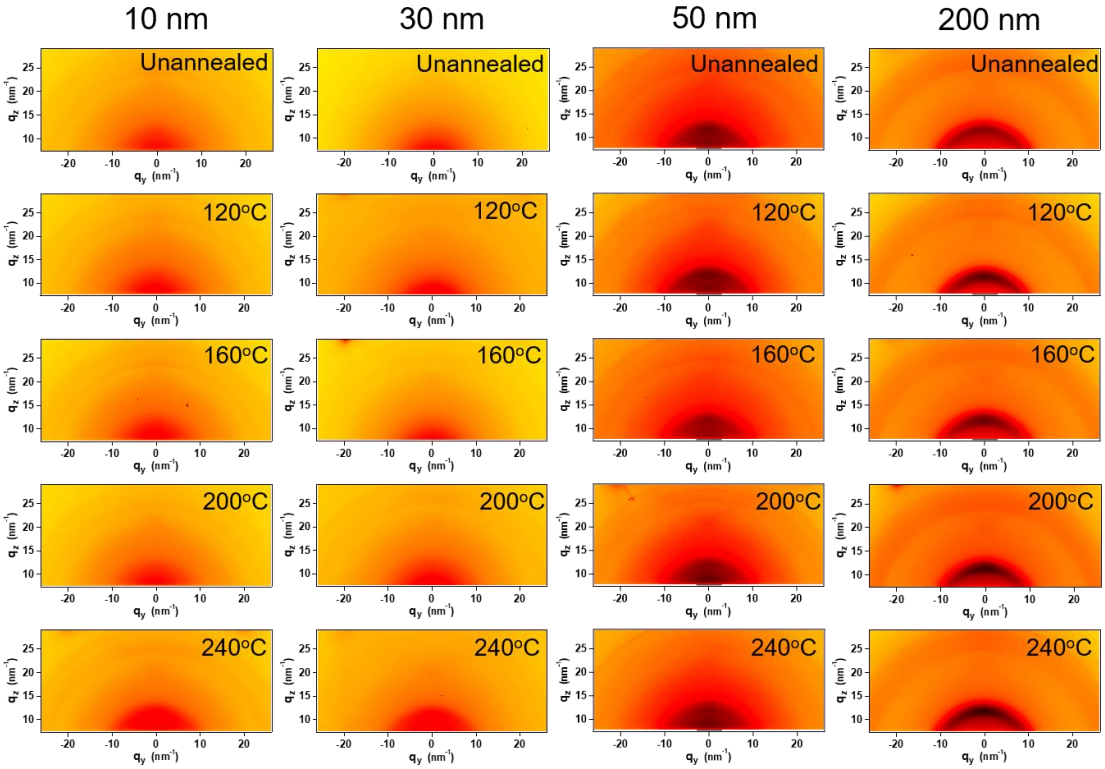

Figure 4. The GIWAXS 2D patterns of Nafion thin films with various thicknesses and annealing temperatures under 80% RH at 25°C.

crystalline peak was observed above the melting temperature at around 250–300°C. Thus, the annealing process does not to cause the film to melt in this study, which is also confirmed by the ellipsometry (not shown).[35-36] In the GIWAXS patterns of the Nafion thin film, board peaks attributed to the combination of CF_2 chain amorphous and crystalline structures appear at q=10.5 nm^{-1} and 12 nm^{-1}, respectively.[23, 47] For further investigation, the board peak observed in Figure 5 could be deconvoluted into the amorphous and crystalline peaks. The degree of crystallinity of the Nafion thin films, χ_c, can be estimated based on previous research.[48] In this study, both crystalline and amorphous components are calculated along the in-plane and out-of-plane directions using Equation [5]. As shown in Figure 4, the degree of crystallinity, χ_c, generally increased with an increase in annealing temperature and was heavily dependent on thickness. Although the degree of crystallinity along the out-of-plane direction exhibited a slightly higher value, there is no obvious anisotropic behavior observed. For the 200 nm-thick Nafion thin films, χ_c significantly increased to 61% after the annealing

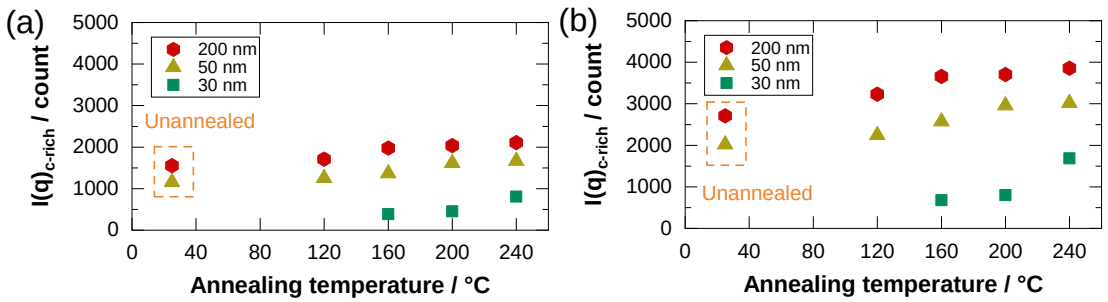

Figure 5. The calculated degree of crystallinity for the Nafion thin films with various thicknesses and annealing treatments along the (a) in-plane and (a) out-of-plane directions.

temperature increased to 160°C and then slightly increased as the temperature continued to increase. For 50 nm-thick Nafion thin films, χ_c gradually increased as the annealing treatment increased and then increased by almost 80% after the annealing treatment at 200°C. The 10 nm-thick Nafion thin film results differed from the other samples and exhibited a unique behavior in that the crystalline peak did not appear until the annealing temperature increased to 240°C. The crystallinity of dispersion cast Nafion N112 and N117 film membranes has been reported to be 55-75%,[19, 49-50] which is comparable to that of the $\geqslant$ 50 nm-thick unannealed Nafion thin films in the study. Therefore, the degree of crystallinity of the Nafion thin films estimated here is reasonable and correctly reflects the nanostructure of the hydrophobic domain. The annealing treatment involves heating the thin films above their T_α, thereby giving the polymer chains enough mobility to reorient and pack themselves into crystallites.[34] This behavior can be linked to the formation of crystallinity in Nafion thin films, where the high crystallinity increased the mechanical energy for hydrophilic/hydrophobic phase-

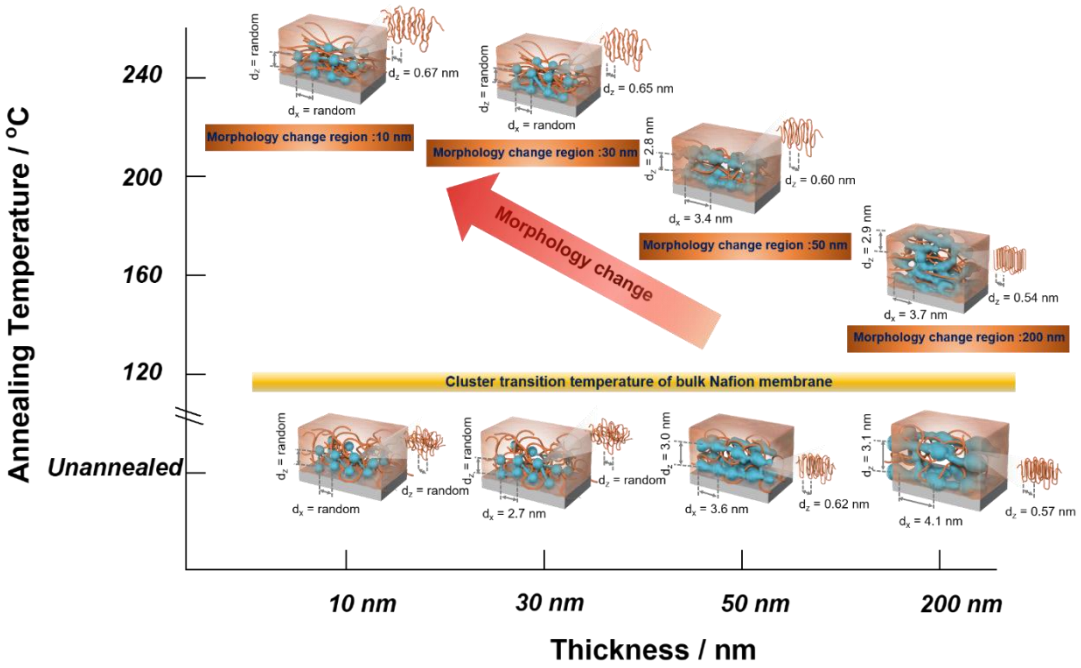

Figure 6 The schematic image of Nafion thin film morphology variation for different film thicknesses and annealing temperatures under 80% RH 25°C. dx and dz represents the average *d*-spacing of the hydrophilic domain along the in-plane and out-of-plane directions, respectively. The temperature at which morphology significantly changes showed a dependence on film thickness. The cluster transition temperature of the bulk Nafion membrane is 105–120°C.[52-54]

separation. Annealing at temperatures above the Tα induced crystallinity in thin films and limited the hydrophilic/hydrophobic phase separation. These changes are consistent with the reduced conductivity due to a stronger mechanical force in the mechanical and chemical energy balance that controls proton transport.[20, 51] The difference in T_α between this study and previous work is related to wettability.

Herein, we promote a conceptual model to further understand the morphological changes related to Tα in terms of hydrophilic and hydrophobic phase variations after different annealing treatments. For Nafion thin films with thicknesses of 10 nm, 30 nm, 50 nm, and 200 nm, Tα exists in three ranges as shown in Figure 6: (1) 120–160°C for film 200 nm in thickness, (2) 160–200°C for film 50 nm in thickness, and (3) 200–

240°C for film 30 nm or 10 nm in thickness. As thickness decreased, Tα increased due to the amplified hydrogen bonding interactions between the ionomer and Pt substrate.

2.4 Conclusion

This study systematically investigated the morphological and proton transporting properties of Nafion thin films on Pt substrates with various thicknesses and annealing treatments via GISAXS/GIWAXS and the electrochemical impedance method. Both the morphology and proton transporting properties of the films were significantly changed after annealing them above the cluster transition temperature. The temperature at which the conductivity significantly decreased is consistent with the temperature at which the ionic domain constrained and subsequently enhanced structural crystallinity. For the 200 nm-thick film, morphology changes due to bulky dominant properties occurred at the lowest temperature. Since there are strong electrostatic interactions between the ionomer and substrate, as the film thickness approached the characteristic polymer domain size, the thickness-confined Nafion thin films under 30 nm required a significantly higher temperature to induce morphology changes. The findings of this study are expected to further the understanding of catalysts/ionomer interfacial phenomena during the hot-pressing process in PEFCs.

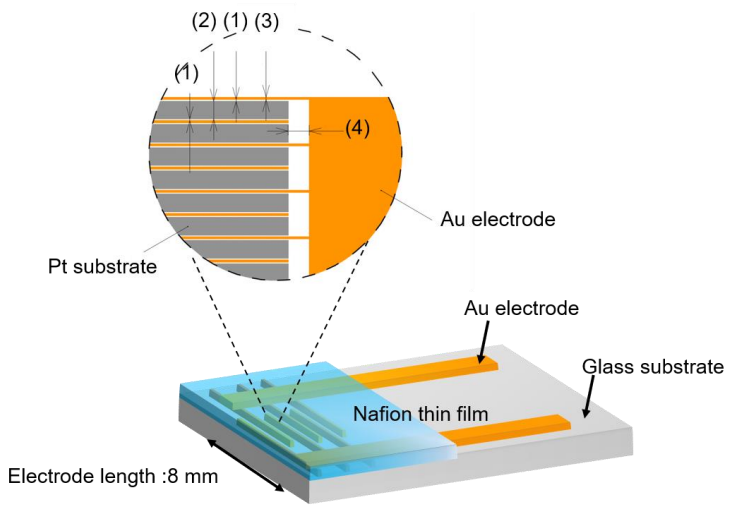

(1) Distance between electrode and Pt substrate : 0.008 mm
(2) Width of Pt substrate : 0.084 mm
(3) Width of Au electrode : 0.01 mm
(4) Spacing between Pt substrate to side : 0.1 mm

Electrode numbers : 72

Figure S1. The geometry of interdigitated array (IDA) electrodes used for EIS measurements.

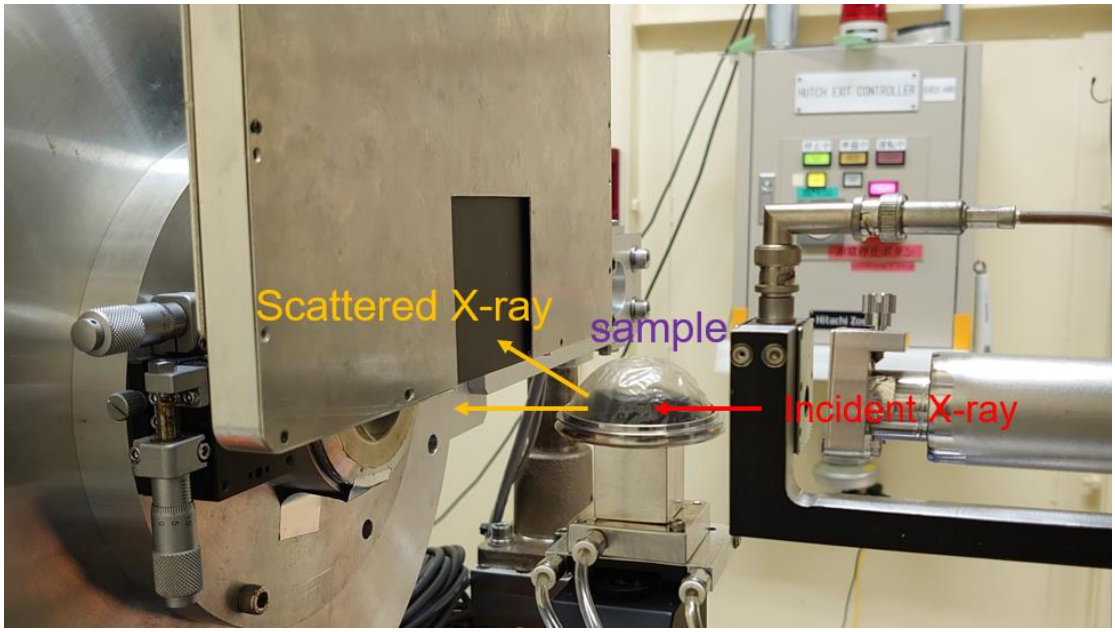

Figure S2. The schematic image of GISAXS/GIWAXS measurement. Continuous N_2 flow was transport into chamber with 25 μm PEEK film to maintain constant humidity level. In this way, GISAXS and GIWAXS patterns were collected at the same time.

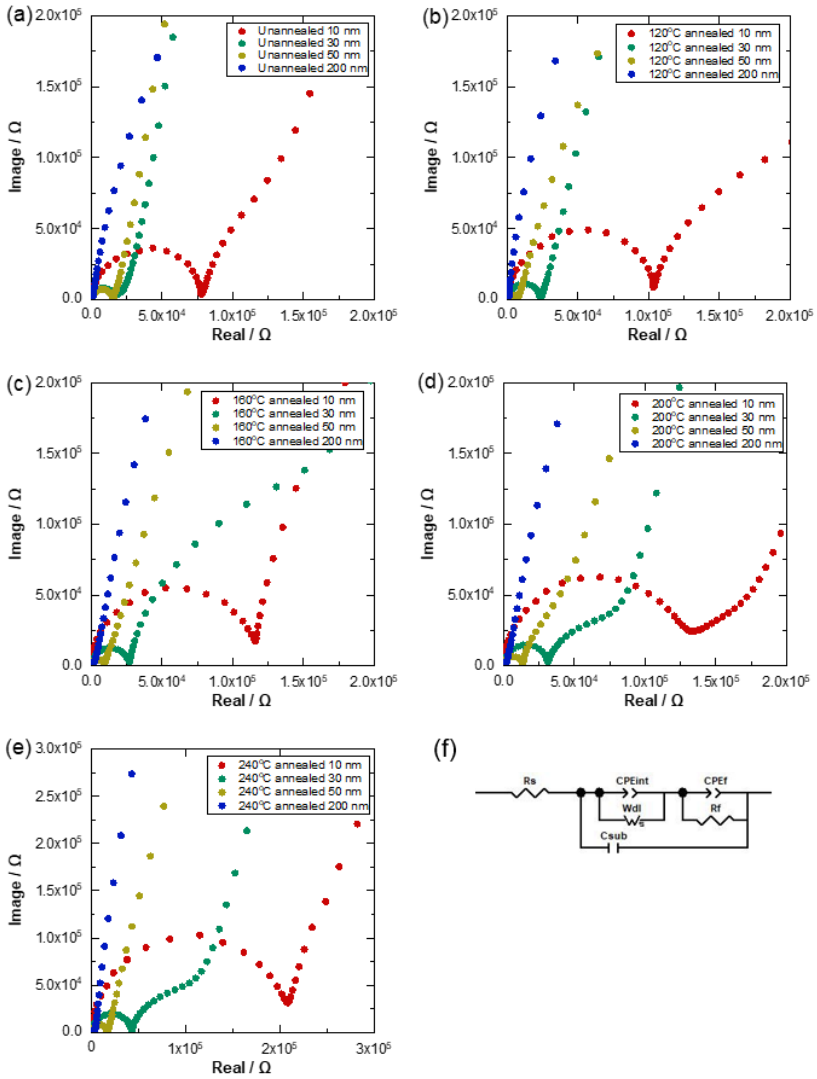

Figure S3. The Nyquist plot of prepared Nafion thin-films with thickness and post-treatment (a) unannealed, (b) 120°C (c) 160°C (d) 200°C and (e) 200 nm with various annealing temperature. The EIS measurements were performed under 80%RH at 25°C. (f) The equivalent circuit model used for the fitting of the Nyquist plots.

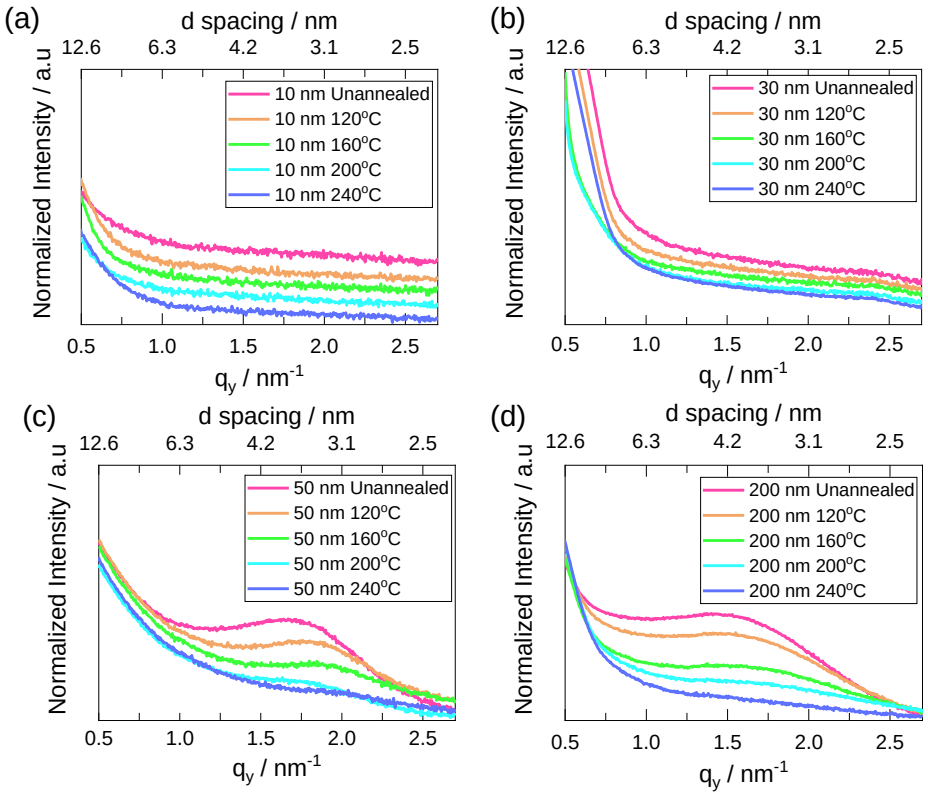

Figure S4. The 1D line-profile of the Nafion thin-films with various thicknesses ((a):10 nm, (b): 30 nm, (c):50 nm, (d):200 nm) before and after annealing with various temperatures.

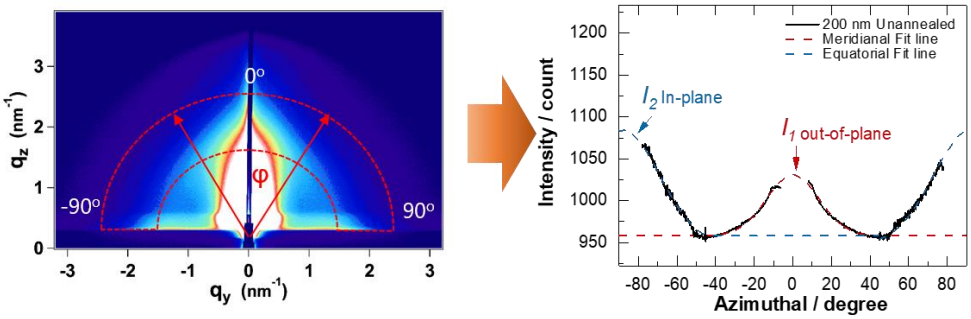

Figure S5. The illustration of normalization method used in this manuscript. Ionomer peak was extracted from the scattering from in 2D pattern(left) to azimuthal plot and fitted with Gaussian function.

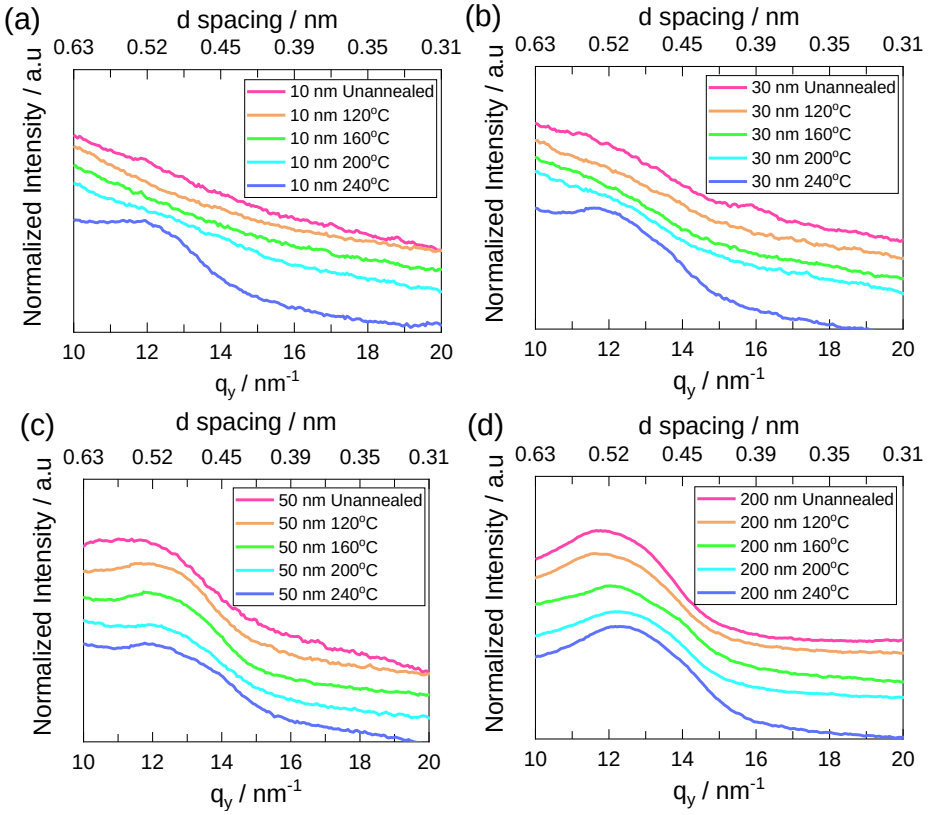

Figure S6. The 1D line-profile extracted from GIWAXS for the Nafion thin-films with various thicknesses ((a):10 nm, (b):30 nm, (c):50 nm, (d):200 nm) before and after annealing with various temperatures.

REFERENCE

(1) Santos, E.; Schmickler, W. *Catalysis in Electrochemistry: From Fundamental Aspects to Strategies for Fuel Cell Development*; Wiley, 2011.

(2) Pu, H. *Polymers for PEM Fuel Cells*; Wiley, 2014.

(3) O'Hayre, R.; Cha, S. W.; Prinz, F. B.; Colella, W. *Fuel Cell Fundamentals*; Wiley, 2016.

(4) Mauritz, K. A.; Moore, R. B. State of Understanding of Nafion. *Chem. Rev.* **2004,** *104* (10), 4535.

(5) Zhang, H.; Shen, P. K. Recent Development of Polymer Electrolyte Membranes for Fuel Cells. *Chem. Rev.* **2012,** *112* (5), 2780.

(6) Holdcroft, S. Fuel Cell Catalyst Layers: A Polymer Science Perspective. *Chem. Mater* **2014,** *26* (1), 381.

(7) Kusoglu, A.; Weber, A. Z. New Insights into Perfluorinated Sulfonic-Acid Ionomers. *Chem. Rev* **2017,** *117* (3), 987.

(8) Rollet, A.-L.; Diat, O.; Gebel, G. A New Insight into Nafion Structure. *J. Phys. Chem. B* **2002,** *106* (12), 3033.

(9) Rodgers, M. P.; Bonville, L. J.; Kunz, H. R.; Slattery, D. K.; Fenton, J. M. Fuel cell perfluorinated sulfonic acid membrane degradation correlating accelerated stress testing and lifetime. *Chem. Rev.* **2012,** *112* (11), 6075.

(10) Weber, A. Z.; Newman, J. Modeling Transport in Polymer-Electrolyte Fuel Cells. *Chem. Rev.* **2004,** *104* (10), 4679.

(11) Inzelt, G.; Pineri, M.; Schultze, J. W.; Vorotyntsev, M. A. Electron and proton conducting polymers: recent developments and prospects. *Electrochim. Acta* **2000,** *45* (15), 2403.

(12) Maldonado, L.; Perrin, J.-C.; Dillet, J.; Lottin, O. Characterization of polymer electrolyte Nafion membranes: Influence of temperature, heat treatment and drying protocol on sorption and transport properties. *J. Memb. Sci* **2012,** *389*, 43.

(13) Page, K. A.; Landis, F. A.; Phillips, A. K.; Moore, R. B. SAXS Analysis of the Thermal Relaxation of Anisotropic Morphologies in Oriented Nafion Membranes. *Macromolecules* **2006,** *39* (11), 3939.

(14) Iden, H.; Sato, K.; Ohma, A.; Shinohara, K. Relationship among Microstructure, Ionomer Property and Proton Transport in Pseudo Catalyst Layers. *J. Electrochem. Soc.* **2011,** *158* (8), B987.

(15) Jiang, R.; Mittelsteadt, C. K.; Gittleman, C. S. Through-Plane Proton Transport Resistance of Membrane and Ohmic Resistance Distribution in Fuel Cells. *J. Electrochem. Soc.* **2009,** *156* (12), B1440.

(16) Tesfaye, M.; Kushner, D. I.; McCloskey, B. D.; Weber, A. Z.; Kusoglu, A. Thermal Transitions in Perfluorosulfonated Ionomer Thin-Films. *ACS Macro Lett.* **2018**,

(17) Osborn, S. J.; Hassan, M. K.; Divoux, G. M.; Rhoades, D. W.; Mauritz, K. A.; Moore, R. B. Glass Transition Temperature of Perfluorosulfonic Acid Ionomers. *Macromolecules* **2007,** *40* (10), 3886.

(18) Starkweather Jr, H. W. Crystallinity in perfluorosulfonic acid ionomers and related polymers. *Macromolecules* **1982,** *15* (2), 320.

(19) Brown, E. N.; Rae, P. J.; Bruce Orler, E.; Gray, G. T.; Dattelbaum, D. M. The effect of crystallinity on the fracture of polytetrafluoroethylene (PTFE). *Materials Science and Engineering: C* **2006,** *26* (8), 1338.

(20) Paul, D. K.; Karan, K. Conductivity and Wettability Changes of Ultrathin Nafion Films Subjected to Thermal Annealing and Liquid Water Exposure. *J. Phys. Chem. C* **2014,** *118* (4), 1828.

(21) Paul, D. K.; Shim, H. K. K.; Giorgi, J. B.; Karan, K. Thickness dependence of thermally induced changes in surface and bulk properties of Nafion®nanofilms. *J. Polym. Sci. B* **2016,** *54* (13), 1267.

(22) de Almeida, S. H.; Kawano, Y. Thermal Behavior of Nafion Membranes. *J. Therm. Anal. Calorim* **1999,** *58* (3), 569.

(23) Kusoglu, A.; Kushner, D.; Paul, D. K.; Karan, K.; Hickner, M. A.; Weber, A. Z. Impact of Substrate and Processing on Confinement of Nafion Thin Films. *Adv.*

Funct. Mater **2014,** *24* (30), 4763.

(24) Paul, D. K.; Karan, K.; Docoslis, A.; Giorgi, J. B.; Pearce, J. Characteristics of Self-Assembled Ultrathin Nafion Films. *Macromolecules* **2013,** *46* (9), 3461.

(25) Davis, E. M.; Stafford, C. M.; Page, K. A. Elucidating Water Transport Mechanisms in Nafion Thin Films. *ACS Macro Lett.* **2014,** *3* (10), 1029.

(26) Dishari, S. K.; Hickner, M. A. Antiplasticization and Water Uptake of Nafion Thin Films. *ACS Macro Lett.* **2012,** *1* (2), 291.

(27) Tesfaye, M.; Kushner, D. I.; Kusoglu, A. Interplay between Swelling Kinetics and Nanostructure in Perfluorosulfonic Acid Thin-Films: Role of Hygrothermal Aging. *ACS Applied Polymer Materials* **2019,** *1* (4), 631.

(28) Jinnouchi, R.; Kudo, K.; Kitano, N.; Morimoto, Y. Molecular Dynamics Simulations on O2 Permeation through Nafion Ionomer on Platinum Surface. *Electrochim. Acta* **2016,** *188*, 767.

(29) Paul, D. K.; McCreery, R.; Karan, K. Proton Transport Property in Supported Nafion Nanothin Films by Electrochemical Impedance Spectroscopy. *J. Electrochem. Soc.* **2014,** *161* (14), F1395.

(30) Siroma, Z.; Kakitsubo, R.; Fujiwara, N.; Ioroi, T.; Yamazaki, S.-i.; Yasuda, K. Depression of proton conductivity in recast Nafion® film measured on flat substrate. *J. Power Sources* **2009,** *189* (2), 994.

(31) Siroma, Z.; Ioroi, T.; Fujiwara, N.; Yasuda, K. Proton conductivity along interface in thin cast film of Nafion®. *Electrochem. Commun.* **2002,** *4* (2), 143.

(32) Ono, Y.; Nagao, Y. Interfacial Structure and Proton Conductivity of Nafion at the Pt-Deposited Surface. *Langmuir* **2016,** *32* (1), 352.

(33) Tesfaye, M.; MacDonald, A. N.; Dudenas, P. J.; Kusoglu, A.; Weber, A. Z. Exploring substrate/ionomer interaction under oxidizing and reducing environments. *Electrochem. Commun.* **2018,** *87*, 86.

(34) Martin, R. T.; Kevin, P. D.; Katherine, D. L.; Charles, W. M. ACS symposium series, 1989.

(35) Gierke, T. D.; Munn, G. E.; Wilson, F. C. The morphology in nafion perfluorinated membrane products, as determined by wide- and small-angle x-

ray studies. *J. Polym. Sci. B* **1981,** *19* (11), 1687.

(36) Fujimura, M.; Hashimoto, T.; Kawai, H. Small-angle x-ray scattering study of perfluorinated ionomer membranes. 1. Origin of two scattering maxima. *Macromolecules* **1981,** *14* (5), 1309.

(37) Moore, R. B.; Martin, C. R. Morphology and chemical properties of the Dow perfluorosulfonate ionomers. *Macromolecules* **1989,** *22* (9), 3594.

(38) Kusoglu, A.; Savagatrup, S.; Clark, K. T.; Weber, A. Z. Role of Mechanical Factors in Controlling the Structure–Function Relationship of PFSA Ionomers. *Macromolecules* **2012,** *45* (18), 7467.

(39) Lee, K.; Ishihara, A.; Mitsushima, S.; Kamiya, N.; Ota, K.-i. Effect of Recast Temperature on Diffusion and Dissolution of Oxygen and Morphological Properties in Recast Nafion. *J. Electrochem. Soc.* **2004,** *151* (4), A639.

(40) Wang, J.; Yang, M.; Dou, P.; Wang, X.; Zhang, H. Influences of Annealing on the Perfluorosulfonate Ion-Exchanged Membranes Prepared by Melt Extrusion. *Ind. Eng. Chem. Res* **2014,** *53* (36), 14175.

(41) Divoux, G. M.; Finlay, K. A.; Park, J. K.; Song, J.-M.; Yan, B.; Zhang, M.; Dillard, D. A.; Moore, R. B. Morphological Factors Affecting the Behavior of Water in Proton Exchange Membrane Materials. **2011,** *41* (1), 87.

(42) Singhal, N.; Datta, A. Reversible tuning of chemical structure of Nafion cast film by heat and acid treatment. *J. Phys. Chem. B* **2015,** *119* (6), 2395.

(43) Luan, Y.; Zhang, Y.; Zhang, H.; Li, L.; Li, H.; Liu, Y. Annealing effect of perfluorosulfonated ionomer membranes on proton conductivity and methanol permeability. *J. Appl. Polym. Sci* **2008,** *107* (1), 396.

(44) Li, J.; Yang, X.; Tang, H.; Pan, M. Durable and high performance Nafion membrane prepared through high-temperature annealing methodology. *J. Memb. Sci* **2010,** *361* (1), 38.

(45) Modestino, M. A.; Kusoglu, A.; Hexemer, A.; Weber, A. Z.; Segalman, R. A. Controlling Nafion Structure and Properties via Wetting Interactions. *Macromolecules* **2012,** *45* (11), 4681.

(46) Kido, M.; Nojima, S.; Ishige, R.; White, K. L.; Kamitani, K.; Ohta, N.; Hirai,

T.; Takahara, A. Effect of molecular weight on microcrystalline structure formation in polymer with perylenediimide side chain. *J. Polym. Sci. B* **2016,** *54* (22), 2275.

(47) van der Heijden, P. C.; Rubatat, L.; Diat, O. Orientation of Drawn Nafion at Molecular and Mesoscopic Scales. *Macromolecules* **2004,** *37* (14), 5327.

(48) Mendil-Jakani, H.; Pouget, S.; Gebel, G.; Pintauro, P. N. Insight into the multiscale structure of pre-stretched recast Nafion® membranes: Focus on the crystallinity features. *Polymer* **2015,** *63*, 99.

(49) Brown, E.; Rae, P.; Dattelbaum, D.; Clausen, B.; Brown, D. J. E. m. In-situ measurement of crystalline lattice strains in polytetrafluoroethylene. *Experimental Mechanics* **2008,** *48* (1), 119.

(50) Schlick, S.; Gebel, G.; Pineri, M.; Volino, F. J. M. Fluorine-19 NMR spectroscopy of acid Nafion membranes and solutions. **1991,** *24* (12), 3517.

(51) Karan, K. PEFC catalyst layer: Recent advances in materials, microstructural characterization, and modeling. *Abbreviation: Curr. Opin. Electrochem* **2017,** *5* (1), 27.

(52) Page, K. A.; Cable, K. M.; Moore, R. B. Molecular Origins of the Thermal Transitions and Dynamic Mechanical Relaxations in Perfluorosulfonate Ionomers. *Macromolecules* **2005,** *38* (15), 6472.

(53) Fan, Y.; Tongren, D.; Cornelius, C. J. The role of a metal ion within Nafion upon its physical and gas transport properties. *Eur. Polym. J.* **2014,** *50*, 271.

Chapter 3 Elucidation of Substrate Influence on Morphology and Proton Transportation of Perfluorosulfonated Ionomer Thin Film

3.1 Introduction

Research activities in energy generation, conversion, and storage have dramatically increased due to the need for a sustainable energy infrastructure.[1-4] Among these new energy sources, polymer electrolyte fuel cells (PEFCs) are known for their high current density and use in sustainable stationary energy solutions.[5-8] In typical polymer electrolyte fuel cells, the electrochemical reactions occur on the carbon-supported platinum (Pt/C) covered by a solid-state proton conducting electrolyte. Among proton conducting materials, perfluorinated sulfonic-acid ionomer (Nafion), is one of the most widely used due to its high proton conductivity, and its thermal and chemical stability.[9-11] On the Pt/C catalyst, Nafion forms a semi-continuous film with nano-order thickness, and mass transport of such as protons, water, and oxygen, is performed through the film.[12-16] Controlling the structure of the Nafion thin-film on the Pt/C catalyst is important because the mass transport properties depend on the structure.

Nafion is composed of a hydrophobic polytetrafluoroethylene backbone (-CF_2-) with perfluorinated ether side-chains terminated by hydrophilic sulfonic acid groups (-SO_3H). The sulfonic acid groups exhibit high proton conductivity in a hydrophilic ionic domain.[14, 17-18] Free-standing Nafion membranes, which are a few hundred micrometers thick, have been widely investigated in past decades.[19-21] Several studies have revealed that cluster-networks or the parallel water channel model well describe the nanostructure in the Nafion membrane and proton conductivity ranging from ~10^{-1} to ~10^2 mS/cm is exhibited under 10–100% relative humidity at 25°C.[22-23]

However, Nafion thin-films on the Pt/C catalyst have a different structure from the free-standing Nafion membrane because of a strong confinement interaction between Nafion and the catalyst.[24-27] The proton conductivity of the Nafion thin-films is 1–2 orders of magnitude lower than that of a free-standing Nafion membrane and shows strong thickness-dependence under a certain relative humidity.[13, 18, 28] The confinement

effect is known to influence the phase behavior of uncharged block-copolymer systems.[29-35] In thin-films, both interactions with the substrate, and thickness confinement as small as the characteristic domain size of the copolymers, can cause anisotropy in the orientation of domains, resulting in morphologies that differ from that of the bulk membrane. [36-38]

In Nafion thin-films with thickness ranging from 35 to 80 nm cast on Pt over a C substrate, an ionomer peak attributed to the hydrophilic domain was observed in grazing-incidence small-angle X-ray scattering (GISAXS) experiments.[24-27] Among the results, the ionomer peak of Nafion thin film on Pt substrate showed the best-defined shape, while thin films on carbon substrate exhibited the most isotropic behavior among all sample on Au and Pt substrates. This was confirmed by Hicker using in situ ellipsometry.[32, 39] Other neutron experiments indicated that ionomer thin films are composed of alternating water-rich and Nafion-rich layers at the Nafion/SiO_2 interface, while such multilayer lamellae structure were not observed for Nafion on Au and Pt surfaces.40 These results suggest that thickness and substrate/film interactions control the reorganization and alignment of a phase-separated nanostructure, thereby altering the water-transport swelling properties.[32, 40-42] Although many studies have focused on the Nafion/substrate interfacial region, these have been limited to substrate dependency issues and to morphological changes due to substrate differences.

This work systematically analyzes the effect of confinement on platinum and carbon structures in Nafion thin films 10-200 nm thick on substrates. The morphology and proton conductivity of Nafion thin films were investigated using GISAXS/GIWAXS and electrochemical impedance, respectively. The confinement effect on the proton transport property of different substrates is discussed.

3.2 Experimental

Sample preparations

The Nafion dispersion solution was prepared by diluting 5 wt% Nafion (Aldrich, equivalent weight (EW) = 1100 stock dispersion) to 0.1-1.6 wt% with 99.5% 1,1,1,3,3,3-hexafluoro-2-propanol (Wako Pure Chemical Industries, Ltd.). All diluted solutions were given 30 min to equilibrate.

For conductivity measurements, as-prepared Nafion dispersion thin films were spin-cast onto as-prepared interdigitated array electrodes, of which details will be introduced below. As-prepared Nafion dispersion was dripped onto interdigitated array electrodes rotating at 800-1600 rpm for 2 min via the spin-cast method.

For GISAXS/GIWAXS measurements, a 20 nm Cr buffer layer was deposited on P-doped Si substrate (1×1 cm) using a Magnetron sputter device (MSP-30T, Vacuum Devices, Inc., Japan) under Ar gas at 8.0 $\times 10^{-1}$ Pa and 150 mA, for 1 min 47 s. Then, to mimic the Pt catalyst surface, a 30 nm Pt layer was fabricated in the same way on the as-prepared Si@Cr substrate under Ar gas at 8.0×10^{-1} Pa. Next, a 55-nm carbon layer was added to the same Si substrate used above, by the vacuum deposition method (VC-100S, VACUUM DEVICE). The same method was used to cast the Nafion thin films aforementioned. The rotation condition was set at 800-1600 rpm for 2 min.

Proton conductivity

Self-designed interdigitated array electrodes were fabricated by Osaka Vacuum Industrial Co., Ltd., of which the geometric details are shown in Figure S1. As shown in Figure S1, a 100 nm Pt layer was precisely deposited between Au-tooth electrodes with 0.008 mm spacing to avoid direct contact. Interdigitated array electrodes over carbon substrates were fabricated using the same method as aforementioned. Before being used, the interdigitated array electrodes were soaked in acetone solution for at least 1 h; then were sonicated for 5 min in isopropanol (Wako Pure Chemical Industries, Ltd.), acetone (Wako Pure Chemical Industries, Ltd.), and Millipore water, in succession. Finally, the interdigitated array electrodes were washed again in a sequence

of isopropanol, acetone, and Millipore water three times; then dried at 60 °C for at least 2 h.

The proton conductivity of the Nafion thin-films applied to the interdigitated array electrodes was measured using electrochemical impedance spectroscopy under a flow of dry N_2 gas through water tank. All measurements were conducted at 25 °C with 20-90% relative humidity (RH). The impedance data were collected by applying an alternative potential of 100 mV over a frequency ranging from 7 MHz to 0.01 Hz using a multi-potentiostat (VSP-300, Bio-logic). For equivalent circuit model design and data fitting, EC-lab (Version 11.18, Bio-logic) software was adopted.

GISAXS/GIWAXS

GISAXS and GIWAXS measurements were conducted in Spring at the BL40B2 beamline in Hyogo, Japan, where 12.4-keV X-ray GISAXS/GIWAXS measurements were conducted with 80% RH and at 25 °C. The GISAXS 2D image was collected with a Dectris Pilatus imaging plate (0.172 mm ×0.172 mm, C9729DK-10) and the GIWAXS detector used was a flat panel sensor (0.05 mm, Hamamatsu Photonics K. K., Japan). The sample-to-detector distance was set at 2200 mm and 60 mm for GISAXS and GIWAXS, respectively. GISAXS and GIWAXS were measured at an incidence angle 0.14° and the exposure time was 100 s for all samples. Silver behenate and CeO_2 were used for calibration of the beam center and sample detector distance for GISAXS and GIWAXS, respectively. The experimental setup is shown in Figure S2 (supporting information).

3.3 Results and Discussion

Figure 1 shows the proton conductivity of Nafion thin films cast on Pt and carbon substrates at 25 °C and various RH values. The collected Nyquist plot are shown in Figure S5 in the supporting information. Both Pt- and carbon-supported Nafion thin

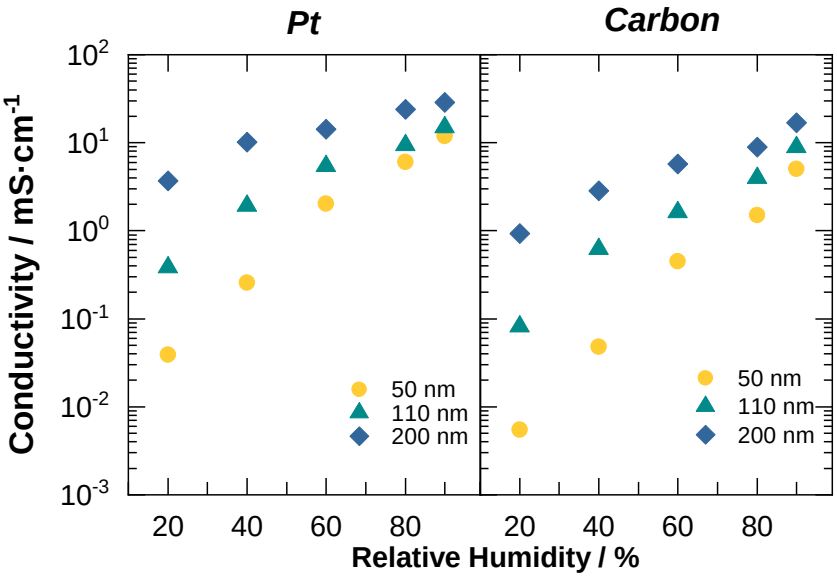

Figure 1 The Proton conductivity of Nafion thin films on Pt and carbon substrates with a variety of thicknesses and relative humidity at 25 °C

films exhibit thickness dependence. Compared to the carbon-supported films, the Pt-supported films showed higher conductivity values at the same RH. In the case of 50-nm-thick films, proton conductivity of the Pt-supported specimen was almost an order of magnitude higher than that of the carbon-supported specimen. However, as the thickness approached 200 nm, the difference in proton conductivity of Pt and carbon-supported films reduced by an order of magnitude. This trend indicates that the bulk structure of the ionomer has more influence on the conductivity than its interaction with the substrate, as the thickness increases. Karan and Nagao's groups reported that the conductivity of Nafion thin film on SiO_2 showed similar tendencies and values.[13, 18] Thus, it is considered that the results in Figure 1 correctly reflect the actual differences in conductivity on these different substrates.

GISAXS measurements were performed to examine the morphological change of Nafion thin films relative to their thickness. Comparisons of GISAXS 2D patterns of Nafion thin films on Pt and carbon substrates are shown in Figure 2. The scattering patterns are plotted in two dimensions as a function of the scattering vector q, which is defined in equation (1).

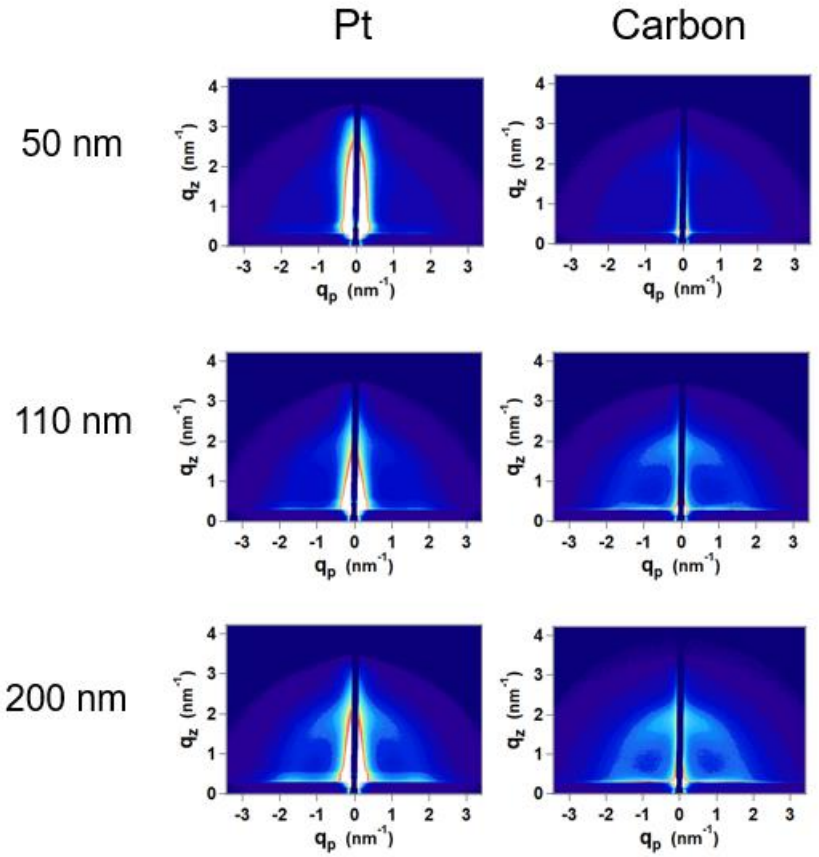

Figure 2 GISAXS 2D patterns of Nafion thin films with a variety of thicknesses (50-200 nm) and substrate (Pt, carbon) measured at 80% RH and 25 °C.

$$\mathbf{q} = \begin{pmatrix} q_x \\ q_y \\ q_z \end{pmatrix} = \frac{2\pi}{\lambda} \begin{pmatrix} \cos 2\Theta \cos \alpha_f - \cos \alpha_i \\ \sin 2\Theta \cos \alpha_f \\ \sin \alpha_i + \cos \alpha_f \end{pmatrix} \quad [1]$$

Here, λ represents the wavelength of the incident X-rays. The thickest film exhibited a scattering ring at q ~1.5–2 nm^{-1}, which is assigned to the ordered structure of the hydrophilic domains in Nafion thin film, and is called the "ionomer peak".[30] Examination of the Pt- and carbon-supported samples at high humidity (Figure 2) demonstrates that increasing thickness seems to cause more significant changes in films on Pt substrates than in films on carbon substrates.

To explore the variation of ionomer peaks in relation to the film thickness, line integral analysis was utilized to extract the I-q line profile. The cut lines along the

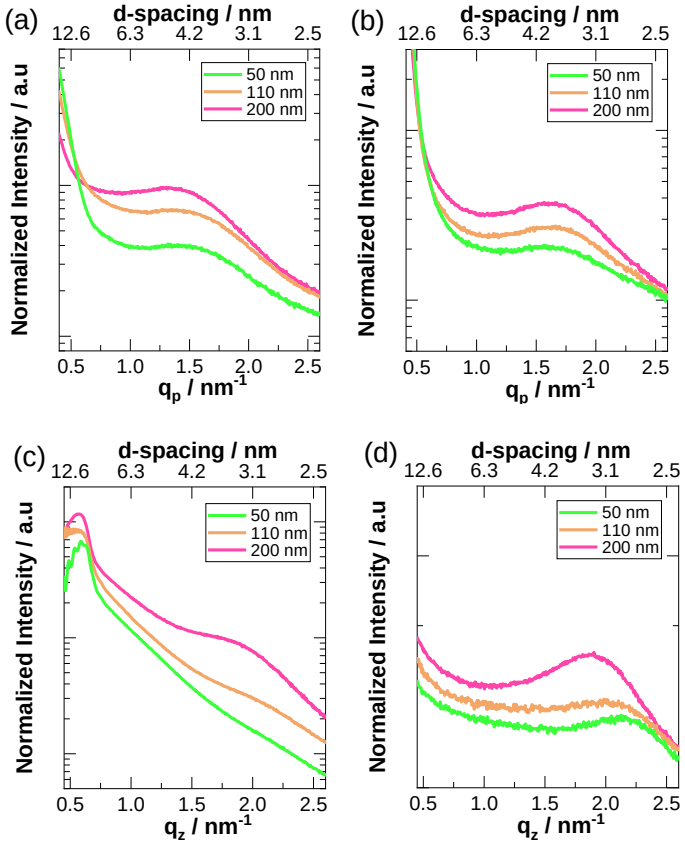

Figure 3 GISAXS 1D line-profile along the in-plane: (a) Pt and (b) Carbon, and out-of-plane: (c) Pt and (d) Carbon

equatorial and meridional direction reflect the ordered structure in-plane and out-of-plane, respectively. The as-obtained line-profiles of the Nafion thin films on Pt and carbon are shown in Figure 3. It was found that the ionomer peak on Pt had a better-defined and sharper ionomer peak than carbon along the in-plane direction (a and b), suggesting a better-defined order in the ionic domain. However, when the film thickness decrease, the ionomer scattering peaks were not obvious, which indicate the existence of a less-ordered domain structure due to the strong confinement effect. Similar tendencies were found in the out-of-plane direction (Figure 3c and d) as well.

Ionomer conductivity is a strong function of the humidity level and the proximity of adjacent ionic clusters. The former can be related to the relative humidity, and the latter can be interpreted as d-spacing. The latter is also a precursor and indicator of the ease of forming an H-bond network. Such a network is critical, especially with low relative

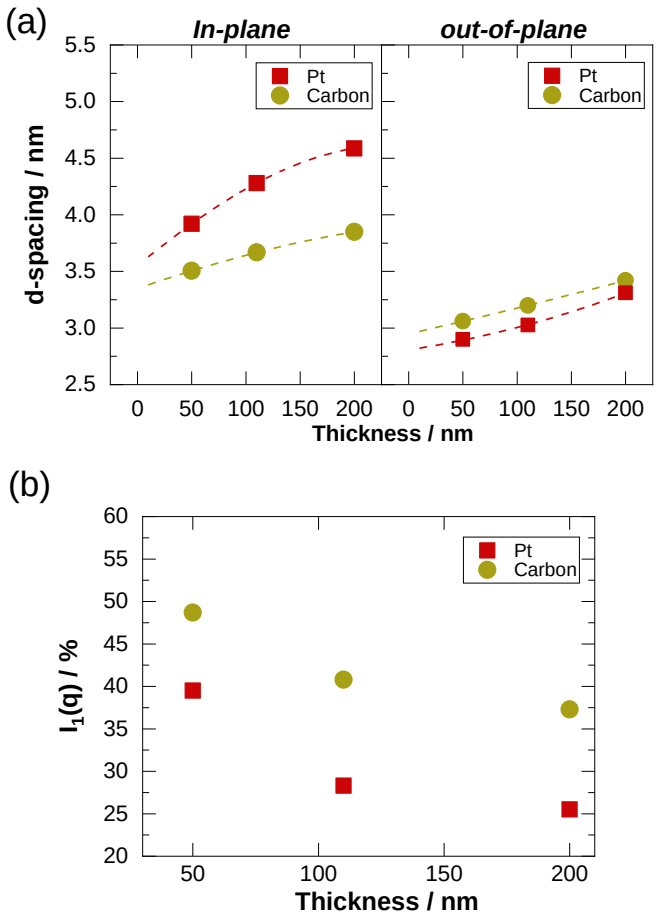

Figure 4 (a) d-spacing of hydrophilic ionic domain extracted from Figure 3 in-plane and out-of-plane with 80% RH at 25 °C. (b) Ratio of the ionomer contribution along the out-of-plane direction. The values were calculated on the basis of $I_1(q) / (I_1(q) + I_2(q)) \times 100$.

humidity.[42] The ionomer peak observed in Figure 3 was fitted to a Gaussian function, and the peak position values along the in-plane and out-of-plane directions were estimated (Figure 3(a)). The scattering vector q, expressed in reciprocal space, was converted to d-spacing in real space using the following equation:

$$d = \frac{2\pi}{q} \qquad [2]$$

As shown in Figure 3(a), the ionomer peak shifted to higher d-spacing values with increasing film thickness in both samples owing to the growth of the ionic domains.

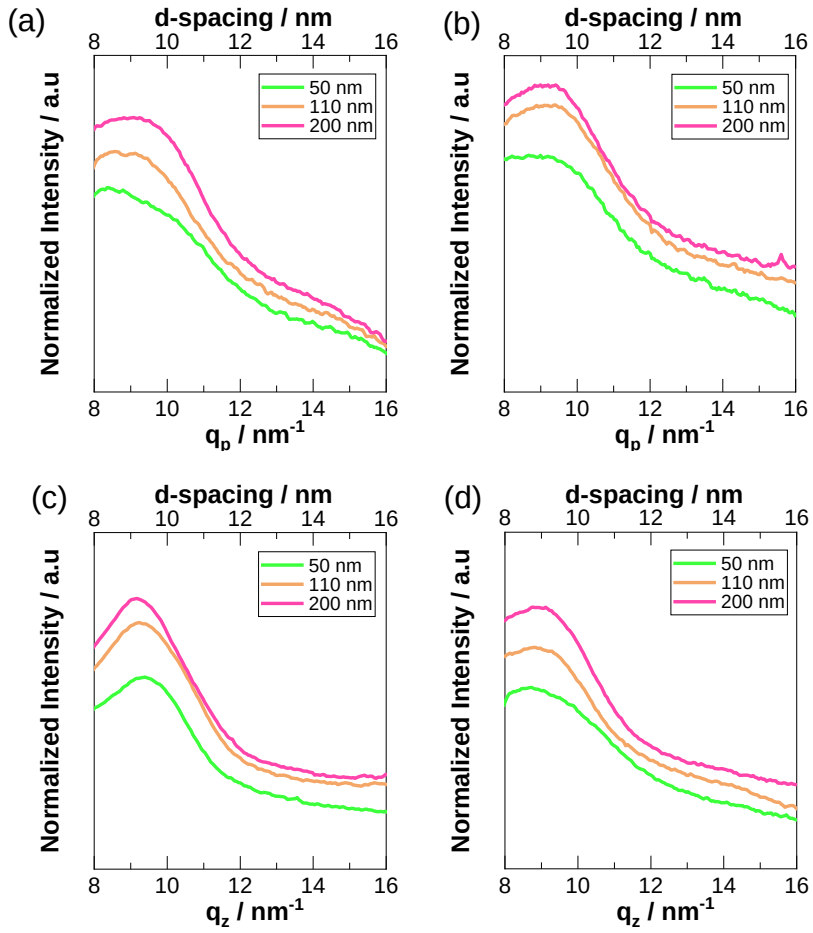

Figure 5 GIWAXS line-profile extracted from 2D patterns of Nafion thin films in-plane: (a) Pt and (b) Carbon, and out-of-plane: (c) Pt and (d) Carbon.

Along the in-plane direction, the d-spacing of the ionic domains in Pt- and carbon supported films increased from 3.9 to 4.6 nm and from 3.5 to 3.7 nm, respectively.

Periodic ionic domains and semi-crystalline hydrophobic structures were formed in the 50-nm-thick films, which led to higher conductivity values. For the Nafion thin films with thickness over 110 nm, the hydrophilic domains grew considerably because of the relatively stronger nanophase separation than that in the thinner films. The hydrophilic domains, which act as the protonic path, grew larger with increasing humidity and thickness, leading to a lower activation energy of the proton conduction process.

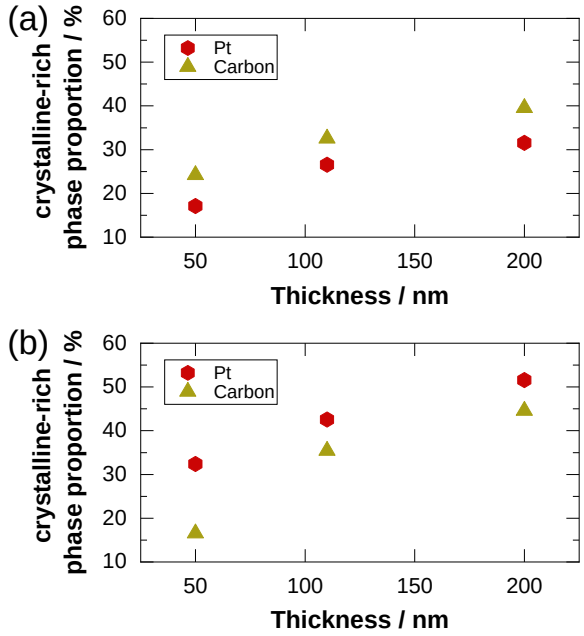

Figure 6 The Crystalline-rich phase proportion in Nafion thin films of various thicknesses and on different substrates along (a) In-plane and (b) Out-of-plane directions.

In order to quantitatively comparison of the intensity of ionomer peak along meridional and equatorial axes, represented as I_1 and I_2, respectively, we normalized the curves using the integrated intensity of ionomer peak with same method as our previous work.[38] I_1 (out-of-plane) and I_2 (in-plane) are assumed to be Gaussian distribution functions of the azimuthal angle φ, with peaks along the meridional (φ = 0°) and equatorial (φ = 90°) direction, respectively. The obtained I_1 (φ) and I_2 (φ) were then used to determine the normalized intensity I(q), as defined by the following equation.[43]

$$I_i(q) \approx \int_0^{\frac{\pi}{2}} I_i(\varphi) 2\pi q \left|\sin\varphi\right| d\varphi \qquad [3]$$

The normalized intensity of the ionomer peak along the meridian (i = 1) and the equator (i = 2) was evaluated using equation (3). An illustration of a typical azimuthal plot fitting is shown in Figure S6. For all samples, a low χ^2 value ($\leqslant$ 2.19) was obtained.

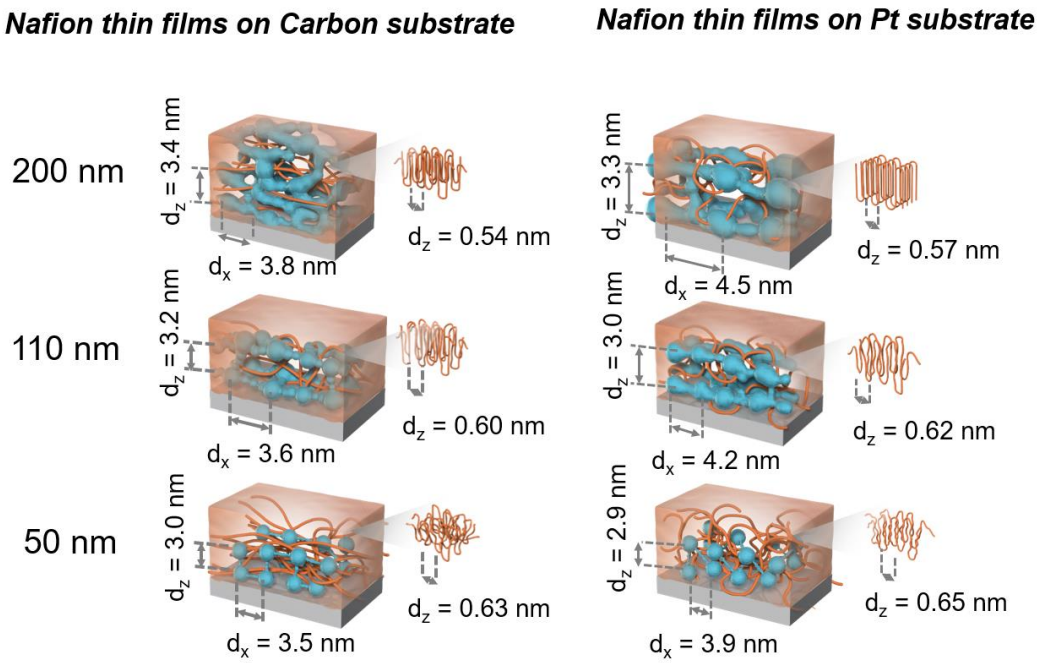

Figure 7 Schematic image of Nafion thin film structure with different morphological behavior on carbon and Pt substrates.

As shown in Figure 4(b), the I_I(q) (%) increased with decreasing thickness, regardless of substrate, which indicate that the contribution of out-of-plane component comparatively increased as decreasing thickness. Additionally, the I_I(q) on the Pt was comparatively lower than that on the carbon, which suggest that the hydrophilic domain in Pt-supported Nafion is more orientated. Furthermore, it might indicate the hydrophilic domains grew better along the in-plane direction on Pt than on carbon. The hydrophilic domains in Nafion thin films show different anisotropic behavior depending on the substrate. The substrate influences the crystalline phase of the fluorocarbon backbone as well as the hydrophilic ionic domains in the Nafion films. To examine the molecular aggregation in the hydrophobic domains of the Nafion films, GIWAXS measurements were performed at 25 °C and 80 % RH. Figure S7 shows the 2D GIWAXS patterns and Figure 5 shows the GIWAXS line profiles of the Nafion thin films on Pt and carbon substrates.

The influence of the substrate was evident from variation of a scattering halo indicative of amorphous/crystalline component. For instance, the line profiles (Figure 5(a)) showed that increasing thickness caused a crystalline peak to appear near q = 11 nm^{-1}, which was next to the amorphous peak at 9.5 nm^{-1}.[29, 44-45] This thickness-induced crystalline order, with a characteristic spacing around 0.5 nm, corresponds to the (-CF_2-) backbone chains of the polytetrafluoroethylene crystallites, similar to the typical wide angle X-ray scattering peak observed for the free-standing Nafion membranes.[29] These crystallites form a crystalline structure, which leads to physical crosslinking of the (-CF_2-) backbone and consequent reduction in the proton conductivity. The formation of a crystalline order was observed in Figure 5 by the shifts in the crystalline peak around q = 11 nm^{-1}. For both Pt- and carbon-supported thin films, as the film thickness decreased to 50 nm, (Figure 5(a) and (b)), the crystalline order is expected to decrease, because the backbone chains become topologically confined at such a thickness.[33] Additionally, in case of Pt-supported Nafion thin films, it is notable that the observed amorphous/crystalline peak in out-of-plane component is more defined and sharper than that of in-plane component. The opposite phenomenon was observed for carbon-supported thin films.

Here, we introduced an indicator: crystalline-rich domain proportion ($P_{c\text{-}rich}$), to gain further insight regarding the relative variation in the semi-crystalline (-CF_2-) backbone aggregation on different substrates. Figure 6 shows the Pc-rich in various Nafion thin films; the $P_{c\text{-}rich}$ values were extracted from the as-obtained 2D scattering parttern (Figure S7). The detail of the calculation method is described in Figure S8 and our previous study.[38] Generally, the Pc showed thickness dependence on both substrates. Interestingly, $P_{c\text{-}rich}$ of the thin films on the Pt substrate along the out-of-plane direction showed higher values than that on the carbon substrate, while showing the opposite trend along the in-plane direction.

We have shown our conceptual model of the morphology of Nafion thin films with thickness ranging from 50-200 nm on Pt and carbon substrates in Figure 7. In the case of the Nafion thin film with 50 nm thickness, the hydrophilic domain along in-plane

direction in Pt-supported Nafion thin films is comparatively larger than carbon supported Nafion thin films. This is because the interaction between the sulfonic acid and Pt is relatively strong than the interaction between the sulfonic acid and carbon.[29] The development of hydrophilic domain on Pt substrate increase the proton conductivity, compared to carbon substrate as shown in Figure 1. The in-plane proton conductivity difference between Pt and carbon become small as the thickness of Nafion thin-film increases because the interaction between ionomer and substrate become relatively small. On the other hand, we proved that the hydrophilic domain along in-out-of-plane direction in Pt-supported Nafion thin films is comparatively smaller than carbon supported Nafion thin films. It is anticipated that the proton conductivity along out-of-plane direction in Pt supported Nafion thin films is not as high as in carbon supported thin films based on the relationship between the hydrophilic domain and proton conductivity of in-plane in Nafion thin films.

3.4 Conclusion

We focused on a series of Nafion films with thickness ranging from 50 to 200 nm to reveal differences in confinement effect and impacts from type of substrate. This was done in terms of morphology and proton transport property via GISAXS/GIWAXS and the electrochemical impedance method. Within this range of film thickness, substrate/ionomer interaction are expected to have a significant impact on the structure of the ionomer. Thin films on Pt exhibit completely different anisotropic behavior than those on carbon substrate. In the case of Pt, that the hydrophilic ionic domain along the in-plane direction is more developed than that along the out-of-plane shows obviously significant behavior. Interestingly, as the film thickness reaches, in essence, bulk phase (200 nm), the difference in conductivity between carbon and Pt substrates becomes almost negligible. It is anticipated that the proton in-plane conductivity in the Nafion thin films is higher than out-of-plane conductivity, because the in-plane size of the hydrophilic domains is larger than their out-of-plane size. The knowledge about the

relationship between the proton transport and morphology of Pt and carbon supported Nafion thin films, is useful to design proton transport pathway of practical catalyst.

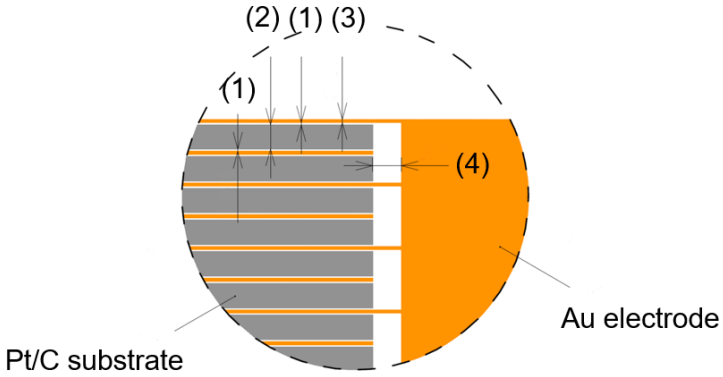

(1) Distance between electrode and Pt or carbon substrate : 0.008 mm
(2) Width of Pt or carbon substrate : 0.084 mm
(3) Width of Au electrode : 0.01 mm
(4) Spacing between Pt or carbon substrate to side : 0.1 mm

Electrode numbers : 72

Figure S1. The schematic image of interdigitated array (IDA) electrode used for proton conductivity measurement. Au electrodes were deposited on glass substrate. The detailed information of IDAs were described in the main text

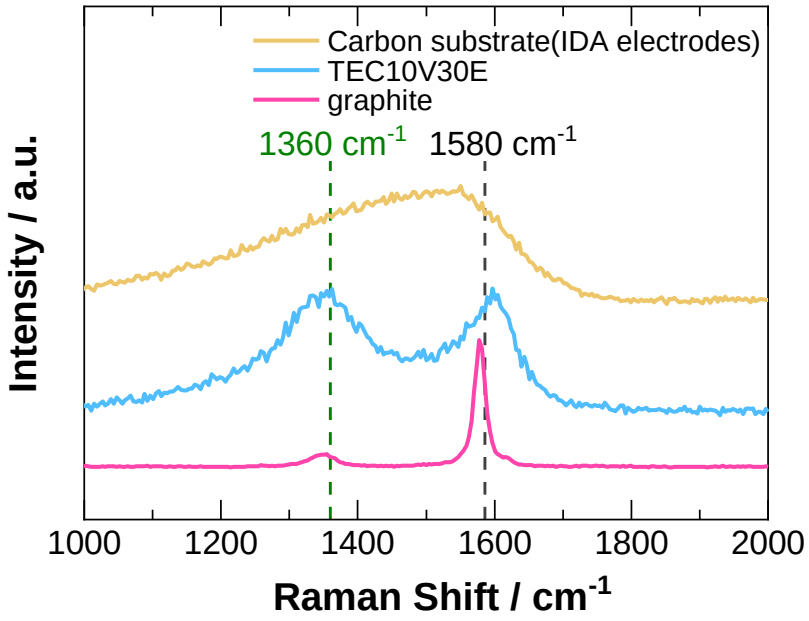

Figure S3. The Raman spectroscopy of carbon substrate of IDA electrodes (yellow), TEC10V30E (blue) and graphite (pink). The TEC10V30E and graphite here are used as reference. The peak around 1360 cm^{-1} and 1580 cm^{-1} are assigned to D band and G band. The carbon substrate of IDA electrodes used in this study exhibited amorphous-like structure.

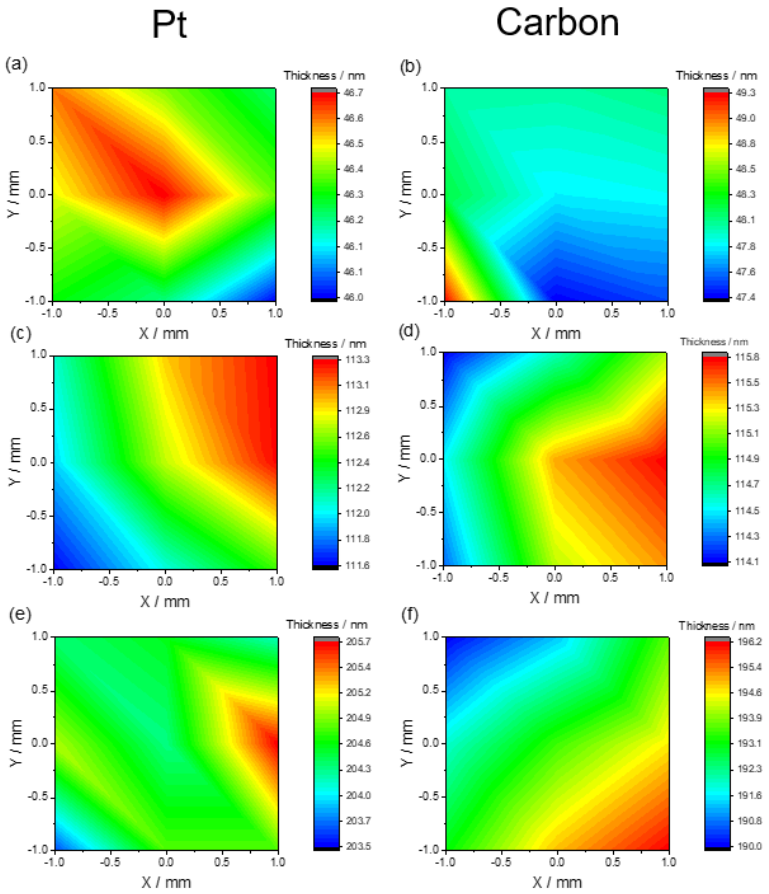

Figure S3. The ellipsometry mapping of cast thin films with various thicknesses on Pt ((a) 50 nm (c) 110 nm (e) 200 nm) and carbon((b) 50 nm (d) 110 nm (f) 200 nm) substrate. The difference in film thickness on Pt substrate was 0.7 nm, 1.7 nm and 2.2 nm for 50, 110 and 200 nm thick Nafion thin films. For carbon supported thin films, the difference was 1.9 nm, 1.7 nm and 6.2 nm for 50, 110 and 200 nm thick Nafion thin films.

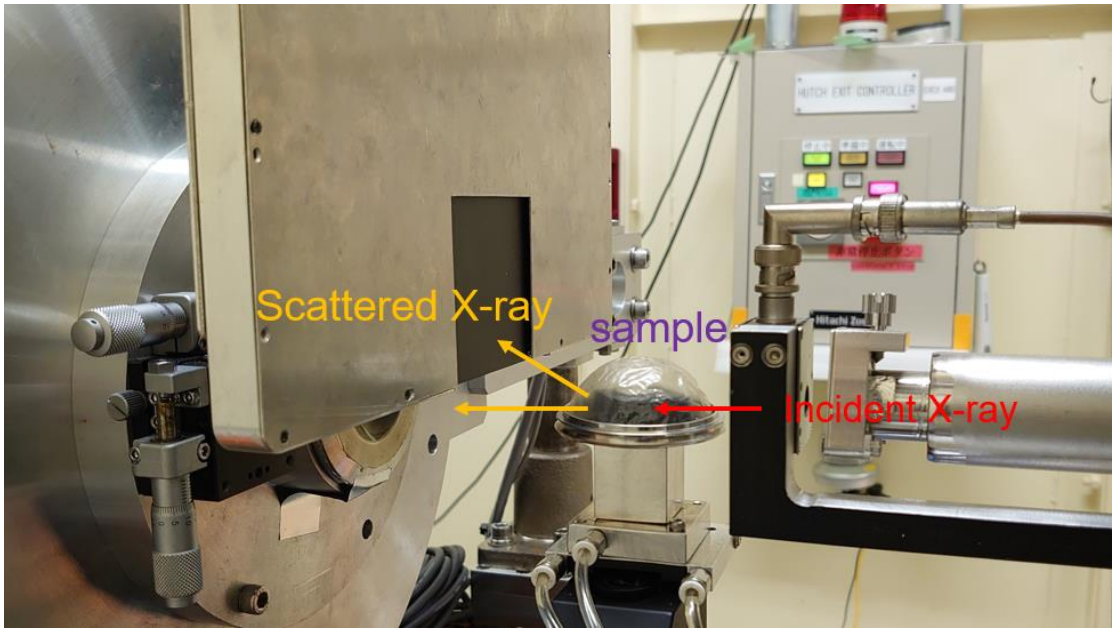

Figure S4. The schematic image of GISAXS/GIWAXS measurement. Continuous N2 flow was transport into chamber with 25 μm PEEK film to maintain constant humidity level.

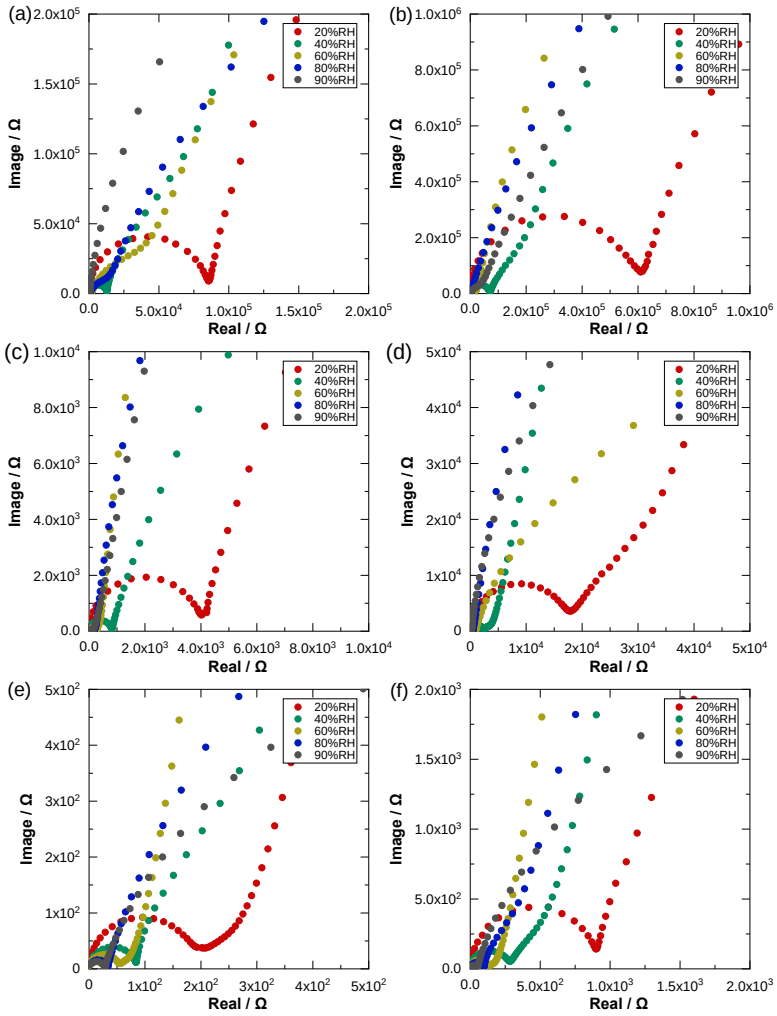

Figure S5. Nyquist plot of Nafion thin film with various thickness and Pt ((a): 50 nm, (c): 110 nm, (e): 200 nm,) and carbon ((b): 50 nm, (d): 110 nm, (f): 200 nm) with various relative humidity under 25oC via electrochemical impedance method.

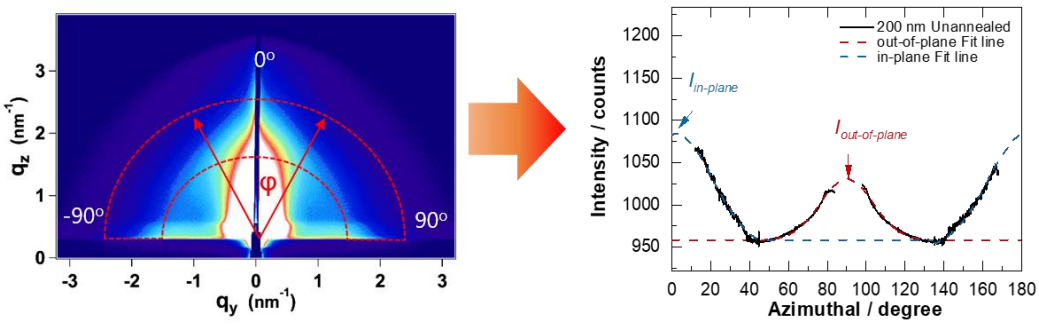

Figure S6. The illustration of normaalization method used in this manuscript. Ionomer peak was extracted from the scattering from in 2D pattern(left) to azimuthal plot and fitted with Gaussian function.

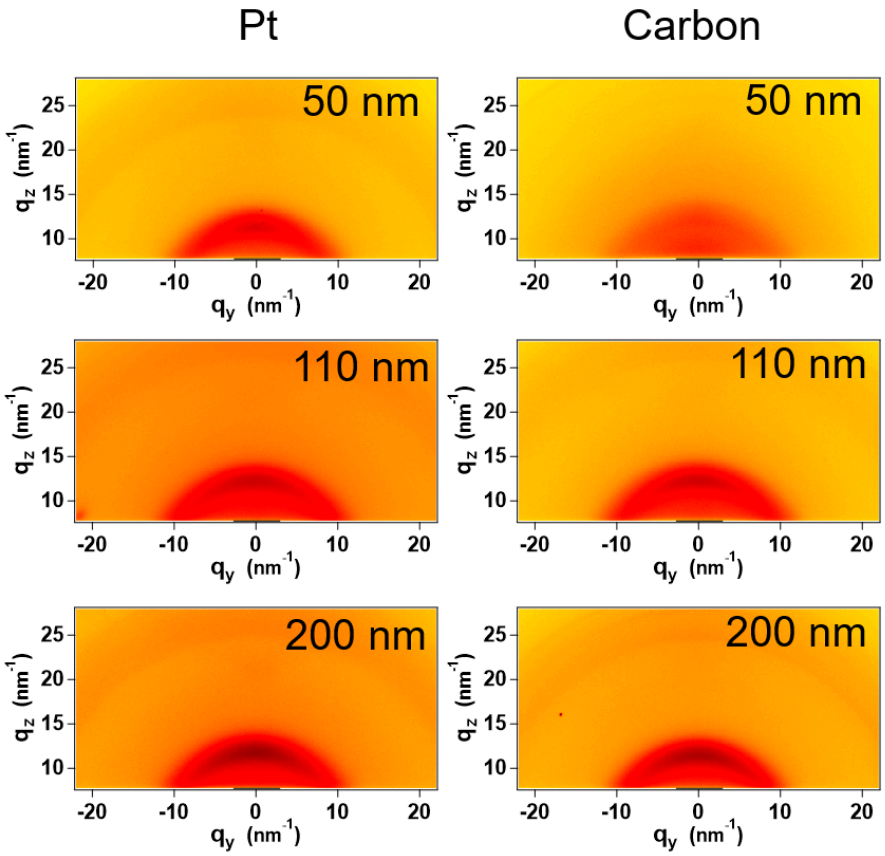

Figure S7. GIWAXS 2D pattern of Nafion thin film with various thicknesses on Pt and Carbon substrate at 25oC 80%RH.

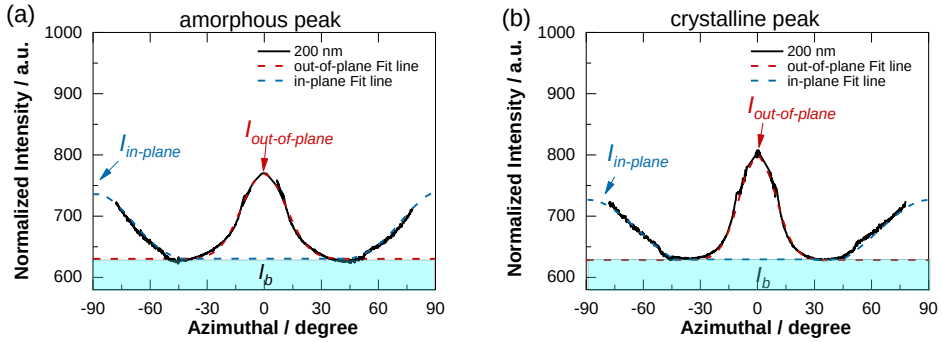

Figure S8. The typical illustration of crystalline-rich phase proportion fitting results of 200 nm thick Pt supported Nafion thin films. Azimuthal plot was extracted from GIWAXS 2D patterns shown in Figure S3. The in-plane and out-of-plane fit line are best-fit curve of the amorphous/crystalline peak. Ib represents the non-orientation component in hydrophobic domain, which is considered as the background. The detailed information of calculation procedure was based on our previous work.

Reference

(1) Eikerling, M.; Kulikovsky, A. *Polymer Electrolyte Fuel Cells: Physical Principles of Materials and Operation*; CRC Press, 2014.

(2) Franco, A. A. Polymer Electrolyte Fuel Cells: Science, *Applications, and Challenges*; Pan Stanford Publishing, 2016.

(3) Kreuer, K. D. Fuel Cells: *Selected Entries from the Encyclopedia of Sustainability Science and Technology*; Springer New York, 2012.

(4) Li, H.; Knights, S.; Shi, Z.; Van Zee, J. W.; Zhang, J. *Proton Exchange Membrane Fuel Cells: Contamination and Mitigation Strategies*; CRC Press, 2010.

(5) O'Hayre, R.; Cha, S. W.; Prinz, F. B.; Colella, W. *Fuel Cell Fundamentals*; Wiley, 2016.

(6) Pu, H. *Polymers for PEM Fuel Cells*; Wiley, 2014.

(7) Santos, E.; Schmickler, W. *Catalysis in Electrochemistry: From Fundamental Aspects to Strategies for Fuel Cell Development*; Wiley, 2011.

(8) Zhang, J.; Wu, J.; Zhang, H. *PEM Fuel Cell Testing and Diagnosis*; Elsevier Science, 2013.

(9) Mauritz, K. A.; Moore, R. B. State of Understanding of Nafion. *Chem. Rev*. **2004**, *104* (10), 4535.

(10) Sheng, W.; Chen, S.; Vescovo, E.; Shao-Horn, Y. Size Influence on the Oxygen Reduction Reaction Activity and Instability of Supported Pt Nanoparticles. *J. Electrochem. Soc*. **2012**, *159* (2), B96.

(11) Holdcroft, S. Fuel Cell Catalyst Layers: A Polymer Science Perspective. *Chem. Mater.* **2014**, *26* (1), 381.

(12) Jinnouchi, R.; Kudo, K.; Kitano, N.; Morimoto, Y. Molecular Dynamics Simulations on O_2 Permeation through Nafion Ionomer on Platinum Surface. *Electrochim. Acta* **2016**, *188*, 767.

(13) Paul, D. K.; McCreery, R.; Karan, K. Proton Transport Property in Supported

Nafion Nanothin Films by Electrochemical Impedance Spectroscopy. *J. Electrochem. Soc*. **2014**, *161* (14), F1395.

(14) Modestino, M. A.; Paul, D. K.; Dishari, S.; Petrina, S. A.; Allen, F. I.; Hickner, M. A.; Karan, K.; Segalman, R. A.; Weber, A. Z. Self-Assembly and Transport Limitations in Confined Nafion Films. *Macromolecules* **2013**, *46* (3), 867.

(15) Siroma, Z.; Ioroi, T.; Fujiwara, N.; Yasuda, K. Proton conductivity along interface in thin cast film of Nafion®. *Electrochem. Commun.* **2002**, *4* (2), 143.

(16) Siroma, Z.; Kakitsubo, R.; Fujiwara, N.; Ioroi, T.; Yamazaki, S.-i.; Yasuda, K. Depression of proton conductivity in recast Nafion® film measured on flat substrate. *J. Power Sources* **2009**, *189* (2), 994.

(17) Schmidt-Rohr, K.; Chen, Q. Parallel cylindrical water nanochannels in Nafion fuel-cell membranes. Nat. Mater. **2008**, *7* (1), 75.

(18) Ono, Y.; Nagao, Y. Interfacial Structure and Proton Conductivity of Nafion at the Pt-Deposited Surface. *Langmuir* **2016**, *32* (1), 352.

(19) Kusoglu, A.; Weber, A. Z. New Insights into Perfluorinated Sulfonic-Acid Ionomers. *Chem. Rev*. **2017**, *117* (3), 987.

(20) Kreuer, K.-D.; Paddison, S. J.; Spohr, E.; Schuster, M. Transport in Proton Conductors for Fuel-Cell Applications: Simulations, Elementary Reactions, and Phenomenology. *Chem. Rev*. **2004**, *104* (10), 4637.

(21) Kreuer, K.-D.; Portale, G. A Critical Revision of the Nano-Morphology of Proton Conducting Ionomers and Polyelectrolytes for Fuel Cell Applications. *Adv. Funct. Mater.* **2013**, *23* (43), 5390.

(22) Berrod, Q.; Lyonnard, S.; Guillermo, A.; Ollivier, J.; Frick, B.; Manseri, A.; Améduri, B.; Gébel, G. Nanostructure and Transport Properties of Proton Conducting Self-Assembled Perfluorinated Surfactants: A Bottom-Up Approach toward PFSA Fuel Cell Membranes. *Macromolecules* **2015**, *48* (17), 6166.

(23) Rodgers, M. P.; Bonville, L. J.; Kunz, H. R.; Slattery, D. K.; Fenton, J. M. Fuel cell perfluorinated sulfonic acid membrane degradation correlating accelerated stress testing and lifetime. *Chem. Rev*. **2012**, *112* (11), 6075.

(24) Paul, D. K.; Fraser, A.; Karan, K. Towards the understanding of proton conduction mechanism in PEMFC catalyst layer: Conductivity of adsorbed Nafion films. *Electrochem. Commun.* **2011**, *13* (8), 774.

(25) Paul, D. K.; Karan, K. Conductivity and Wettability Changes of Ultrathin Nafion Films Subjected to Thermal Annealing and Liquid Water Exposure. *J. Phys. Chem. C* **2014**, *118* (4), 1828.

(26) Frieberg, B. R.; Page, K. A.; Graybill, J. R.; Walker, M. L.; Stafford, C. M.; Stafford, G. R.; Soles, C. L. Mechanical Response of Thermally Annealed Nafion Thin Films. *Appl. Mater. Interfaces* **2016**, *8* (48), 33240.

(27) Nagao, Y. Highly Oriented Sulfonic Acid Groups in a Nafion Thin Film on Si Substrate. *J. Phys. Chem. C* **2013**, *117* (7), 3294.

(28) Dishari, S. K.; Hickner, M. A. Confinement and Proton Transfer in NAFION Thin Films. *Macromolecules* **2013**, *46* (2), 413.

(29) Kusoglu, A.; Kushner, D.; Paul, D. K.; Karan, K.; Hickner, M. A.; Weber, A. Z. Impact of Substrate and Processing on Confinement of Nafion Thin Films. *Adv. Funct. Mater.* **2014**, *24* (30), 4763.

(30) Kusoglu, A.; Dursch, T. J.; Weber, A. Z. Nanostructure/Swelling Relationships of Bulk and Thin-Film PFSA Ionomers. *Adv. Funct. Mater.* **2016**, *26* (27), 4961.

(31) Plazanet, M.; Torre, R.; Sacchetti, F. Confinement, entropic effects and hydrogen bond network fluctuations of water in Nafion membrane. *J. Mol. Liq* **2016**, *219*, 1161.

(32) Tesfaye, M.; MacDonald, A. N.; Dudenas, P. J.; Kusoglu, A.; Weber, A. Z. Exploring substrate/ionomer interaction under oxidizing and reducing environments. *Electrochem. Commun.* **2018**, *87*, 86.

(33) Karan, K. Interesting Facets of Surface, Interfacial, and Bulk Characteristics of Perfluorinated Ionomer Films. *Langmuir* **2019**, *35*(42), 13489

(34) Page, K. A.; Kusoglu, A.; Stafford, C. M.; Kim, S.; Kline, R. J.; Weber, A. Z. Confinement-driven increase in ionomer thin-film modulus. *Nano Lett.* **2014**, 14 (5), 2299.

(35) Tesfaye, M.; Kushner, D. I.; Kusoglu, A. Interplay between Swelling Kinetics

and Nanostructure in Perfluorosulfonic Acid Thin-Films: Role of Hygrothermal Aging. *ACS Applied Polymer Materials* **2019**, *1* (4), 631.

(36) Bass, M.; Berman, A.; Singh, A.; Konovalov, O.; Freger, V. Surface Structure of Nafion in Vapor and Liquid. *J. Phys. Chem. B* **2010**, *114* (11), 3784.

(37) Bass, M.; Berman, A.; Singh, A.; Konovalov, O.; Freger, V. Surface-Induced Micelle Orientation in Nafion Films. *Macromolecules* **2011**, *44* (8), 2893.

(38) Gao, X.; Yamamoto, K.; Hirai, T.; Uchiyama, T.; Ohta, N.; Takao, N.; Matsumoto, M.; Imai, H.; Sugawara, S.; Shinohara, K. Morphology Changes in Perfluorosulfonated Ionomer from Thickness and Thermal Treatment Conditions. *Langmuir* **2020**, *36* (14), 3871.

(39) Karan, K. PEFC catalyst layer: Recent advances in materials, microstructural characterization, and modeling. Abbreviation: Curr. Opin. *Electrochem* **2017**, *5* (1), 27.

(40) Kushner, D. I.; Kusoglu, A.; Podraza, N. J.; Hickner, M. A. Substrate - Dependent Molecular and Nanostructural Orientation of Nafion Thin Films. *Adv. Funct. Mater.* **2019**, *29*, 1902699.

(41) Goossens, P. J.; Vallaey, B.; Verlinden, J.; Martens, J. A.; Rongé, J. Interfacial Water Drives Improved Proton Transport in Siliceous Nanocomposite Nafion Thin Films. *ChemPhysChem* **2018**, *19* (4), 538.

(42) Iden, H.; Sato, K.; Ohma, A.; Shinohara, K. Relationship among Microstructure, Ionomer Property and Proton Transport in Pseudo Catalyst Layers. *J. Electrochem. Soc.* **2011**, *158* (8), B987.

(43) Shoji, Y.; Ishige, R.; Higashihara, T.; Morikawa, J.; Hashimoto, T.; Takahara, A.; Watanabe, J.; Ueda, M. Cross-Linked Liquid Crystalline Polyimides with Siloxane Units: Their Morphology and Thermal Diffusivity. *Macromolecules* **2013**, *46* (3), 747.

(44) van der Heijden, P. C.; Rubatat, L.; Diat, O. Orientation of Drawn Nafion at Molecular and Mesoscopic Scales. *Macromolecules* **2004**, *37* (14), 5327.

(45) Giffin, G. A.; Haugen, G. M.; Hamrock, S. J.; Di Noto, V. Interplay between

Structure and Relaxations in Perfluorosulfonic Acid Proton Conducting Membranes. *J. Am. Chem. Soc*. **2013**, *135* (2), 822.

Chapter 4 The role of water of cast Nafion thin films in morphological and proton transport view

4.1 Introduction

Polymer electrolyte fuel cells (PEFCs) have received extraordinary attention for the past several decades due to its high efficiency, high power density and zero emission as fuel cell vehicles to microelectronics.[1-4] In polymer electrolyte fuel cells, oxygen reduction reaction (ORR) occurs on carbon-supported platinum (Pt/C) covered by proton conductive perfluorosulfonated ionomers. Nafion® is the most well-known proton conductive material due to its high proton conductivity, thermal stability and mechanical properties.[5-9] Nafion consists of a hydrophobic polytetrafluoroethylene backbone ($-CF_2-$) with perfluorinated chains on either side that are terminated by hydrophilic sulfonic acid groups ($-SO_3H$).[10,11] In the presence of water, the hydrophilic phase forms an ionic domain responsible for proton transport, while the hydrophobic phase aggregates and provides a high-stability polymer.[8,9,12] The electrochemical properties such as proton conductivity of Nafion thin films on the catalyst is different from those of free-standing Nafion membranes.[13-15] These are because as the ionomer thickness approaches the domain size of the copolymers, the confinement effect caused by the ionomer/electrode interaction can significantly influence the domain orientations and anisotropy in Nafion thin fillms.[16,17] Thus, it is crucial to reveal the relationship between the morphology and electrochemical properties in the Nafion thin films on the catalyst.

In the electrode fabrication for PEFCs, Nafion is cast on the Pt/C catalyst by using catalyst ink of mixture of Nafion dispersion and Pt/C catalyst and exists as a thin-film with a few nanometer thicknesses. It has been reported that the molecular structure and properties of the Nafion in the dispersion is influenced by the solvents.[18-25] In high dielectric constant solvent such as water, the Nafion has a tightly packed structure with the sulfonic group on the outside and the perfluorocarbon backbone on the inside of the molecule.[18,20,21,26] In low dielectric constant solvent such as isopropyl alcohol (IPA),

the Nafion has a loosely packed structure with the perfluorocarbon backbone on the outside and the sulfonic group on the inside of the molecules.[26,27] In mixed solution between water and IPA, the molecular structure of Nafion changes from the tightly packed structure to the loosely packed structure as the [IPA]/[IPA+water] ratio increases.[27] These molecular structures of the Nafion in the dispersion affects the electrode performance of PEFCs.[24,25,27,28] These solvent effect must also change the interaction driving ionomer-particle aggregation in an ink, because inks with different water/alcohol ratios exhibits different aggregate sizes.[29-31] Ngo.el.al. revealed that the aggregate particle size of Nafion molecule decrease with the increasing IPA concentration from 20 to 80 wt% of IPA/water solvents via transmission electron microscopy.[27] The similar tendency was also observed by Neyerlin *et.al*., who revealed that the aggregate size of Nafion molecules increases with increasing water centration.[32] Although, several efforts have been devoted to clarify the molecular structure of Nafion in the dispersion with various solvents, or different IPA/water ratio. However, these studies focused on the Nafion in dispersion state but not the film. Up to now, it has not been clearly understood the relationship among the morphology and proton transport properties of Pt supported Nafion thin-film cast by Nafion dispersion with different IPA/water ratio.

In order to analyze the morphology of thin-film Nafion on catalyst, grazing incidence small angle X-ray scattering (GISAXS) / grazing incidence wide angle X-ray scattering (GIWAXS) are powerful tools.[16,33-36] Our group also proved that the quantitative relationship between morphology and proton transporting properties of Nafion thin films with various thicknesses after annealing treatment on Pt substrate by using these techniques combined with Pt deposited interdigitated array electrodes.[37] Those tools are useful to understand the relationship between morphology and proton conductivity of Nafion thin films cast on Pt electrode by using the Nafion dispersion with different water/alcohol ratio.

In the present work, we examined the correlation between morphology and proton transport behavior of spun cast Nafion thin films with different IPA/water fraction. 50, 110 nm-thick Nafion thin films on Pt substrate cast by Nafion dispersion with different

water/alcohol ratio were systematically investigated via GISAXS/GIWAXS and electrochemical impedance spectroscopy (EIS) method in terms of morphological property and proton transport behavior.

4.2 Experimental

Proton Conductivity measurement

The self-designed Pt deposited interdigitated array (Osaka Vacuum Industrial Co., Ltd) with the same setup of our previous work was used to measure proton conductivity.[37] Nafion dispersion was prepared by diluting 20 wt% Nafion solution to desired solution, in which the solvent compositions were [IPA]/[IPA+water] 2, 17, 34, 54 wt% by addition of Millipore water. Then, Nafion thin films were fabricated by spin-casting method on the interdigitated array electrodes. The thicknesses of as prepared Nafion thin films on interdigitated array electrodes were confirmed by ellipsometry measurement (OTSUKA ELECTRONICS Co., LTD).

The proton conductivity of cast Nafion thin films applied to the interdigitated array electrodes was measured using EIS under a flow of dry N_2 gas through water tank. All measurements were conducted at 25 °C with 20-90% relative humidity (RH). An alternating amplitude potential and frequency range were set at 100 mV and 7 MHz− 0.01 Hz, respectively. To capture the Nafion thin film resistances, the collected impedance data were fitted using analysis software EC-lab (V.11.21)

GISAXS/GIWAXS measurement

The Nafion thin-films for GISAXS/GIWAXS measurements were prepared on Pt sputtered Si substrate as previously reported.37 The prepared Nafion thin films were placed into a cell connected to a humidity controller system for the GISAXS/GIWAXS. The relative humidity was controlled by transporting hydrated N_2 gas to maintain a constant humidity level of 80% RH at 25ºC. GISAXS and GIWAXS were performed in beamline BL40B2 at SPring-8, Hyogo, Japan. The X-ray energy was 12.4 keV, and

the incident X-ray angle was at 0.14º. The GISAXS and GIWAXS 2D image was collected with a Dectris Pilatus imaging plate (0.172 mm x 0.172 mm, C9729DK-10) and a flat panel sensor (0.05 mm, Hamamatsu Photonics K. K. Japan), respectively. The X-ray exposure time for the Nafion thin films in the GISAXS and GIWAXS was 100 s and 10 s, respectively. The distance between the samples and the detector was set at 2200 mm and 60 mm for GISAXS and GIWAXS, respectively. Silver behenate and CeO_2 were used as standard material to calibrate the beam center and the sample-detector distance for the GISAXS and GIWAXS, respectively.

4.3 Results and Discussion

The thickness of the as-prepared Nafion thin-films were 50 and 110 nm, which were characterized by ellipsometry combined with Cauchy model fitting as we reported previously.[37] Figure. 1 shows the proton conductivity of the cast Nafion thin films with different IPA fraction in the solvent and thicknesses ((a) 110 nm, (b) 50 nm) at 25ºC under 20-90%RH. The Nyquist plot are shown in supporting information Figure S1. In the case of 110 nm shown in Figure 1(a), the proton conductivity increased as increasing relative humidity in range of 20-90%RH over all samples, which exhibited humidity dependence as previous work.13 Additionally, the proton conductivity increased with

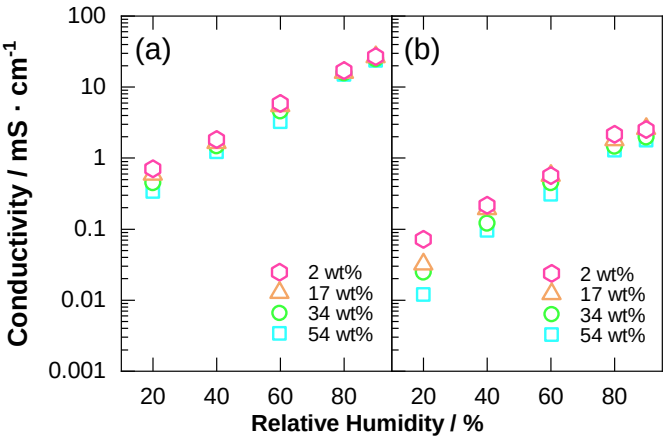

Figure 1. Proton conductivity of Nafion thin films with various thicknesses: (a) 110 nm, (b) 50 nm, cast by different IPA fraction of Nafion dispersion. The electrochemical impedance was conducted under wide range of humidity from 20-90%RH at 25ºC

decreasing IPA fraction in cast solution. Comparing the proton conductivity of Nafion thin films cast by dispersion with IPA fraction of 54 wt% and 2 wt%, the gap at 20%RH showed the most difference (54 wt%: 0.33 mS/cm 2 wt%: 0.70 mS/cm). Similar tendency was observed for 50 nm (Figure 1(b)). These results indicate the proton conductivity of the Pt-supported Nafion thin films affected by the IPA fraction in cast solution. In particular, the difference in proton conductivity between 2 wt% and 54 wt% IPA cast thin films was enlarged as thickness comparatively decreased to 50 nm.

To examine the morphology of the as-prepared Nafion thin films cast by dispersion with various IPA fraction, GISAXS and GIWAXS measurements were performed on the Nafion thin films. Figure 2 exhibits the GISAXS 2D patterns of Nafion thin films with thickness of 50 and 110 nm cast by different IPA fraction of Nafion dispersion. The scattering patterns are plotted as scattering vector q in 2D and the measured intensity is reported as a function of the magnitude of the scattering vector[38]

$$\mathbf{q} = \begin{pmatrix} q_x \\ q_y \\ q_z \end{pmatrix} = \frac{2\pi}{\lambda} \begin{pmatrix} \cos 2\Theta \cos \alpha_f - \cos \alpha_i \\ \sin 2\Theta \cos \alpha_f \\ \sin \alpha_i + \cos \alpha_f \end{pmatrix} \quad [1]$$

where αi is the incidence angle. αf and Θ represent the exit angle along out-of-plane and in-plane, respectively. λ is the wavelength of the incidence X-ray. In the case of the 110 nm-thick Nafion thin films cast by dispersion with 54 wt% IPA fraction, the scattering ring appeared around q = 1-2 nm^{-1}. The scattering ring is named as “ionomer

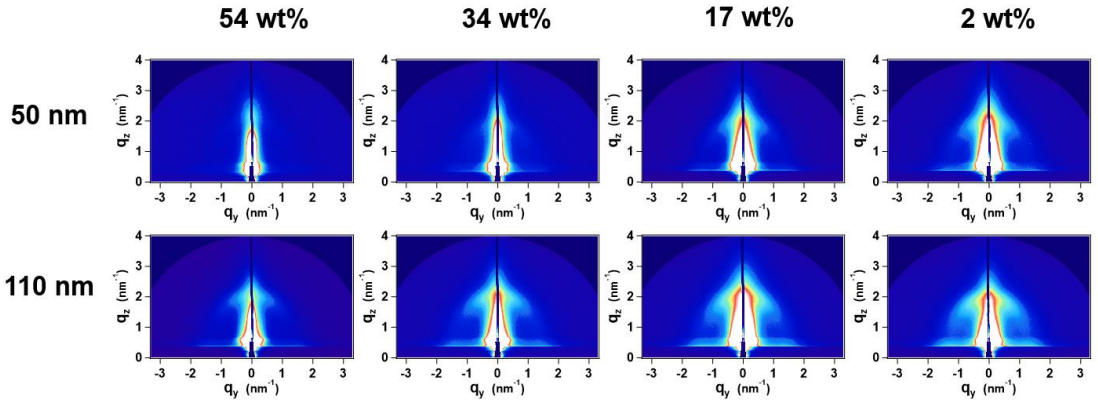

Figure 2. GISAXS 2D patterns of 50 and 110 nm thick Nafion thin films cast by dispersion with various IPA fraction under 80%RH at 25°C

peak", arising from the ordered structure of hydrophilic ionic domain in Nafion thin films.[39,40] As the IPA fraction decreased to 2 wt%, the ionomer peak significantly increased, which indicates that the formation of hydrophilic ionic domain was enhanced. Similar tendency was observed in 50 nm Nafion thin films because the growth of hydrophilic domain along in-plane direction was significantly confined as film thickness approach to domain size.

To further understand how the ionic domain orientation changes, 1D line-integrated analyses along the equatorial (in-plane) and meridional directions (out-of-plane) were extracted from the GISAXS 2D profiles by the same manner as previous report.[37] For the in-plane direction analysis, the distance of cut line was set as q=0.45 nm^{-1} from beam center to avoid the influence from Yoneda peak. For the out-of-plane analysis, the scattering position shift along qz direction could be caused by refraction of X-ray. We confirmed the peak shift along qz direction was negligibly small by calculating the d-spacing taking distorted wave born approximation into consideration.[37] The typical 1D line profiles along the in-plane direction are shown in Figure 3. The scattering vector q expressed in reciprocal space can be converted to d-spacing, which is the distance of the periodic structure in real space, using equation [2].

$$d = \frac{2\pi}{q} \qquad [2]$$

The line profiles along in-plane direction shown in Figure 3 clearly presented the difference of morphology in these Nafion thin films with various thicknesses and IPA

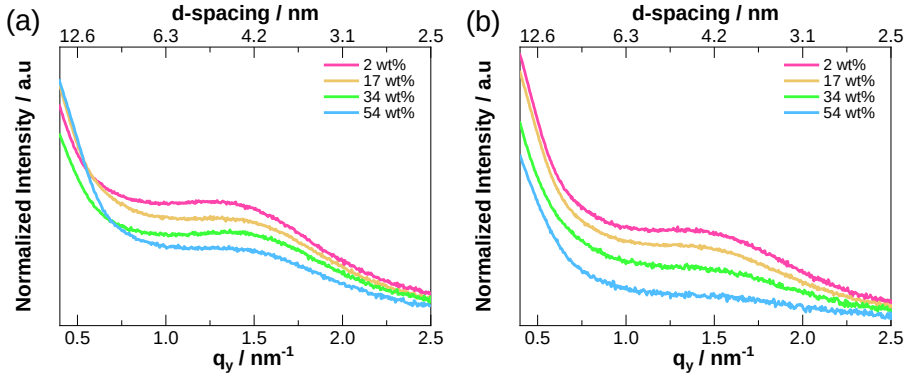

Figure 3. 1D in-plane lineprofile of Naifon thin films cast by Nafion dispersion with various IPA fraction extracted. ((a):110 nm, (b): 50 nm)

fraction. The intensity of ionomer peak found in all 50 nm and 110 nm-thick Nafion thin films increased as decreasing IPA fraction to 2wt% and the peak position slightly shifted to lower q side to about 1.56 nm-1 and 1.48 nm-1, respectively. Similar tendency was observed in case of out-of-plane direction (Figure S2).

The Gaussian function was used to fit the ionomer peak to extract d-spacing of ionomer peak. The typical fitting results are shown in Figure S3. The obtained d-spacing vs. IPA fraction plot is shown in Figure 4(a), (b). For 50 nm and 110 nm Nafion thin films, d-spacing along in-plane direction increased to 3.0 nm and 4.4 nm, respectively, as IPA fraction decreased to 2 wt%. Although the d-spacing value along out-of-plane direction shown in Figure 4(b) basically exhibited the similar tendency as Figure 4(a), the value of out-of-plane was slight lower, compared to that along in-plane direction. Overall, d-spacing showed monotonically decreasing relationship with an increase of IPA fraction of cast Nafion dispersion, which indicates that the alcohol/water ratio in Nafion dispersion directly affects the spacing of order hydrophilic ionic domain in cast Nafion thin films. Furthermore, as the d-spacing along in-plane

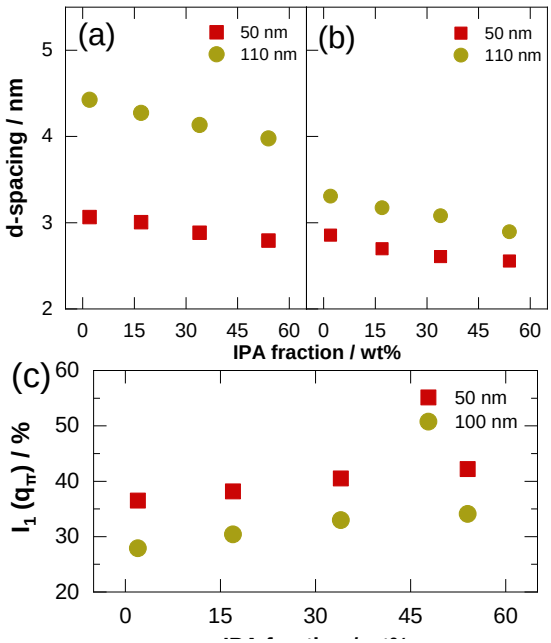

Figure 4. The d-spacing of ionomer peak extracted from lineprofile along (a) in-plane and (b) out-of-plane direction under 80%RH with different IPA fraction. Figure 4(c) present the ratio of contribution of hydrophilic ionic domain along out-of-plane component.

direction showed higher value than of out-of-plane direction under the same condition (IPA fraction, thickness), which indicate that the hydrophilic domain behaves anisotropically.

To quantitatively compare the intensity of the ionomer peak along the meridional and equatorial axes, I_1 and I_2 were utilized, respectively. We normalized the curves by setting the integrated intensity around the ionomer peak to q=1-2 $nm^{-1}$with the same method as we reported previously.[37] It is assumed that I_1 (out-of-plane) and I_2 (in-plane) are both Gaussian distribution functions of the azimuthal angle, φ, shown in Figure S4, with peaks along the meridional (φ=0°) and equatorial (φ=90°) directions. The I_1 (φ) and I_2 (φ) were then used to determine the normalized integral intensity, I(q), which is defined by the following equation[41]

$$I_i(q) \approx \int_0^{\frac{\pi}{2}} I_i(\varphi) 2\pi q \sin|\varphi| d\varphi \qquad [3]$$

The normalized integral intensity of the ionomer peak along the meridian (i=1) and the equator (i=2) was evaluated using Equation [4]. In this study, the meridian and equator scattering patterns represent the in-plane and out-of-plane directions. The estimated normalized integrated intensity of ionomer peak around 1-2 nm^{-1} for 50 and 110 nm-thick Nafion thin films with various IPA fraction was shown in Figure 4(c). Generally, for both 50 and 110 nm, the contribution of orientated component along out-of-plane direction, I_1(q) (%), are slightly increased with increasing IPA fraction. Such result exhibited that the IPA fraction in casting solution make impact on orientation of

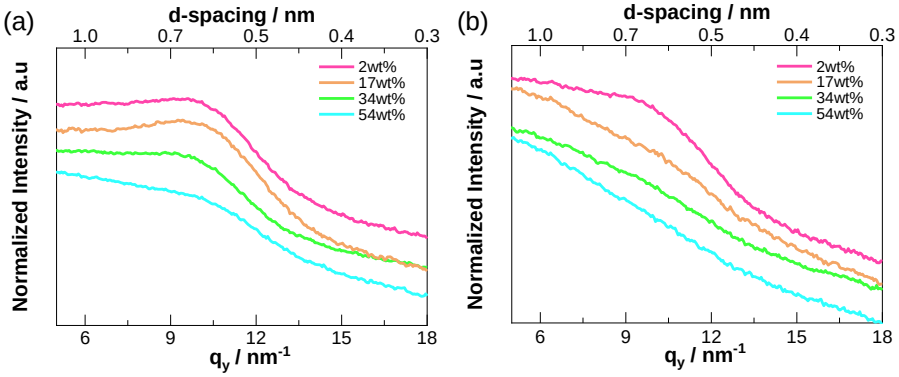

Figure 5. GIWAXS 1D lineprofile ((a):110 nm, (b): 50 nm,) of Nafion thin film cast by Nafion dispersion with different IPA fraction extracted from 2D patterns shown in Figure S5

nanostructure of cast film. Considering the absolute intensity of scattering pattern shown in Figure 2, it is clear that the film cast by lower IPA fraction solution is more inclined to orientated to be aligned parallel to Pt substrate than that film cast by high IPA fraction solution. Similar result was observed by previous report conducted by Cleve *et.al.*, who suggest that the film cast with lower IPA fraction induced more orientated Pt/ionomer interfacial structure due to the Pt-sulfonate interaction.[28]

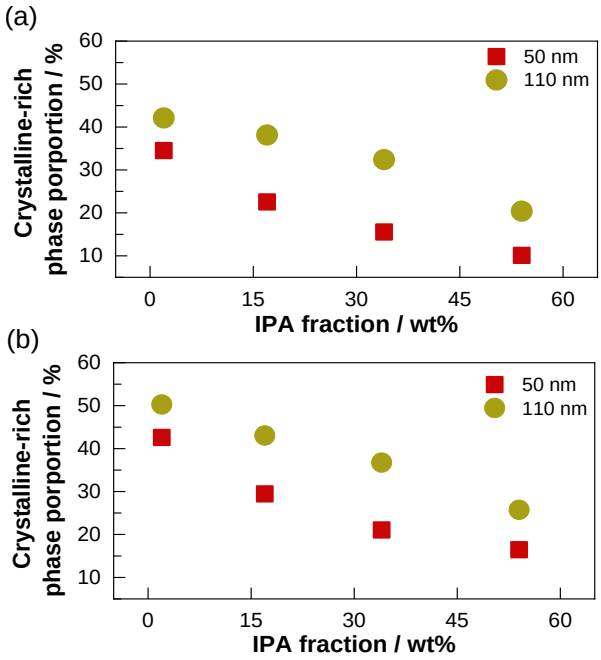

Figure 6. The estimated crystalline-rich phase proportion of Nafion thin films with different IPA fraction along (a) in-plane and (b) out-of-plane direction extracted from GIWAXS 2D patterns.

To examine the molecular aggregation in the hydrophobic domain of the Nafion thin films, GIWAXS was performed under 80% RH at 25ºC. The GIWAXS 1D line profiles along the in-plane direction extracted from 2D GIWAXS patterns (Figure S5) are shown in Figure 5. In the GIWAXS patterns of the Nafion thin film, board peaks attributed to the combination of CF_2 chain amorphous and crystalline structures appear at q=10.5 nm^{-1} and 12 nm^{-1}, respectively.[33,42] For 50 nm-thick Nafion thin films shown in Figure 5(b), amorphous / crystalline peak were found in all samples and decreased as increasing IPA fraction, which indicates that the growth of ordered hydrophobic structure was enhanced as decreasing IPA fraction of Nafion cast dispersion. Compared

to 50 nm samples, the amorphous / crystallinity peak observed in 110 nm (Figure 5(a)) exhibited comparatively sharp due to the fact that bulky properties begin to dominate thin films morphology.[34] For further investigation, the board amorphous / crystallinity peak observed in Figure 5 was deconvoluted into the amorphous and crystalline peak. As our pervious report, crystalline-rich phase proportion, Pc, was introduced here to describe the morphology changes as a function of IPA fraction. The Pc of the Nafion thin films can be estimated based on previous research.[37] The typical fitting results were shown in supporting information (Figure S6). As shown in Figure 6(a), the Pc along in-plane direction generally decreased with an increase in IPA fraction for a given thickness. In the case of the 110 nm-thick Nafion thin films, Pc gradually decreased to 20.4% as the IPA fraction increased 54 wt%. In the case of the 50 nm-thick Nafion thin films, Pc gradually decreased to 10.1% as the IPA fraction increased to 54 wt%. Compared to 110 nm, 50 nm-thick thin films exhibited lower Pc due to the disordered domain structure as aforementioned. Similar tendency was observed in Pc of out-of-plane direction shown in Figure 6(b). Additionally, the Pc along the out-of-plane direction exhibited a slightly higher value than in-plane direction, indicating anisotropic behavior due to the ionomer/substrate interaction. Figure 6 clearly shows that the

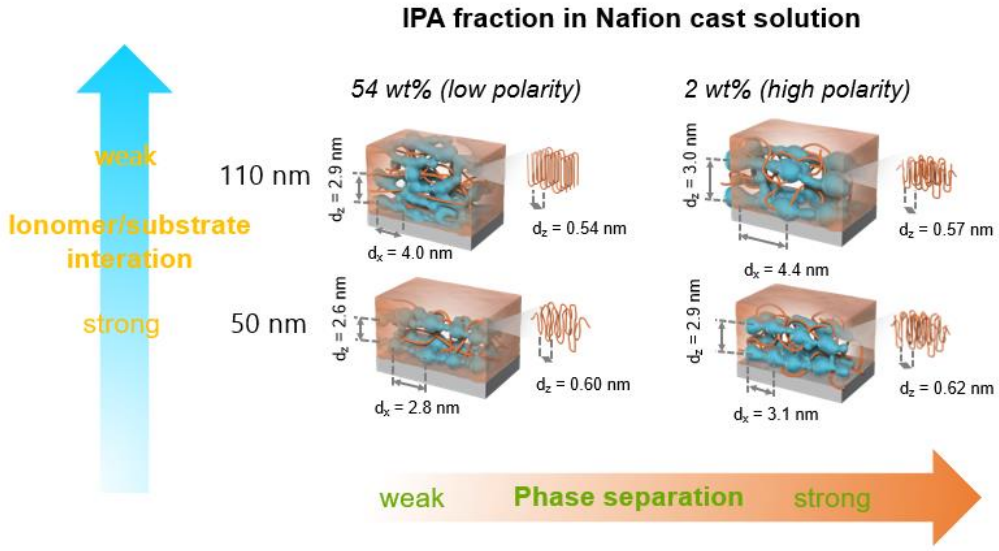

Figure 7 The schematic model of Nafion thin films cast by dispersion with different IPA fraction

crystalline structure of the thin films, depends on dispersion of IPA fraction, thereby implying that state of dispersion influence the structural order of hydrophobic domain in Nafion.

Here we discuss the correlation between the IPA fraction and morphology in the Nafion thin-films. This study shows that both the morphology and proton conductivity of Nafion thin films is influenced by IPA fraction of cast dispersion. It has been reported that the morphology of the Nafion molecules in the dispersion changes with the IPA/water ratio.[43] In the low IPA content, the polar sulfonic groups interact with the water and the non-polar perfluorocarbon backbones association with each other, resulting in a tightly packed structure with the sulfonic group on the outside and the perfluorocarbon backbone on the inside of the Nafion molecules. In the increasing IPA content, the non-polar perfluorocarbon backbones interact with the IPA and the polar sulfonic groups association with each other, resulting in a loosely packed structure with the perfluorocarbon backbone on the outside and the sulfonic group on the inside of the Nafion molecules. Considering the previous reports, in the present study, Nafion molecules in the 2 wt% IPA fraction dispersion have the tightly packed structure with hydrophilic/hydrophobic phase separation because that the large amount of water interacts with sulfonic groups. On the other hand, Nafion molecules in the 54 wt% IPA fraction dispersion have the loosed packed structure with low hydrophilic/hydrophobic phase separation. In the case of 2 wt% IPA fraction dispersion, the tightly packed structure with sulfonic group on the outside of Nafion molecules, enhances the development of hydrophilic/hydrophobic phase separation in the Nafion thin-film because the sulfonic groups interacts with the surface of Pt substrate.[28,34] On the other hand, in the case of 54 wt% IPA fraction dispersion, the loosely packed structure of Nafion molecules, relatively inhibits the development of hydrophilic/hydrophobic phase separation in the Nafion thin-film. In particular, the effect of the molecular structure on the thin-film morphology is pronounced when the thickness of Nafion thin-film is small. These morphological difference of the Nafion thin-films, which are influenced by the Nafion molecular structure in the various IPA fraction dispersion results in the proton conductivity difference. The tendency of domain size various with

IPA or water content is consistent with the previous work conducted by Berlinger et. al., who also suggested that the average cluster size increase with increasing water content.32 In high IPA content solvent, as aforementioned, Nafion molecules tend to form tightly packed structure with high hydrophilic/hydrophobic phase separated structure. In case of this, it is anticipated that proton transport pathway is well grown, which is related to comparatively high proton conductivity. On the other hand, low IPA content solvent result in loosed paced structure where the proton transport pathway is restricted due to the low hydrophilic/hydrophobic phase separation.

4.4 Conclusion

In this study, we systematically investigated the alcohol/water effect in Nafion thin film with thickness of 50-110 nm in terms of morphology and proton transport property via GISAXS/GIWAXS and EIS method. It is obvious that the water/alcohol ratio in cast dispersion directly affect the morphology, connectivity of hydrophilic, hydrophilic/hydrophobic phase separation as well as proton transport behavior in cast films. As IPA fraction decreased to 2wt%, the growth of hydrophilic domain of cast Nafion thin films is accelerated accompany with formation of crystalline-rich phase in hydrophobic domain, which indicate the strongly hydrophilic/hydrophobic phase separation. On the other hand, Nafion thin films cast by 54 wt% IPA fraction exhibited the lowest phase separation, proton conductivity value. All these results indicate the fact that the morphology of cast thin films are strongly influenced by the dispersion state in solution. The findings of this study are expected to further the understanding of catalysts/ionomer interfacial phenomena during the optimized dispersion fabrication process in PEFCs.

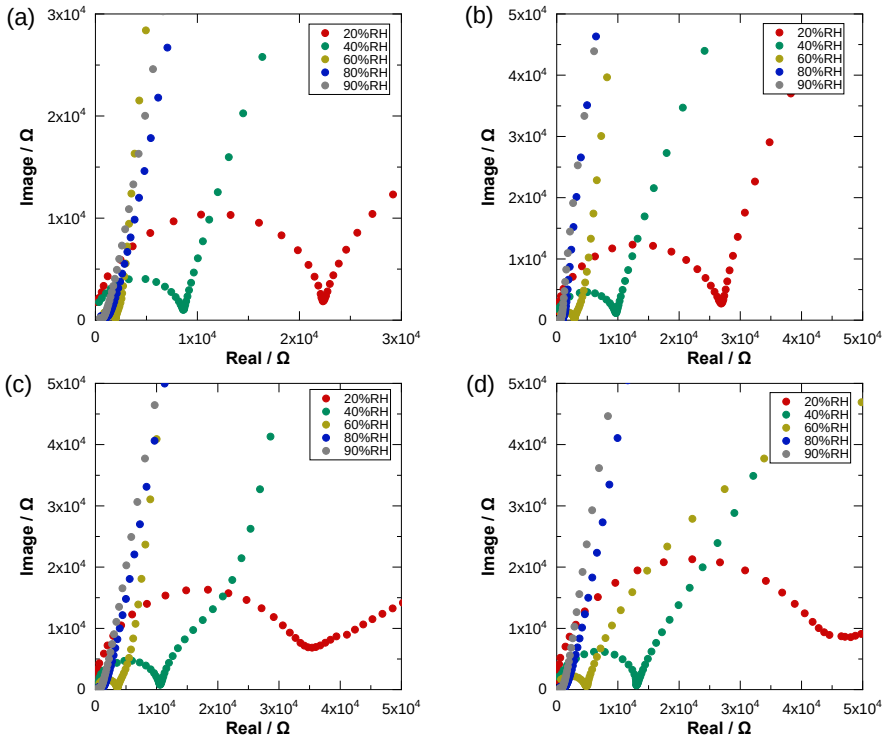

Figure S1. Typical Nyquist plot of Nafion thin films with thickness of 110 nm cast by various IPA fraction of Nafion dispersion (a): 2 wt% (b): 17 wt% (c): 34 wt% (d): 54 wt% under 20-90%RH at 25°C.

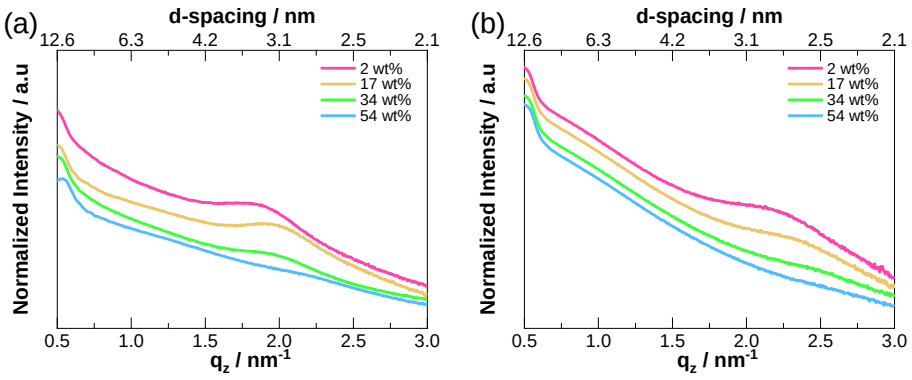

Figure S2. 1D out-of-plane line-profiles of Nafion thin films cast by Nafion dispersion with various IPA fraction extracted. ((a):110 nm, (b): 50 nm)

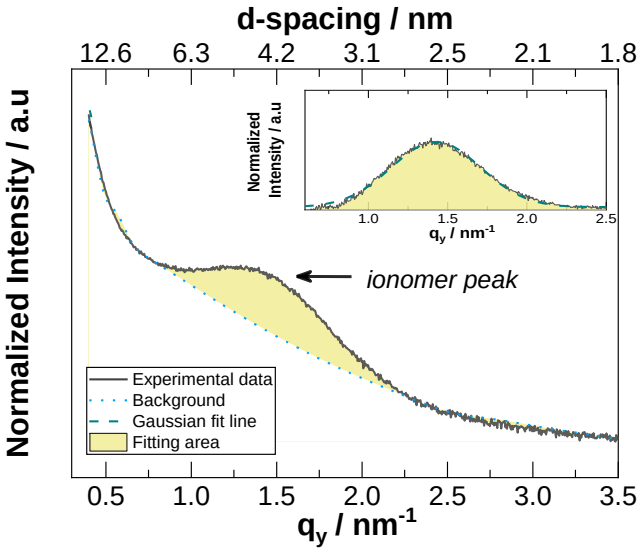

Figure S3. Typical Gaussian fitting result of 1D line profile of 110 nm-thick Nafion thin film cast by dispersion with 2 wt% IPA fraction. The isotropic background was subtracted before Gaussian fitting.

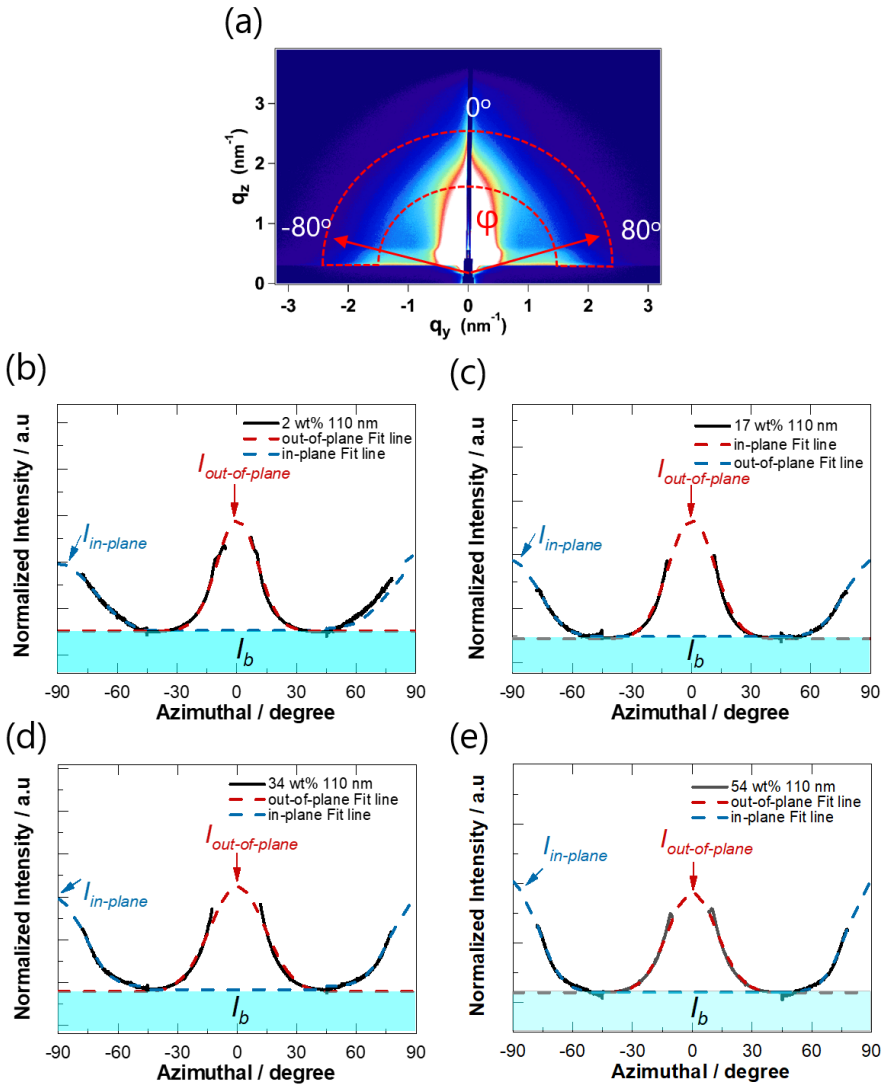

Figure S4. (a) The illustration of normalization method used in this manuscript. Ionomer peak, defined as 1.5-2.5 nm^{-1}, was extracted from the scattering from 2D pattern to azimuthal plot and fitted with Gaussian function for both in-plane and out-of-plane component. The typical fitting results of 110 nm-thick Nafion thin films ((b): 2 wt% (c): 17 wt% (d): 34 wt% (d) 54 wt%) are shown above. Isotropic background was subtracted

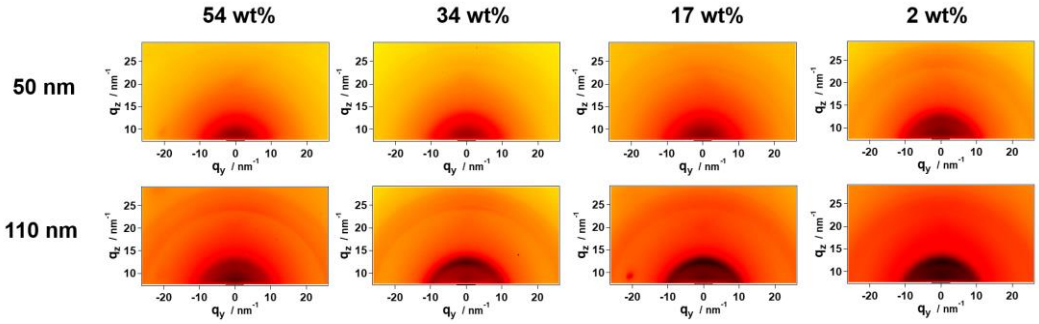

Figure S5. GIWAXS 2D patterns of Nafion thin film cast by dispersion with various IPA fraction.

Reference

(1) Eikerling, M.; Kulikovsky, A. *Polymer Electrolyte Fuel Cells: Physical Principles of Materials and Operation;* CRC Press, 2014.

(2) Franco, A. A. *Polymer Electrolyte Fuel Cells: Science, Applications, and Challenges;* Pan Stanford Publishing, 2016.

(3) Kreuer, K. D. *Fuel Cells: Selected Entries from the Encyclopedia of Sustainability Science and Technology;* Springer New York, 2012.

(4) Li, H.; Knights, S.; Shi, Z.; Van Zee, J. W.; Zhang, J. *Proton Exchange Membrane Fuel Cells: Contamination and Mitigation Strategies*; CRC Press, 2010.

(5) Kreuer, K.-D.; Paddison, S. J.; Spohr, E.; Schuster, M. Transport in Proton Conductors for Fuel-Cell Applications: Simulations, Elementary Reactions, and Phenomenology. *Chem. Rev*. **2004**, 104 (10), 4637.

(6) Divoux, G. M.; Finlay, K. A.; Park, J. K.; Song, J.-M.; Yan, B.; Zhang, M.; Dillard, D. A.; Moore, R. B. Morphological Factors Affecting the Behavior of Water in Proton Exchange Membrane Materials. *ECS Trans*. **2011**, 41 (1), 87.

(7) Kusoglu, A.; Weber, A. Z. New Insights into Perfluorinated Sulfonic-Acid Ionomers. *Chem. Rev.* **2017**, 117 (3), 987.

(8) Mauritz, K. A.; Moore, R. B. State of Understanding of Nafion. *Chem. Rev*. **2004**, 104 (10), 4535.

(9) Rodgers, M. P.; Bonville, L. J.; Kunz, H. R.; Slattery, D. K.; Fenton, J. M. Fuel cell perfluorinated sulfonic acid membrane degradation correlating accelerated stress testing and lifetime. *Chem. Rev*. **2012**, 112 (11), 6075.

(10) Zhang, H.; Shen, P. K. Recent Development of Polymer Electrolyte Membranes for Fuel Cells. *Chem. Rev*. **2012**, 112 (5), 2780.

(11) Holdcroft, S. Fuel Cell Catalyst Layers: A Polymer Science Perspective. *Chem. Mater* **2014**, 26 (1), 381.

(12) Weber, A. Z.; Borup, R. L.; Darling, R. M.; Das, P. K.; Dursch, T. J.; Gu, W.;

Harvey, D.; Kusoglu, A.; Litster, S.; Mench, M. M.et al. A Critical Review of Modeling Transport Phenomena in Polymer-Electrolyte Fuel Cells. *J. Electrochem. Soc*. **2014**, 161 (12), F1254.

(13) Paul, D. K.; McCreery, R.; Karan, K. Proton Transport Property in Supported Nafion Nanothin Films by Electrochemical Impedance Spectroscopy. *J. Electrochem. Soc*. **2014**, 161 (14), F1395.

(14) Paul, D. K.; Shim, H. K. K.; Giorgi, J. B.; Karan, K. Thickness dependence of thermally induced changes in surface and bulk properties of Nafion®nanofilms. *J. Polym. Sci. B* **2016**, 54 (13), 1267.

(15) Jinnouchi, R.; Kudo, K.; Kitano, N.; Morimoto, Y. Molecular Dynamics Simulations on O_2 Permeation through Nafion Ionomer on Platinum Surface. *Electrochim. Acta* **2016**, 188, 767.

(16) Tesfaye, M.; Kushner, D. I.; Kusoglu, A. Interplay between Swelling Kinetics and Nanostructure in Perfluorosulfonic Acid Thin-Films: Role of Hygrothermal Aging. *ACS Applied Polymer Materials* **2019**, 1 (4), 631.

(17) Kushner, D. I.; Kusoglu, A.; Podraza, N. J.; Hickner, M. A. Substrate - Dependent Molecular and Nanostructural Orientation of Nafion Thin Films. *Adv. Funct. Mater*. **2019**, 1902699.

(18) Aldebert, P.; Dreyfus, B.; Pineri, M. Small-angle neutron scattering of perfluorosulfonated ionomers in solution. Macromolecules 1986, 19 (10), 2651.

(19) Aldebert, P.; Gebel, G.; Loppinet, B.; Nakamura, N. Polyelectrolyte effect in perfluorosulfonated ionomer solutions. *Polymer* **1995**, 36 (2), 431.

(20) Loppinet, B.; Gebel, G.; Williams, C. E. Small-Angle Scattering Study of Perfluorosulfonated Ionomer Solutions. *J. Phys. Chem. B* **1997**, 101 (10), 1884.

(21) Szajdzinska-Pietek, E.; Schlick, S.; Plonka, A. Self-Assembling of Perfluorinated Polymeric Surfactants in Water. Electron-Spin Resonance Spectra of Nitroxide Spin Probes in Nafion Solutions and Swollen Membranes. *Langmuir* **1994**, 10 (4), 1101.

(22) Szajdzinska-Pietek, E.; Schlick, S.; Plonka, A. Self-assembling of

perfluorinated polymeric surfactants in nonaqueous solvents. Electron spin resonance spectra of nitroxide spin probes in Nafion solutions and swollen membranes. *Langmuir* **1994**, 10 (7), 2188.

(23) Li, H.; Schlick, S. Effect of solvents on phase separation in perfluorinated ionomers, from electron spin resonance of VO2+ in swollen membranes and solutions. *Polymer* **1995**, 36 (6), 1141.

(24) Lin, H. L.; Yu, T. L.; Huang, C. H.; Lin, T. L. Morphology study of Nafion membranes prepared by solutions casting. *J. Polym. Sci. B* **2005**, 43 (21), 3044.

(25) Ma, C.-H.; Yu, T. L.; Lin, H.-L.; Huang, Y.-T.; Chen, Y.-L.; Jeng, U.-S.; Lai, Y.-H.; Sun, Y.-S. Morphology and properties of Nafion membranes prepared by solution casting. *Polymer* **2009**, 50 (7), 1764.

(26) Tarokh, A.; Karan, K.; Ponnurangam, S. Atomistic MD Study of Nafion Dispersions: Role of Solvent and Counterion in the Aggregate Structure, Ionic Clustering, and Acid Dissociation. *Macromolecules* **2019**.

(27) Ngo, T. T.; Yu, T. L.; Lin, H.-L. Influence of the composition of isopropyl alcohol/water mixture solvents in catalyst ink solutions on proton exchange membrane fuel cell performance. *J. Power Sources* **2013**, 225, 293.

(28) Van Cleve, T.; Khandavalli, S.; Chowdhury, A.; Medina, S.; Pylypenko, S.; Wang, M.; More, K. L.; Kariuki, N.; Myers, D. J.; Weber, A. Z. Dictating Pt-Based Electrocatalyst Performance in Polymer Electrolyte Fuel Cells, from Formulation to Application. *Appl. Mater. Interfaces* **2019**, 11 (50), 46953.

(29) Li, S.; Terao, K.; Sato, T. Colloidal Dispersion of a Perfluorosulfonated Ionomer in Water–Methanol Mixtures. *Polymers* **2018**, 10 (1), 72.

(30) Yang, F.; Xin, L.; Uzunoglu, A.; Qiu, Y.; Stanciu, L.; Ilavsky, J.; Li, W.; Xie, J. Investigation of the interaction between nafion ionomer and surface functionalized carbon black using both ultrasmall angle X-ray scattering and Cryo-TEM. *Appl. Mater. Interfaces* **2017**, 9 (7), 6530.

(31) Takahashi, S.; Shimanuki, J.; Mashio, T.; Ohma, A.; Tohma, H.; Ishihara, A.; Ito, Y.; Nishino, Y.; Miyazawa, A. Observation of ionomer in catalyst ink of polymer electrolyte fuel cell using cryogenic transmission electron microscopy.

Electrochim. Acta **2017**, 224, 178.

(32) Berlinger, S. A.; McCloskey, B. D.; Weber, A. Z. Inherent acidity of perfluorosulfonic acid ionomer dispersions and implications for ink aggregation. *J. Phys. Chem. B* **2018**, 122 (31), 7790.

(33) Kusoglu, A.; Dursch, T. J.; Weber, A. Z. Nanostructure/Swelling Relationships of Bulk and Thin-Film PFSA Ionomers. *Adv. Funct. Mater.* **2016**, 26 (27), 4961.

(34) Kusoglu, A.; Kushner, D.; Paul, D. K.; Karan, K.; Hickner, M. A.; Weber, A. Z. Impact of Substrate and Processing on Confinement of Nafion Thin Films. *Adv. Funct. Mater*. **2014**, 24 (30), 4763.

(35) Tesfaye, M.; MacDonald, A. N.; Dudenas, P. J.; Kusoglu, A.; Weber, A. Z. Exploring substrate/ionomer interaction under oxidizing and reducing environments. *Electrochem. Commun.* **2018**, 87, 86.

(36) Dudenas, P. J.; Kusoglu, A. Evolution of Ionomer Morphology from Dispersion to Film: An in Situ X-ray Study. *Macromolecule*s **2019**, 52 (20), 7779.

(37) Gao, X.; Yamamoto, K.; Hirai, T.; Uchiyama, T.; Ohta, N.; Takao, N.; Matsumoto, M.; Imai, H.; Sugawara, S.; Shinohara, K. Morphology Changes in Perfluorosulfonated Ionomer from Thickness and Thermal Treatment Conditions. *Langmuir* **2020**, 36 (14), 3871.

(38) Saito, I.; Miyazaki, T.; Yamamoto, K. Depth-resolved structure analysis of cylindrical microdomain in block copolymer thin film by grazing-incidence small-angle x-ray scattering utilizing low-energy x-rays. *Macromolecules* **2015**, 48 (22), 8190.

(39) Bass, M.; Berman, A.; Singh, A.; Konovalov, O.; Freger, V. Surface Structure of Nafion in Vapor and Liquid. *J. Phys. Chem. B* **2010**, 114 (11), 3784.

(40) Bass, M.; Berman, A.; Singh, A.; Konovalov, O.; Freger, V. Surface-Induced Micelle Orientation in Nafion Films. *Macromolecules* **2011**, 44 (8), 2893.

(41) Kido, M.; Nojima, S.; Ishige, R.; White, K. L.; Kamitani, K.; Ohta, N.; Hirai, T.; Takahara, A. Effect of molecular weight on microcrystalline structure formation in polymer with perylenediimide side chain. *J. Polym. Sci. B* **201**6, 54 (22), 2275.

(42) Kusoglu, A.; Modestino, M. A.; Hexemer, A.; Segalman, R. A.; Weber, A. Z. Subsecond Morphological Changes in Nafion during Water Uptake Detected by Small-Angle X-ray Scattering. *ACS Macro Lett.* **2011**, 1 (1), 33.

(43) Karan, K. Interesting Facets of Surface, Interfacial, and Bulk Characteristics of Perfluorinated Ionomer Films. *Langmuir* **2019**, 35 (42), 13489.

Chapter 5 Plasticization effect in Nafion thin film on Pt substrate

5.1 Introduction

Finding sustainable solutions to the looming energy crisis on both small and environmental friendly has become one of the most urgent challenges to reduce our dependence on conventional energy source[1-4] PEFCs, a next generation energy conversion system, offer the advantages of high power density with zero-emission, which is considered as the one of the most promising energy source in the future. In practical PEFCs, oxygen reduction reaction occurs (ORR) the interface of carbon-supported Pt covered by proton conducting electrolyte. Nafion, a benchmark of perfluorosulfonated ionomer (PFSI), is the most commonly used as ion conducting electrolyte material in PEFSs due to its high proton conductivity, high thermal and mechanical properties.[5-8] As ionomer/catalysts act as a reaction field in PEFCs, which is essential parts to improve efficiency and performance, therefore elucidation of the structure of Nafion on the Pt/C catalysts is related to oxygen reaction reduction activity.[9-11]

Nafion consists of hydrophobic perfluorocarbon backbone ($-CF_2$) and hydrophilic sulfonate side chains ($-SO_3H$). The physical properties of these materials are dictated by the coulombic interactions between the ion-pairs along the backbone. These electrostatic interactions lead to the formation of stable ionic associations that behave in many ways as cross-links. In particular, the relaxation behavior of these materials is greatly affected by the associations, and the resulting aggregates (multiplets), and has been the focus of several rheological studies.[12-15]

Up to now, several studies have shown that the rheological behavior of these materials can be altered simply by changing the degree of neutralization or through the choice of counterion, factors that can be expected to influence the strength of the associations.[16-18] In particular, and pertinent to later discussion, early patent literature describes the neutralization of ionomers with alkyl ammonium ions and subsequent

changes in the rheological properties. In addition, Weiss et al. observed a decrease in the viscosity of alkylamine neutralized polystyrene ionomers with an increase in the bulkiness of the counterion and found that electrostatic interactions predominate for smaller counterions, while plasticization effect is more important as the counterion becomes sufficiently bulky.[19] These, and other studies, show that by changing the overall number and strength of the electrostatic interactions, a large degree of control can be exerted over the relaxation processes in these materials.[20-24]

Recent simulations of ionomer self-assembly by Kumar provide some basic insights into the nature of these fluids.[25] Upon cooling process, there is first a thermal transition, termed as "Tα", depend on the ion valence and size asymmetry of ion, where the counterions pair with the ions on the chain backbone to form small ion-multiplet structures that remain quite mobile. The long-range interactions of the small ion-multiplet structures lead to the supermolecular assembly of the small ion-multiplets in a well-defined order-disorder transition upon further cooling characterized by a maximum in the specific heat and a sharp drop in the mobility of counterions that have been incorporated into the self-assembled structures.[26] Pages et.al. suggest that this transition can be identified with the "cluster T_g" or α transition temperature.[12-18] The second, lower T_g, is naturally attributed to the conventional T_g of the polymeric structures with the large-scale supermolecularly assembled ionomer multiplet structures. The description put forth by the simulations of Kumar et al. It is apparent that the "self-assembly" of the ion pairs into supermolecular structures that they observe upon cooling corresponds to the same process involved in destabilization of the electrostatic network upon heating. At temperatures in the vicinity of the α-relaxation, an obvious destabilization of the electrostatic network may occur which results in the activation of a dynamic network facilitated through the ion hopping process. In contrast, the β-relaxation was associated with the onset of hydrophobic segmental motions (basically backbone motions) within the framework of a static physically cross-linked network of chains.[27-30]

The two predominant relaxation processes governing the melt rheological behavior

of ionomers. Generally, they are (1) the terminal relaxation time of the polymer chains and (2) the average lifetime of the ionic associations. The terminal relaxation time is dictated by the time that an ion pair resides in an aggregate before “hopping” to another aggregation site. This process was named as “ion-hopping”. Ion-hopping has been identified as a basic phenomenon in the mechanism for the cluster α-relaxation process in Nafion membrane.

In this study, we investigated the morphological and proton transporting behavior in Nafion thin films with the thickness of 50 and 200 nm under a series temperature ranging from 25-120°C under wet conditions to revealed the effect of plasticizer, water molecules. The electrochemical impedance was utilized to collect the information of proton transport behavior under wet condition upon heating. Additionally, we used GISAXS and GIWAXS to obtain a direct measure of morphological information, such as the d-spacing of hydrophilic and hydrophobic periodic structure and characterize the ion-hopping process.

5.2 Experimental

Sample preparation

The pretreatment of geometry detail of self-designed interdigitated arrays electrodes were described in our previous leterature.32 5 wt% Nafion dispersion was diluted to desired concentration with 1,1,1,3,3,3-Hexafluoro-2-propano (Wako). Then, spin casting method was used to fabricate Nafion thin film. The spin coater equipment was Opticoat MS-A100 (MIKASA CO., LTD). As-prepared Nafion dispersion was dropped on Si@Cr@Pt substrate immediately after chuck spun at 800-1600 rpm for 2 min. After the rotation returned to rest, each sample was placed under airflow until completely dried. The as-prepared thin film was placed into a cell connected to a humidity controller system. The steady humidity was made by transporting hydrated N_2 gas.

First, 20 nm Cr buffer layer was deposited on P doped-Si substrate (1 cm x 1cm) by

using Magnetron sputter (MSP-30T, Vacuum Devices Inc. Japan) under 8.0 $x10^{-1}$ Pa Ar atmosphere, 150 mA, 1 min 47 s. Then, to mimic the Pt catalyst surface, 30 nm Pt layer was fabricated in the same way on the as-prepared Cr/Si substrate under Ar atmosphere 8.0 $x10^{-1}$ Pa, 150 mA, 1 min 23 s.

Proton conductivity

The proton conductivity of the prepared Nafion thin-films on the interdigitated array electrode was measured by EIS method under hydrated N_2 gas flow condition. The humidity gas with constant flow rate (relative humidity: 80% at 25°C) was continuously transferred into self-designed chamber where IDA electrodes was set up. The temperature range was set as 25-125°C. The impedance data were collected by applying an alternative potential of 100 mV over a frequency ranging from 7 MHz-0.01 Hz by multi potentiostat (VSP-300, Bio-logic). For equivalent circuit model design and data fitting, EC-lab (Version 11.18, Bio-logic) software was adopted. The detailed of fitting model was described in our previous work.[32]

GISAXS/GIWAXS

GISAXS and GIWAXS measurement were conducted in beamline BL40B2 at Spring, Hyogo, Japan att BL40B2 and X-ray with 12.4 keV were sued. The GISAXS 2D image was collected with a Dectris Pilatus imaging plate (0.172 mm x 0.172 mm, C9729DK-10) and GIWAXS detector was used flat panel sensor (0.05 mm, Hamamatsu Photonics K. K. Japan). GISAXS and GIWAXS were measured at an incidence angle 0.14^o and the exposure time was 100s for all samples. The silver behenate and CeO_2 were used for calibration of beam center and sample detector distance for GISAXS and GIWAXS, respectively.

5.3 Results and Discussion

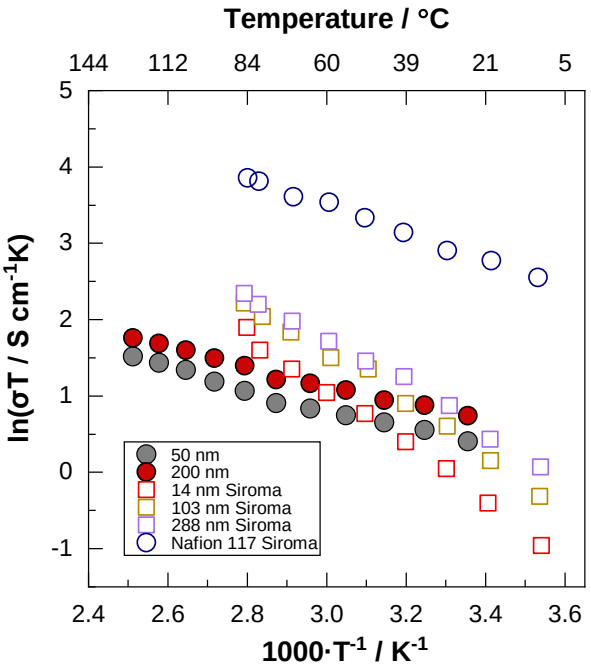

Figure 1. The Arrhenius plot of Proton conductivity as a function of temperature (25-125°C.) for the Pt-supported Nafion thin films with thicknesses of 50 nm and 200 nm. Hollow circle and square represent the Arrhenius plot of proton conductivity for Nafion thin films with various thicknesses under constant relative humidity of 85% reported in previous leterature.33

Figure. 1 shows the Arrhenius plot of proton conductivity for Nafion thin-films with thicknesses of 50 nm and 200 nm. The collected EIS spectra were shown in Figure S3 in the supporting information. Generally, it is obvious that the proton conductivity increased as increasing temperature, which showed strongly dependent on temperature for both 50 nm and 200 nm-thick films. In the case of 200 nm, conductivity gradually increased under 80°C, after then it obviously increased with a larger slop and reached 1.76 $S \cdot cm^{-1} \cdot K$ as temperature increased 125°C. Compared to 200 nm, 50 nm showed the similar tendency but comparatively decreased proton conductivity value on the whole temperature range. Different with 200 nm-thick thin films, the point that the proton conductivity significantly increased is almost at 105°C, which showed a higher value than that of 200 nm thin films. Such a phenomenon is considered to be linked with the increased mobility of sulfonic groups as the temperature approached to thermal transition. For comparison, the plot extracted from previous work conducted by Siroma et al., who conducted the proton conductivity of Nafion thin films on SiO_2 substrate

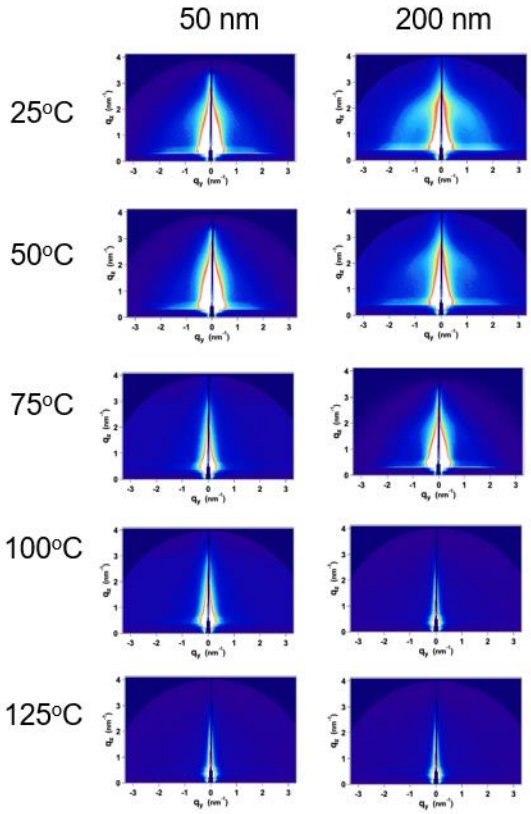

Figure 2. GISAXS 2D patterns of Pt-supported Nafion thin films substrate under different temperature ranging from 25-120°C.

were incorporated in Figure 1. Despite the different substrate, the curve shown in Figure 1 showed the similar tendency. Since the thickness of film.

Comparisons of 2D GISAXS patterns of Nafoin thin films with the thickness of 50 and 200 nm at a various temperature ranging from 25-120°C, are shown in Figure 2((a), (b)). The scattering ring around q=1.5-2 nm^{-1} is defined as the ionomer peak due to the formation of periodic structure of hydrophilic ionic domain. The scattering patterns are plotted in two-dimension as a function of the scattering vector q, which is defined as the following equation [2]

$$\mathbf{q} = \begin{pmatrix} q_x \\ q_y \\ q_z \end{pmatrix} = \frac{2\pi}{\lambda} \begin{pmatrix} \cos 2\Theta \cos \alpha_f - \cos \alpha_i \\ \sin 2\Theta \cos \alpha_f \\ \sin \alpha_i + \cos \alpha_f \end{pmatrix} \quad [1]$$

Here, λ presents the incidence wavelength. In case of 200 nm 2D patterns, ionic domain was clearly observed at 25°C and evidently almost disappeared after 80°C.

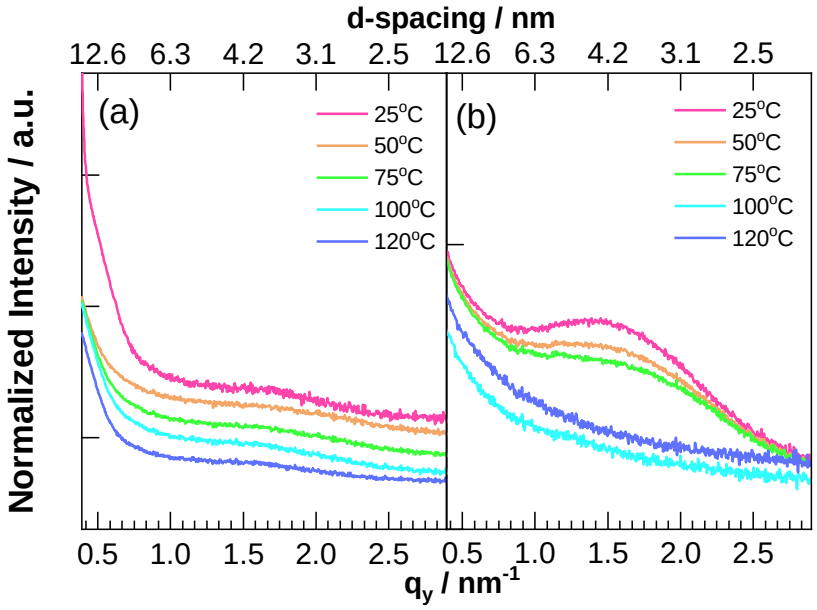

Figure 3. GISAXS 1D in-plane direction lineprofile of Pt-supported Nafion thin films with thicknesss of (a) 50 and (b) 200 nm at 25-120°C

However, 50 nm showed similar tendency with different temperature(100°C) at which the conductivity significantly increased. Such phenomenon is considered to be correlated to the increased mobility caused result from high temperature. Compared to our previous work, in which we annealed 50 and 200 nm thick.

Furthermore, 1D intensity lineprofile was extracted from Figure 2 to give an insight of variation of hydrophilic ionic domain along in-plane and out-of-plane direction shown in Figure 3. The scattering vector q expressed in reciprocal space was converted to d-spacing in real space by using Equation

$$d = \frac{2\pi}{q} \qquad [3]$$

the d is the spacing of periodic structure in real space. In the case of 50 nm thin film along in-plane direction (Figure 3(a)), as temperature increased, the intensity of the ionomer peak relatively gradually decreased and almost disappeared after 100ºC. On the other hand, in case of the 200 nm-thick Nafion thin film, the reduction of ionomer peak accompanying with increasing temperature is more pronounced and the tune point that the peak intensity significantly decreased changed to 80ºC.

2D GIWAXS patterns of Nafoin thin films with the thickness of 50 and 200 nm at a

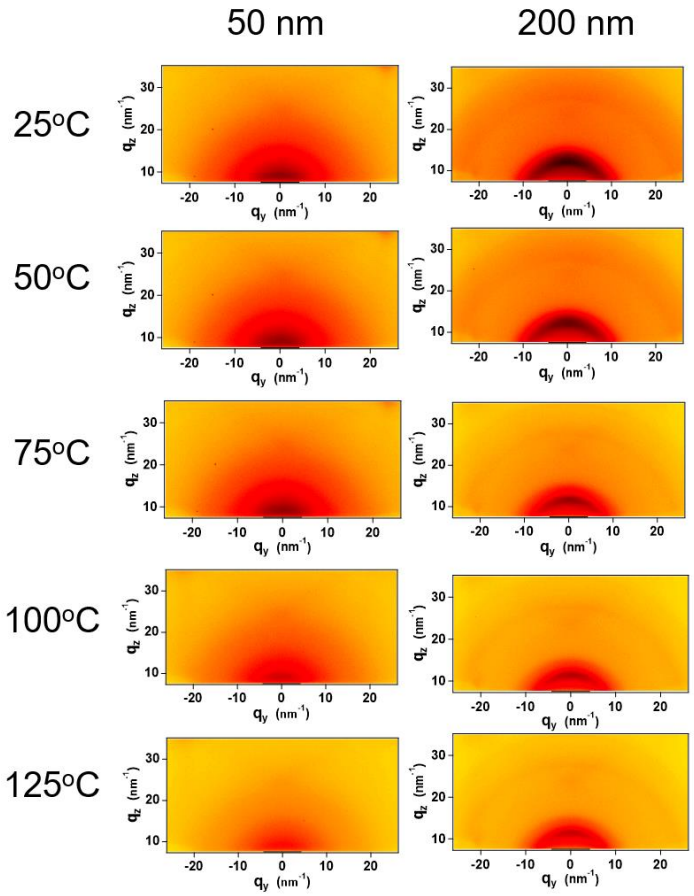

Figure 4. GIWAXS 2D patterns of Pt-supported Nafion thin films substrate under different temperature ranging from 25-120°C.

various temperature ranging from 25-120°C, are shown in Figure 4. In the GIWAXS patterns of the Nafion thin film, board peaks attributed to the combination of CF2 chain amorphous and crystalline structures appear at q=10.5 nm^{-1} and 12 nm^{-1}, respectively. It is obvious that, the increased temperature also caused the morphological changes in hydrophobic backbone in Pt-supported Nafion thin films. Generally, the increased temperature caused the hydrophobic backbone turn in less-ordered structure as temperature exceed above Tα. To investigate further the hydrophobic nanostructural variation, 2D scattering patterns was reduced 1D lineprofile as shown in Figure 5. Compared to 200 nm-thick Nafion thin films, 50 nm required higher temperature to cause the amplitude of the motions of backbone due to the relatively stronger ionomer/electrode interactions as temperature exceed Ta. And the transition temperature is lower than that of our previous work,[32] which evidence that the water

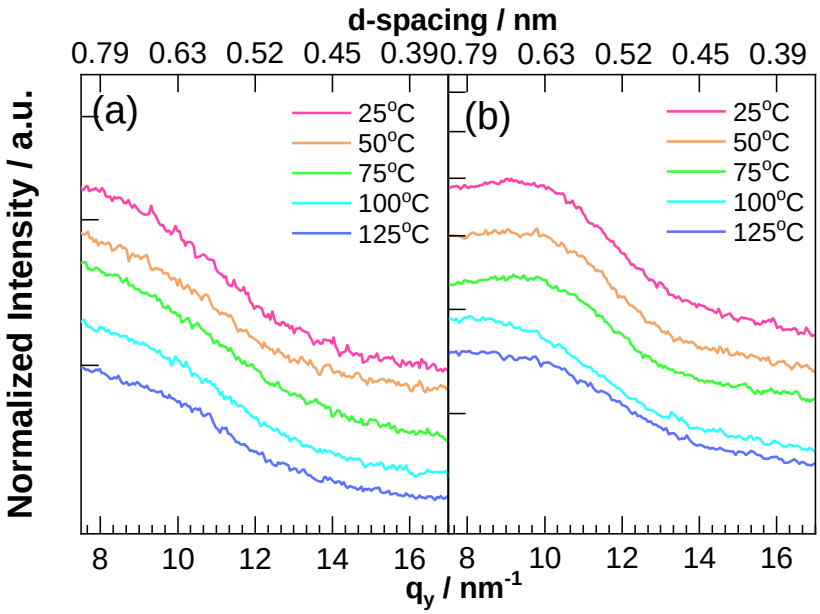

Figure 5. GIWAXS line profile along in-plane and out-of-plane direction of Nafion thin films with thickness of 50 nm and 200 nm.

molecule works as the plasticizer. This effect is strongly depend on the thickness of the cast film due to the fact the specific adsorption of Pt/sulfonate groups.

Herein, we promote a conceptual model to further understand the morphological changes related to Tα in terms of hydrophilic and hydrophobic phase variations upon increasing temperature For Nafion thin films with thicknesses 50 nm and 200 nm, the transition temperature are obviously reduced as the existence of water molecule which play as a role of plasticizer since the water molecule increased the mobility of side chains in Nafion. As the thickness confined to the size of hydrophilic/hydrophobic domain ionomer/electrode interaction become dominate and require more heat energy to cause morphological changes as we shown in Figure 6.

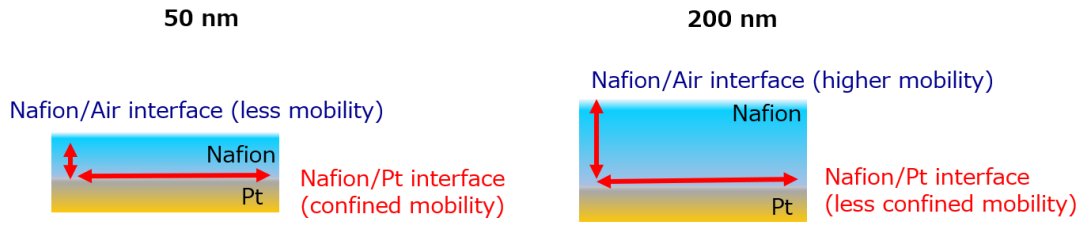

Figure 6. The schematic images of Pt-supported Nafion thin films with various 50 and 200 nm under wet conditions.

5.4 Conclusion

We focused on the plasticization effect of water in Nafion films with thicknesses of 50 and 200 nm at various temperature ranging from 25-120°C via GISAXS/GIWAXS and EIS method. As a result, the proton conductivity increased significantly as temperature increased over the transition temperature, Tα. Long-range mobility of the counterions was closely linked with the R-relaxation in these materials measured by GISAXS and GIWAXS The thinner the film is, the stronger substrate/ionomer interaction affects the mobility of the hydrophilic domain formed by the affinity of sulfonic groups. The compelling evidence confirmed by GISAXS/GIWAXS exhibited that the hydrophilic ionic domain and hydrophobic backbone turned to less phase-separated structure as the temperature exceed Tα. These data provide further fundamental understanding of the link between electrostatic interactions and dynamics in PFSI materials

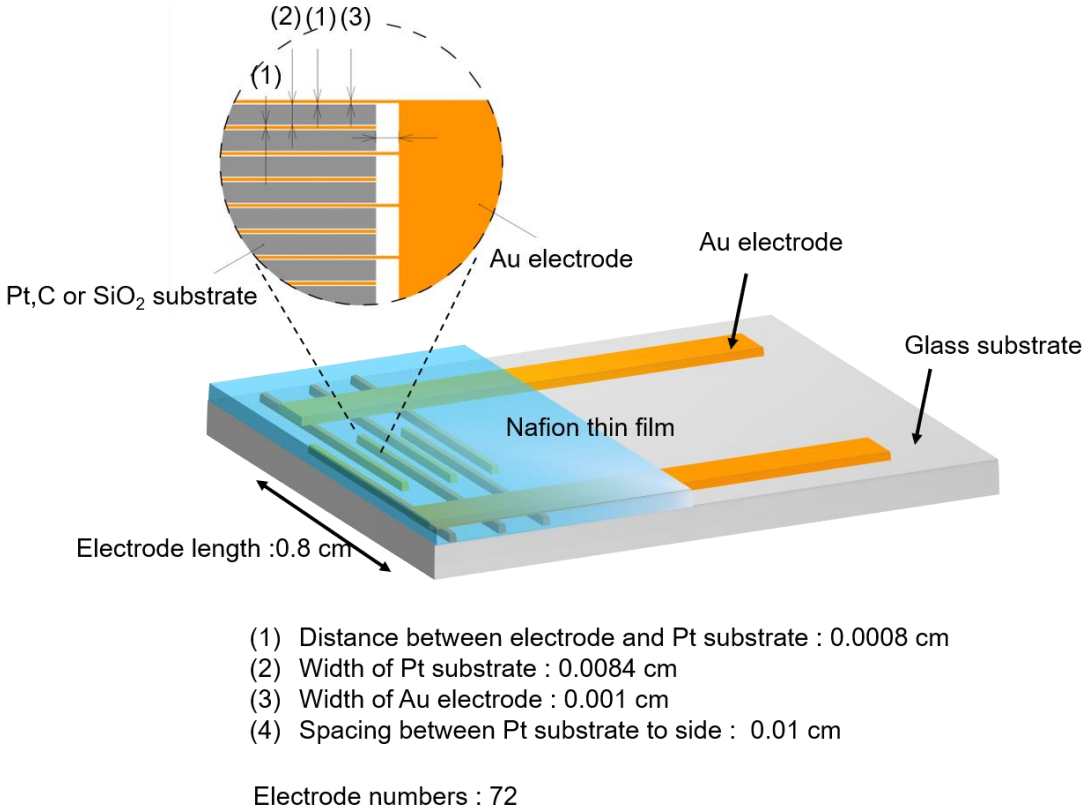

Figure 1. GISAXS 2D patterns of Nafion thin films with various thicknesses on different substrate under 20%RH.

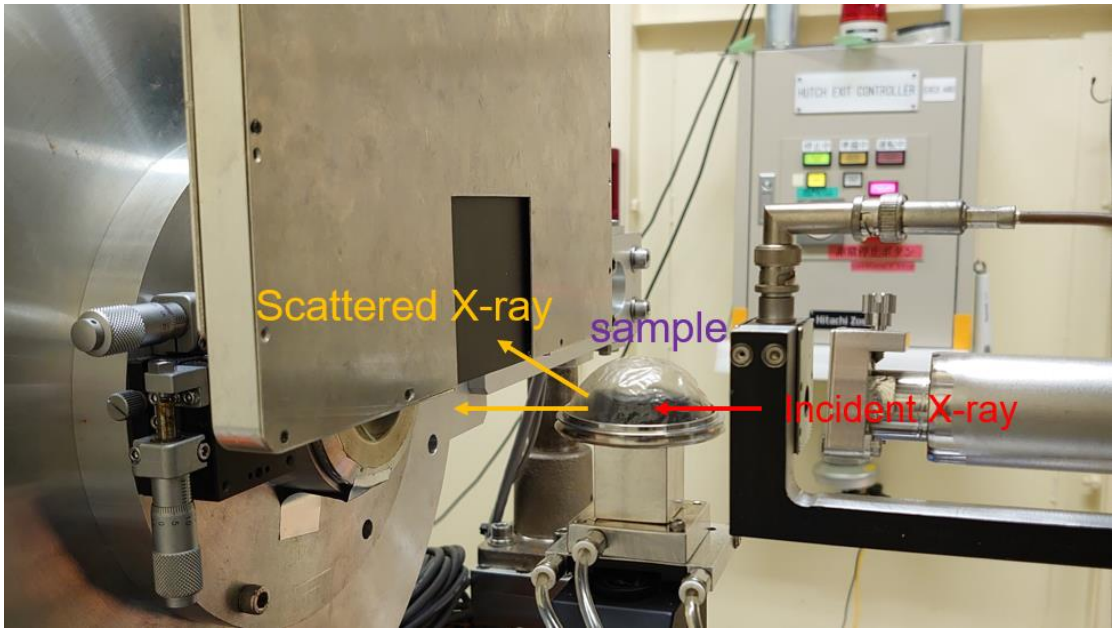

Figure S2. The schematic image of GISAXS/GIWAXS measurement. Continuous N_2 flow was transport into chamber with 25 μm PEEK film to maintain constant humidity level.

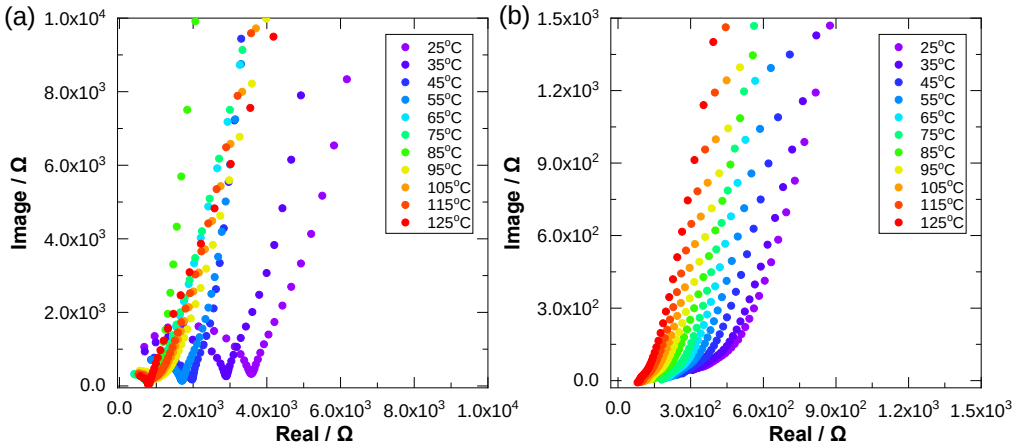

Figure S3. Nyquist plot of Nafion thin film with thickness of 50 nm and 200 nm on Pt substrate under 25-120°C via electrochemical impedance method.

Reference

(1) Eikerling, M.; Kulikovsky, A. Polymer Electrolyte Fuel Cells: Physical Principles of Materials and Operation; CRC Press, 2014.

(2) Franco, A. A. Polymer Electrolyte Fuel Cells: Science, Applications, and Challenges; Pan Stanford Publishing, 2016.

(3) Kreuer, K. D. Fuel Cells: Selected Entries from the Encyclopedia of Sustainability Science and Technology; Springer New York, 2012.

(4) Li, H.; Knights, S.; Shi, Z.; Van Zee, J. W.; Zhang, J. Proton Exchange Membrane Fuel Cells: Contamination and Mitigation Strategies; CRC Press, 2010.

(5) Kushner, D. I.; Kusoglu, A.; Podraza, N. J.; Hickner, M. A. Substrate‐Dependent Molecular and Nanostructural Orientation of Nafion Thin Films. *Adv. Funct. Mater*. **2019**, 1902699.

(6) Kusoglu, A.; Dursch, T. J.; Weber, A. Z. Nanostructure/Swelling Relationships of Bulk and Thin-Film PFSA Ionomers. Adv. Funct. Mater. **2016**, *26* (27), 4961.

(7) Kusoglu, A.; Hexemer, A.; Jiang, R.; Gittleman, C. S.; Weber, A. Z. Effect of compression on PFSA-ionomer morphology and predicted conductivity changes. *J. Memb. Sci*. **2012**, *421-422*, 283.

(8) Kusoglu, A.; Karlsson, A. M.; Santare, M. H. Structure-property relationship in ionomer membranes. *Polymer* **2010**, *51* (6), 1457.

(9) Matos, B. R.; Dresch, M. A.; Santiago, E. I.; Moraes, L. P. R.; Carastan, D. J.; Schoenmaker, J.; Velasco-Davalos, I. A.; Ruediger, A.; Tavares, A. C.; Fonseca, F. C. Nafion membranes annealed at high temperature and controlled humidity: structure, conductivity, and fuel cell performance. *Electrochim. Acta* **2016**, *196*, 110.

(10) Modestino, M. A.; Kusoglu, A.; Hexemer, A.; Weber, A. Z.; Segalman, R. A. Controlling Nafion Structure and Properties via Wetting Interactions. *Macromolecules* **2012**, *45* (11), 4681.

(11) Kusoglu, A.; Weber, A. Z. New Insights into Perfluorinated Sulfonic-Acid

Ionomers. *Chem. Rev.* **2017**, *117* (3), 987.

(12) Shi, S.; Dursch, T. J.; Borup, R. L.; Weber, A. Z.; Kusoglu, A. Effect of Hygrothermal Ageing on PFSA Ionomers' Structure/Property Relationship. *ECS Trans*. **2015**, *69* (17), 1017.

(13) Page, K. A.; Cable, K. M.; Moore, R. B. Molecular Origins of the Thermal Transitions and Dynamic Mechanical Relaxations in Perfluorosulfonate Ionomers. *Macromolecules* **2005**, *38* (15), 6472.

(14) Page, K. A.; Jarrett, W.; Moore, R. B. Variable temperature 19F solid-state NMR study of the effect of electrostatic interactions on thermally-stimulated molecular motions in perfluorosulfonate ionomers. *J. Polym. Sci. B* **2007**, *45* (16), 2177.

(15) Page, K. A.; Kusoglu, A.; Stafford, C. M.; Kim, S.; Kline, R. J.; Weber, A. Z. Confinement-driven increase in ionomer thin-film modulus. *Nano Lett.* **2014**, *14* (5), 2299.

(16) Page, K. A.; Landis, F. A.; Phillips, A. K.; Moore, R. B. SAXS Analysis of the Thermal Relaxation of Anisotropic Morphologies in Oriented Nafion Membranes. *Macromolecules* **2006**, *39* (11), 3939.

(17) Page, K. A.; Park, J. K.; Moore, R. B.; Garcia Sakai, V. Direct Analysis of the Ion-Hopping Process Associated with the α-Relaxation in Perfluorosulfonate Ionomers Using Quasielastic Neutron Scattering. *Macromolecules* **2009**, *42* (7), 2729.

(18) Page, K. A.; Rowe, B. W.; Masser, K. A.; Faraone, A. The effect of water content on chain dynamics in nafion membranes measured by neutron spin echo and dielectric spectroscopy. J. Polym. Sci. B **2014**, *52* (9), 624.

(19) Page, K. A.; Shin, J. W.; Eastman, S. A.; Rowe, B. W.; Kim, S.; Kusoglu, A.; Yager, K. G.; Stafford, G. R. In Situ Method for Measuring the Mechanical Properties of Nafion Thin Films during Hydration Cycles. *ACS Appl. Mater. Interfaces* **2015**, *7* (32), 17874.

(20) Weiss, R.; Agarwal, P.; Lundberg, R. Control of ionic interactions in sulfonated polystyrene ionomers by the use of alkyl-substituted ammonium counterions. *J. Appl. Polym. Sci* **1984**, *29* (9), 2719.

(21) Davis, E. M.; Stafford, C. M.; Page, K. A. Elucidating Water Transport Mechanisms in Nafion Thin Films. *ACS Macro Lett*. **2014**, *3* (10), 1029.

(22) Eastman, S. A.; Kim, S.; Page, K. A.; Rowe, B. W.; Kang, S.; Soles, C. L.; Yager, K. G. Effect of Confinement on Structure, Water Solubility, and Water Transport in Nafion Thin Films. *Macromolecules* **2012**, *45* (19), 7920.

(23) Frieberg, B. R.; Page, K. A.; Graybill, J. R.; Walker, M. L.; Stafford, C. M.; Stafford, G. R.; Soles, C. L. Mechanical Response of Thermally Annealed Nafion Thin Films. *ACS Appl. Mater. Interfaces* **2016**, *8* (48), 33240.

(24) Kim, S.; Dura, J. A.; Page, K. A.; Rowe, B. W.; Yager, K. G.; Lee, H.-J.; Soles, C. L. J. M. Surface-induced nanostructure and water transport of thin proton-conducting polymer films. *Macromolecules* **2013**, *46* (14), 5630.

(25) Nadermann, N. K.; Davis, E. M.; Page, K. A.; Stafford, C. M.; Chan, E. P. Using Indentation to Quantify Transport Properties of Nanophase-Segregated Polymer Thin Films. *Adv. Mater*. **2015**, *27* (33), 4924.

(26) Goswami, M.; Kumar, S. K.; Bhattacharya, A.; Douglas, J. F. Computer simulations of ionomer self-assembly and dynamics. *Macromolecules* **2007**, *40* (12), 4113.

(27) Dudenas, P. J.; Kusoglu, A. Evolution of Ionomer Morphology from Dispersion to Film: An in Situ X-ray Study. *Macromolecules* **2019**, *52* (20), 7779.

(28) Elliott, J. A.; Hanna, S.; Newton, J. N.; Elliott, A. M. S.; Cooley, G. E. Elimination of orientation in perfluorinated ionomer membranes. *Polym. Eng. Sci*. **2006**, *46* (2), 228.

(29) Jung, H.-Y.; Kim, J. W. Role of the glass transition temperature of Nafion 117 membrane in the preparation of the membrane electrode assembly in a direct methanol fuel cell (DMFC). *International Journal of Hydrogen Energy* **2012**, *37* (17), 12580.

(30) Osborn, S. J.; Hassan, M. K.; Divoux, G. M.; Rhoades, D. W.; Mauritz, K. A.; Moore, R. B. Glass Transition Temperature of Perfluorosulfonic Acid Ionomers. *Macromolecules* **2007**, *40* (10), 3886.

(31) Ozmaian, M.; Naghdabadi, R. Molecular dynamics simulation study of glass transition in hydrated Nafion. *J. Polym. Sci. B* **2014**, *52* (13), 907.

(32) Gao, X.; Yamamoto, K.; Hirai, T.; Uchiyama, T.; Ohta, N.; Takao, N.; Matsumoto,

M.; Imai, H.; Sugawara, S.; Shinohara, K. Morphology Changes in Perfluorosulfonated Ionomer from Thickness and Thermal Treatment Conditions. *Langmuir* **2020**, *36* (14), 3871.

(33) Siroma, Z.; Kakitsubo, R.; Fujiwara, N.; Ioroi, T.; Yamazaki, S.-i.; Yasuda, K. Depression of proton conductivity in recast Nafion® film measured on flat substrate. *J. Power Sources* **2009**, *189* (2), 994.

Chapter 6 General Conclusion

Polymer electrolyte fuel cells are widely used in various electronic devices, vehicles, stationary energy supplement. For further utilization, it is still need to improve the energy density, durability and industrial cost. Therefore, this work concentrated on fundamental research in term of ionomer/electrode interfacial regime, especially interfacial phenomena in proton conducting electrolyte.

In chapter 1, the overview of PEFCs and recent progress in Nafion membrane and thin film for the past two decades. Especially the background introduction for proton transport phenomenon and its mechanism in ionomer/electrode interface was briefly introduced.

In chapter 2, the morphological property and proton conductivity of Nafion thin film cast on Pt substrate with various thermal and thickness condition were systematically evaluated by GISAXS/GIWAXS and electrochemical impedance method. It is cleared that Nafion thin film with thicknesses under 30 nm formed a comparatively stable state upon annealing treatment compared to the bulky-like Nafion thin films with thickness of 200 nm. The temperature at which morphology and proton transporting properties significantly changed strongly depend on film thickness.

In chapter 3, different type of substrate impact on morphological and proton transporting properties of Nafion thin film was discussed. The findings demonstrate a complex interplay between the perfluorosulfonic-acid ionomer and the various substrates. Compared to Nafion thin films cast on C substrate didn't exhibit anisotropic behavior. Au showed similar trend with Pt with suppressed growth of ionic domain. These results indicate that sulfonate groups have a great interact with substrate thus the morphology significantly influence by their property.

In chapter 4, The swelling phenomenon in ionomer thin films interacting with a substrate is more complex than that in the microscale due to the infl uence of the interface. The interactions between the ionomer moieties and the substrate control the polymer chains' orientation at the interface, which diminishes beyond a critical

thickness and results in “bulk-like” behavior. This also explains why the 3M PFSA chemistry favors phase separation, especially for fi lms thinner than 50 nm. The reason is that the shorter side-chains bring the backbone main chains closer to the substrate, resulting in increased interactions between the substrate and sulfonic-acid groups. This behavior favors phase separation and potentially leads to a more effi cient packing of nanodomains. that governs their strength and nature. It is known that metallic substrates exhibit stronger interactions for Nafion than those of Si examined herein. Yet, even though substrates have additional influence on the thin-film’s structure and properties, it is the thickness, and therefore the confi nement, that dominates the overall fi lm behavior; the changes in swelling/uptake due to the substrate are smaller in magnitude than the changes caused by the thickness.

In chapter 5, The morphology of Nafion thin film on different substrate present behavior. Nafion thin film on metallic substrate Au, Pt exhibited more anisotropy behavior than that on carbon. While, in case of the comparatively hydrophilic SiO_2 substrate, the ionic domain strongly orientated along out-of-plane direction and exhibit extraordinary anisotropic behavior. These results indicate the morphology of Nafion thin films with thicknesses from 5-200 nm are strongly affected by type of substrate. It is considered that the physical properties such as proton transportation and oxygen diffusion also influenced by substrate.

In chapter 6, the results of previous studies were summarized. GISAXS/GISAXS provide a new insight and effective way to investigate Nafion thin film in term of morphology. By combing with EIS, the correlation of physical property and nanostructure can be established. This thesis mainly focuses on the correlation of structure-property relationship in proton conducting material, Nafion thin film. For deep understanding about interfacial phenomena based on kinetics, such as factors influence on oxygen permeation is required to enhance high performance of PEFCs.

Acknowledgement

The study on this thesis has been carried out at Graduate School of Human and Environmental Studies, Kyoto University.

First of all, I would like to wish to express my special gratitude to Prof. Yoshiharu Uchimoto at Graduate School of Human and Environmental Studies, Kyoto University, for his precise indications and valuable advices. I am also grateful to Assitant prof. Kentaro Yamamoto at Graduate School of Human and Environmental Studies, Kyoto University, for his useful comments and discussions.

I would like to appreciate Associated Prof. Tomoyasu Hirai at Department of Applied Chemistry, Osaka Institute of Technology, for his effective suggestions and helps on analysis GISAXS/GISAXS spectra. I would also like to appreciate Dr. Noboru Ohta at Japan Synchrotron Radiation Research Institute (JASRI), Kyoto University, for their effective suggestions and measuring GISAXS/GIWAXS.

Special thanks are expressed to Dr. Seiho Sugawara and Dr. Kazuhiko Shinohara at Fuel Cell Cutting-Edge Research Center Technology Research Association, for his useful proposal on proton conductivity measurement.

I would like to thank to all the members of Prof. Uchimoto's laboratory for their helps, discussions and encouragement throughout this study.

Finally, I would like to appreciate my parents and my friend for understanding, support and encouragement.

Xiao Gao

Kyoto, JAPAN, November, 2019